FINAL REPORT

as a partial requirement

for

Major Qualifying Project

ACES characterization of damping in micro-beam resonators

Submitted by:

Xiuping Chen
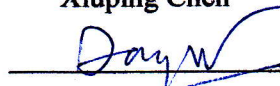
Vu Nguyen
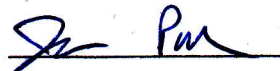
Jason Parker

Submitted to:

Professor Ryszard J. Pryputniewicz

NEST – NanoEngineering, Science, and Technology
CHSLT- Center for Holographic Studies and Laser micro-mechaTronics
Mechanical Engineering Department
School of Engineering
Worcester Polytechnic Institute
Worcester, MA 01609-2280

March 1, 2012

Acknowledgements

The authors would like to offer thanks to Professor Ryszard J. Pryputniewicz for the excellent opportunity he has given us to work in the exciting field of MEMS on this MQP and his valuable advice and direction in the completion of this project. Also, thanks to Mr. Peter Heifti for his assistance with the experimental work, his years of experience in the field of optics were invaluable. Additionally, thanks to Dr. Adriana Hera for her assistance with the computational portion of this project. Thanks to Dr. Boquan Li for assistance with the coating of our samples. Finally, thanks to Professor Nancy A. Burnham and Professor Richard Sisson for additional advice provided in this project.

Contents

List of figures

List of tables

Nomenclature

ACES	Analytical, Computational, and Experimental Solution
MQP	Major Qualifying Project
LDV	Laser Doppler Vibrometer
PZT	Lead Zirconate Titanate
PSA	Prostate Specific Antigen
CCD	Charge Coupled Device
MEMS	Microelectromechanical system
TED	Thermoelastic Damping
CVD	Chemical-Vapor Deposition
Q-factor	quality factor
IC	Integrated Circuit
Q_Z	Q_L calculated by Zener's equation
Q_L	Q-factor calculated by Lifshitz's equation
Q_{anchor}	Q-factor related to anchor damping
$Q_{surface}$	Q-factor related to surface damping
Q_{air}	Q-factor related to air damping
Q_{TED}	Q-factor related to thermoelastic damping
E	Young's modulus
I	area moment of inertia along z axis
A	cross sectional area
$Y(x)$	mode shape of the vibrating beam
β_i	constants that are numerically solved for resonant modes
Fo	amplitude of the applied force
$\mathbf{F_0}(x, y, z)$	value of the light field that is reflected by the cantilever beam at rest
$\mathbf{L}_{t\,(x, y, z, t)}$	displacement vector of one point on the beam
$\mathbf{K_1}(x, y, z)$	illumination propagation vectors
$\mathbf{K_2}(x, y, z)$	observation propagation vectors
J_0	zero order Bessel function of the first kind
ω_0	natural angular frequency
ω	angular frequency of the applied force
σ	stress
ε	strain
ρ	mass density
c_p	heat capacity
k	thermal conductivity
α	thermal expansion coefficient
χ	thermal diffusivity
t	cantilever beam's thickness
L	cantilever beam's length
w	cantilever beam's width
γ	complex eigenfrequency
ω	real frequency of a vibrating body
δ	coating thickness
E_{ds}	dissipative portion of complex modulus of coating

ζ	damping ratio
ξ	a coefficient in Lifshitz's equation for Q_L
ξ_{anchor}	damping coefficient due to anchor loss
λ, μ	lamé coefficients
f_D	doppler frequency shift
f_n	n[th] resonant frequency
v	velocity
ν	Poisson ratio
λ_L	laser wavelength
σ_{ij}	stress tensor
C_{ijkl}	6x6 stiffness matrix
ε_{kl}	strain tensor
δ_{ij}	Kronecker delta
ΔT	temperature variation from the initial temperature
PBS	Polaraizing Beam Splitter
QWP	Quarter Wave Plate
BC	Bragg Cell
ω_c	reference frequency
PD	Photo Detector
FFT	Fast Fourier Transform

Abstract

Recent advances in microelectromechanical systems (MEMS) technology have led to development of a multitude of new sensors and their corresponding applications. Great many of these sensors (e.g., microgyroscopes, accelerometers, biological, chemical, etc.) rely on vibrations of either sensing elements or elastic suspensions that resonate. Regardless of their applications, sensors are always designed to provide the most sensitive responses to the signals they are developed to detect and/or monitor. One way to describe this sensitivity is to use the Quality factor (*Q-factor*). Most recent experimental evidence indicates that as physical sizes of sensors decrease (especially because of advances in fabrication by surface micromachining) the corresponding *Q-factors* increase. This report develops a preliminary model of *Q-factors of MEMS resonators* using Analytical, Computational, and Experimental Solutions (ACES) methodology to investigate the effects of various damping mechanisms on the Q-factor of micro mechanical resonators. We have focused on the contributions of air damping, thermoelastic damping (TED), and surface damping to the Q-factor. Laser Doppler Vibrometry (LDV) and Michelson Interferometry were used to characterize the damping of tipless atomic force microscopy (AFM) probes through ring down tests. Tests were performed at various levels of vacuum with different beam geometries and coatings. COMSOL was used to model the TED as well as resonance characteristics of the beams and the computational results were compared to analytical and experimental results. It was found that as surface area to volume ratio increases beyond approximately 1 μm^{-1}, surface damping becomes the dominant damping mechanism. Additionally air damping was significant at a vacuum level greater than approximately 0.1 μbar. It was also found that the surface damping was much greater with an about 28 nm Au-Pd coated

as compared to about 30 nm Al coated and uncoated beams. Finally, the dissipation term in the

analytical approximation of surface damping was calculated for the above coatings.

Project summary

The goal of this Major Qualifying Project (MQP) was to investigate the effects of

material properties and sensor geometry on the Quality factor (Q-factor) of resonating

microscale and nanoscale sensors in order to optimize their sensitivity. The Q-factor is a way to

describe the sensitivity of these resonators. The Q-factor is adversely affected by various

damping mechanisms including TED, air damping, anchor damping, and surface damping.

In order to accomplish this task, analytical solutions for calculating TED based on the

works of Zener (Zener, 1937) and Lifshitz (Lifshitz and Roukes, 1999) for a simple

commercially available Single Crystal Silicon prismatic cantilevered beam were used to

calculate the Q-factor. A finite element solution was also generated using COMSOL

Multiphysics (2011) and compared with the analytical solution. Additionally experiments were

conducted using a Michelson Interferometer and a Laser Doppler Vibrometer (LDV) to attain the

resonant frequency and overall damping ratio, respectively. These data were compared with the

analytical and computational results. Once the analytical and computational methods were

validated, the results were used to investigate the effects of material properties and geometries in

the hopes of improving the Q-factor of current resonators.

It was found that as size of the sensor decreases to the microscale, surface damping

becomes a significant factor on the Q-factor, and for this reason it deserves attention. The

analytical, numerical, and experimental results agreed with the calculated uncertainty so as to

validate our analysis. Based on the experimental, analytical, and numerical analysis we have

developed we have obtained a relationship for the optimum geometry so as to maximize Q-

factor. We have identified the key material properties to focus on in order to maximize Q-factor.

Additionally, the effects of surface damping were clearly shown and the importance of minimizing the surface damping as the sensor reaches the nanoscale has been demonstrated. These results can be used in the fabrication of current and future resonating sensor designs. This will lead to the increased sensitivity of these devices. In addition, our results have the potential to benefit many sectors including but not limited to communication, medical, defense, and aerospace.

I. Introduction

First proposed by Richard Feinman in his 1959 presentation at California Institute of Technology, some 50 years later micro scale and nano scale fabrication has progressed to the point that it is used in objects we rely on every day, including automotive safety systems, and various consumer products such as active stability control in camcorders (Feynman, 1992). This progress has been spurred on by the advances in stereo lithography made by the integrated circuit industry. The progression of micro scale and nano scale devices is continuing to increase with applications in the automotive, medical, entertainment, aerospace, and defense industries.

I.1. Micromechanical resonators

I.1.1. Principles of operation

A particularly important class of MEMS is the micromechanical resonant sensor. The more traditional sensor is based on the effect the measurand has on the capacitance or resistance of the sensor. In the case of the resonant sensor, the resonator is excited at its natural frequency; the measurand shifts the natural frequency of the resonator either by changing its mass or stiffness. A general rule of thumb is that resonating devices can achieve 10 times greater measurement accuracy as compared to capacitive or resistive methods (Gad-el-Hak, 2002).

Micromechanical resonators are produced in various shapes, including beams, diaphragms, "butterfly" structures, and "H" structures. Figure 1 shows some examples of micromechanical resonators (Elwenspoek and Wiegerink, 2001). The dimensions of these structures are on the micrometer scale and now reaching the nanometer scale. Each shape can have several types of vibration, including longitudinal, transverse, torsional, and lateral. Each resonator has infinite degrees of freedom and thus an infinite number of resonant modes,

however each sensor is usually designed so that one type of vibration and resonant mode will

dominate (Elwenspoek and Wiegerink, 2001).
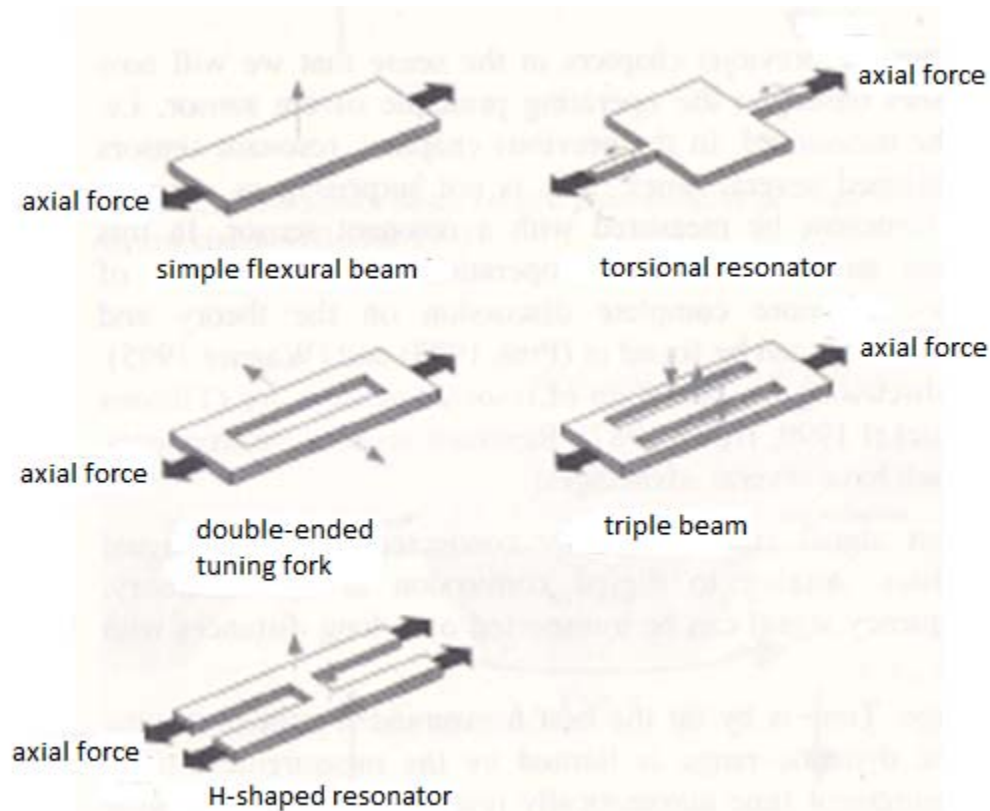
Figure 1. Various structures used in resonant microsensors (Elwenspoek and Wiegerink, 2001).

There are several techniques for exciting resonators into resonance and detecting the shift

in the resonance frequency. Electrostatic excitation and capacitive detection can be used where

the resonator acts as one plate of a capacitor and the substrate acts as the other plate. The charged

capacitor creates a current if the capacitance fluctuates, which occurs based on the displacement

of the resonator. This is a relatively simple method, however, the resonator must be close to the

substrate in order to act as a capacitor, when this occurs squeeze film damping can happen and

negatively impact the performance of the sensor. Additionally, the capacitance of this type of

sensor is usually small and thus leads to a small detection signal (Elwenspoek and Wiegerink, 2001).

Piezoelectric excitation and detection can also be employed. Piezoelectric materials experience a strain when a voltage is applied. In order to exploit this phenomenon, a thin piezoelectric film, such as PZT, is sandwiched between two electrodes and a voltage is applied. This voltage causes a change in the dimensions of the piezoelectric film which forces bridges or membranes into bending. A major benefit to this type of actuation is that frequencies realized by piezoelectrically actuated resonators can be in the GHz range (Lange et al., 2002). However, because two different materials are sandwiched together, temperature can have a large affect on the sensors performance since the two materials will have different coefficients of thermal expansion. The composite structure can also cause unwanted damping of vibrations (Elwenspoek and Wiegerink, 2001).

Electrothermal excitation and piezoresistive detection has been used in resonant sensors. A heat source causes a thermal gradient across the resonator. This thermal gradient leads to bending in the resonator. A typical electrothermally actuated resonator is pictured in Fig. 2, the heat source is located between d_1 and d_2 (Lange et al., 2002). To detect the vibration the change in resistance due to strain is measured. Some materials such as Silicon change resistivity when a stress is applied, this is known as piezoresistivity. This type of actuation is limited to less than 1 MHz (Lange et al., 2002). Additionally, this thermal actuation can lead to high thermal stresses and thermal management becomes more important in sensors actuated this way (Elwenspoek and Wiegerink, 2001).

15
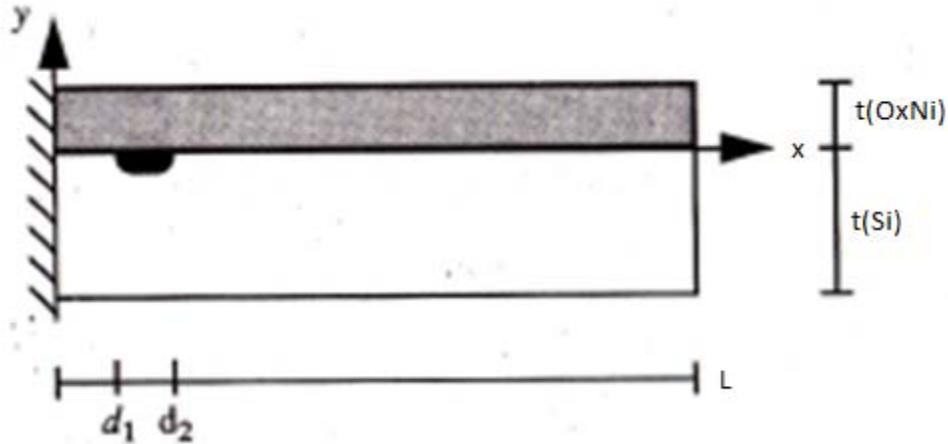
Figure 2. Cross-section of a thermally actuated composite cantilever beam (Lange et al., 2002).

Similar to electrothermal excitation, optothermal excitation relies on creating a thermal gradient in the resonator and thus inducing bending. The heat is generated by the absorption of light. Optical detection is employed and relies on the variation of light transmitted through a gap in a wave guide. Optionally, integrated interferometry can be employed using the surface of the beam and the end of a glass fiber as mirrors (Elwenspoek and Wiegerink, 2001). The benefit of this method of actuation and detection is the fact that it avoids electrical voltages at the sensor which can be important for sensors that operate in explosive regions or in high electric fields.

Magnetic excitation and detection has been used for micromechanical resonators. The resonator is placed in a permanent magnetic field and a harmonic electric current will flow through a bridge type beam resonator and result in a Lorentz force. This force will cause the beam to vibrate and magnetic induction is used to detect this force. In most applications an "H" structure is used where one beam is used for excitation and the other for detection (Elwenspoek and Wiegerink, 2001). This is illustrated in Fig. 3, B is the magnetic field, i is the current and F_L is the induced Lorentz force (Lange et al., 2002). This method uses less power than the electrothermal method and with a large enough magnetic field, excitation can be extended to

frequencies above 1 MHz. The disadvantage is the additional complexity since a permanent

magnet must be integrated into the package (Lange et al., 2002).
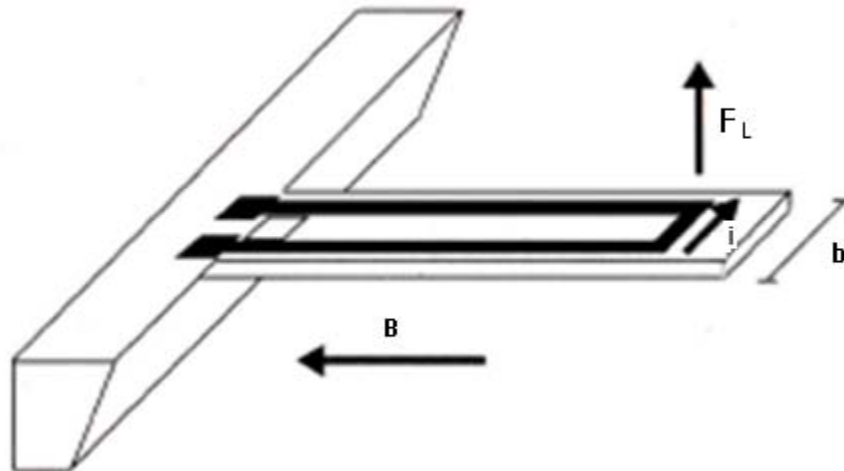
Figure 3. Schematic of a electromagnetically actuated beam.

A final method worth mentioning is that of Dielectric excitation and detection. Similar to

piezoelectric excitation, a thin dielectric film is sandwiched between two electrodes. As a voltage

is applied across the electrodes an electrostatic force is created and causes a lateral deformation

of the film which induces bending of the resonator. The detection is based on the change of

capacitance if the dielectric is deformed. The signals are small, however and require materials

with high dielectric constants (Elwenspoek and Wiegerink, 2001).

I.1.2. Applications

A successful application of the resonant micromechanical sensor is the pressure sensor.

This sensor consists of a membrane onto which is sputtered a thin piezoelectric film. A voltage

causes a lateral strain in the membrane which induces bending. The membrane is exposed to the

medium to be measured and a change in pressure will shift the resonant frequency of the sensor.

This frequency shift can be used to calculate the pressure of the medium. The downside of this

design is that resonant frequency is not only dependent on the pressure but also the mass of the

gas in the vicinity of the membrane so the measurement becomes dependent on the type of gas

being measured. Additionally because the membrane is in direct contact with the gas, corrosion,

chemical absorption, and dust buildup can cause a drift in the readout over time (Elwenspoek and

Wiegerink, 2001). A modified version of this sensor in which the membrane does not vibrate

employs a resonating beam attached to the bottom surface of the membrane or inside the

membrane. An example with the resonators inside the membrane is illustrated in Fig. 4 (Gad-el-

Hak, 2002). As the membrane deflects, strain is induced onto the beam, shifting the resonant

frequency. This design separates the resonator from the atmosphere, thus eliminating some of the

drawbacks of the above design in which the membrane vibrates (Korvink and Paul, 2006).
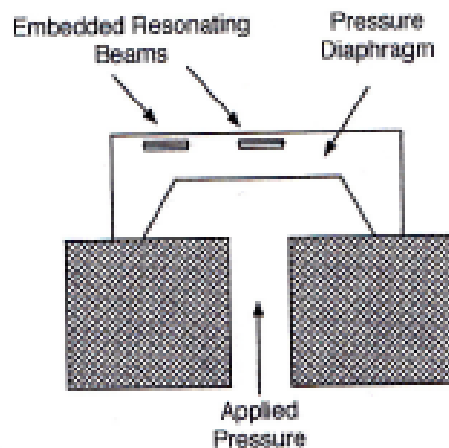
Figure 4. Schematic of a resonating beam pressure sensor (Gad-el-Hak, 2002).

An interesting sensor takes advantage of the stresses induced from the thermal expansion

of a constrained beam. The resonant mass-flow sensor utilizes this phenomenon by relying on

gas flow to control the temperature of a heated beam-type resonator. Heat flow out of the beam

will depend on the velocity of the gas, and since thermal expansion of the beam will induce

mechanical stress, a resonance frequency, which is a function of flow, is obtained. An example

of the resonant mass-flow sensor is illustrated in Fig. 5 (Elwenspoek and Wiegerink, 2001).
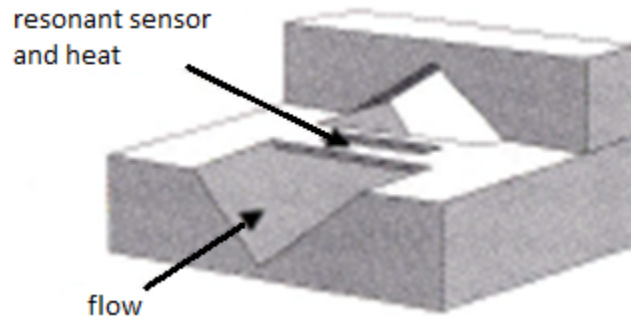
Figure 5. Schematic of a resonant mass flow sensor (Elwenspoek and Wiegerink, 2001).

Another application of the resonant micromechanical sensor is to measure gas

concentration. The resonant vapor sensor employs a cantilever resonating beam coated with a

polymer surface layer. The polymer is used as a sensitive layer that the gas molecules diffuse

into and out of until equilibrium is obtained. The absorption of the gas molecules increases the

mass of the beam and thus produces a shift in the resonant frequency. Mass resolution of better

than 0.4 pg has been obtained. An example of a resonant gas sensor is depicted in Fig. 6 (Lange

et al., 2002).
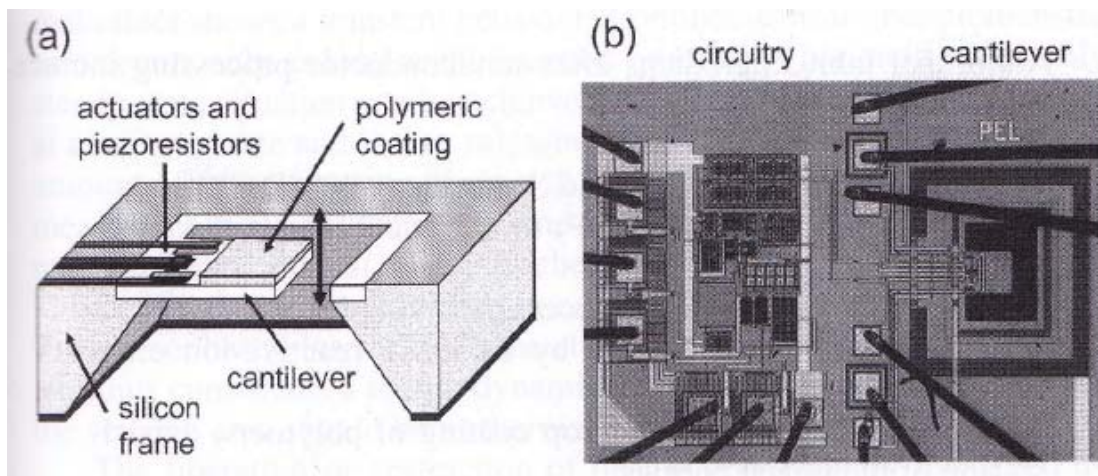
Figure 6. Schematic (a) and micrograph (b) of a thermally acuated, piezoresistive detected
resonant gas sensor (Lange et al., 2002).

Resonant micromechanical sensors have also found a home in acceleration

measurements. In the resonant accelerometer, a proof mass is suspended by four resonating

beams. Acceleration in either direction would cause differential stresses in the corresponding

pair of resonators. The difference in resonant frequency becomes a measure of acceleration. A

typical resonant accelerometer design is depicted in Fig. 7 (Elwenspoek and Wiegerink, 2001).

Resonant micromechanical sensor technology has brought the cost of accelerometers down to

where they are used in automotive applications, such as air bag deployment, stability control, and

electronic suspension control, as well as in biomedical applications and consumer products like

camcorders for active stabilization (Elwenspoek and Wiegerink, 2001).
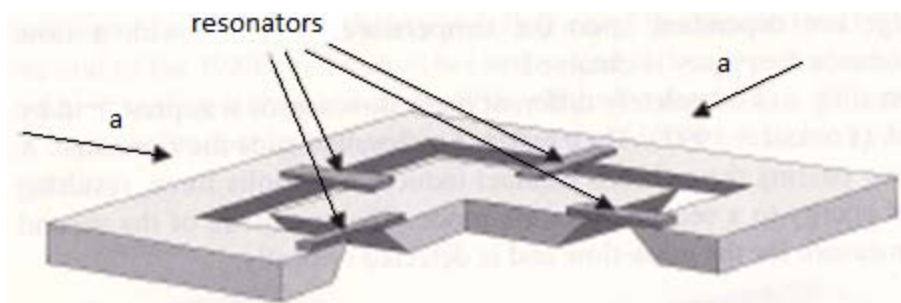
Figure 7. Schematic of a resonant accelerometer (Elwenspoek and Wiegerink, 2001).

Similar to the design of the resonant accelerometer, the resonant yaw rate sensor or

gyroscope measures angular rate by exploiting the Coriolis effect. A proof mass is driven into

oscillation in one axis. Rotation of the reference frame will displace the mass into a second axis;

this reaction causes a shift in the resonant frequency of the beams (Gad-el-Hak, 2002). A

Draper/Honeywell MEMS gyroscope is pictured in Fig. 8 (Weinburg and Kouropenis, 2006).

8(a) is a photomicrograph, in 8(b) and 8(c), silver represents metal, blue represents Silicon

attached to glass, and white indicates suspended Silicon. Electrical contact pads are Right Motor

drive (RM), Right Sense electrode (RS), Motor Pick Off (MPO), Left Sense electrode (LS), Left

Motor drive (LM), and Sense Pick Off (SPO).
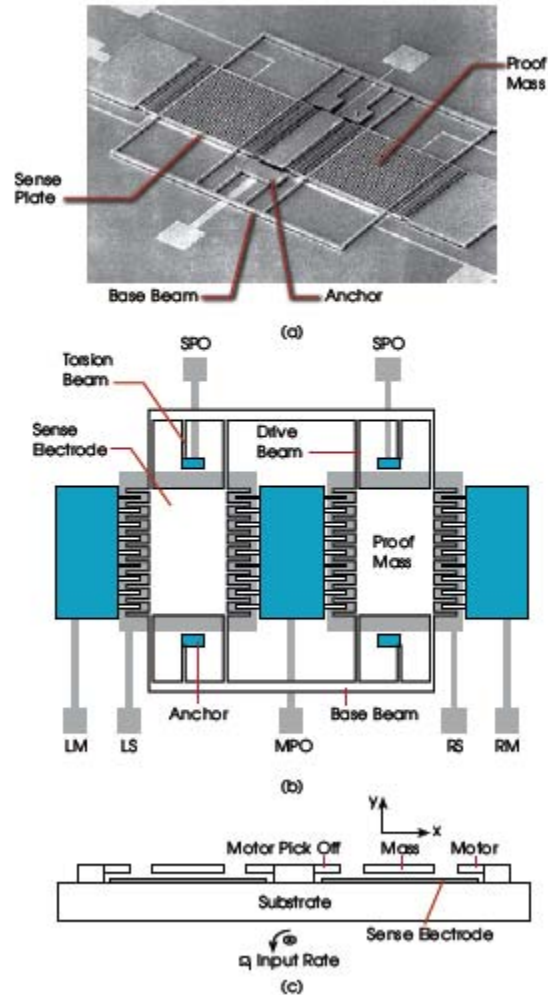
Figure 8. Schematic of a Draper/Honeywell MEMS gyroscope.

The micromechanical resonant sensor also has applications in the medical field as a way

to detect pathogens, including cancer detection. Lee et al. (2004) demonstrated the successful

design of a resonant micromechanical sensor to detect prostate-specific antigen (PSA), the

marker or indicator of prostate cancer. The resonator consisted of a layered Ta/Pt/PZT/Pt/SiO_2

on SiN_x beam with an Au coating. The Au coating was treated with antibodies and immobilized

via calixcrown self-assembled monolayers. PSA is attracted to the antibody and increases the

mass of the beam, shifting the resonant frequency. For a 50 μm x 150 μm x 2.26 μm beam the

authors demonstrated a frequency shift of 273 Hz for 1 ng/ml of PSA (Lee et al., 2004).
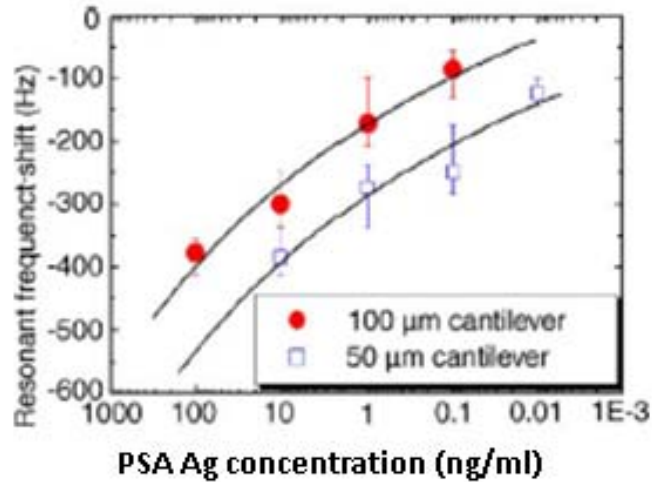
Figure 9. Frequency shift as a function of PSA antigen concentration for two sizes of cantilever
(Lee et al., 2004).

I.1.3. Manufacturing techniques and materials

MEMS industry evolved from integrated circuit (IC) industry, so MEMS manufacturing

techniques are very similar to those used in IC fabrication. MEMS and IC devices are generally

fabricated on a single crystal silicon wafer. To make this wafer, a single crystal silicon bulk is

made from a single crystal silicon seed and drawn into rod shape. This rod is sawed into circular

slices and polished to form wafers. Many identical MEMS devices can be made on one wafer

and are then separated into single device called die for packaging into MEMS chips (Liu, 2011).

The schematic of the process is in Fig.10.
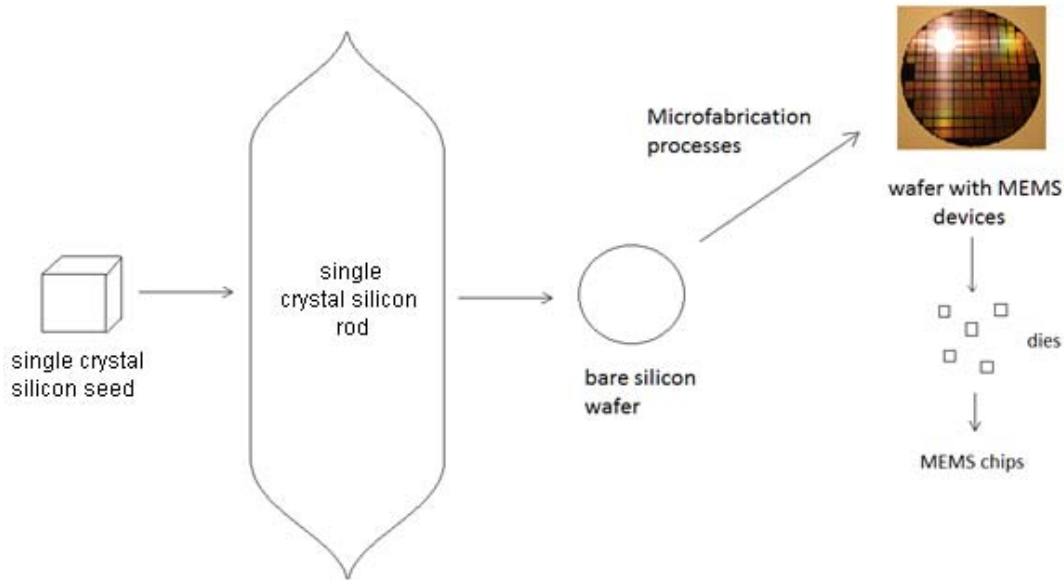
Figure 10. Process flow for MEMS production (Liu, 2011).

Some micro fabrication processes that are most commonly used in MEMS are described

as followed.

I.1.3.1 Thin film deposition

Functional materials can be incorporated on a wafer through an additive deposition

process. This deposition process can involve a direct transfer of material from a source to the
wafer in an atom-by-atom, or layer-by-layer fashion, as shown in Fig.11(Liu, 2011). The source

material can be transferred by evaporation or by sputtering. The achieved thickness is

proportional to the process power and duration (Liu, 2011).

Evaporation involves the heating of the source material to a high temperature to generate

a vapor that condenses on the substrate to form a film. Many elements and compounds can be

evaporated, including Al, Si, Ti, Au, and Al_2O_3. The evaporation process is performed in a

vacuum chamber with pressure typically below 10^{-4} Pa to avoid contaminating the film (Maluf

and Williams, 2004).

23
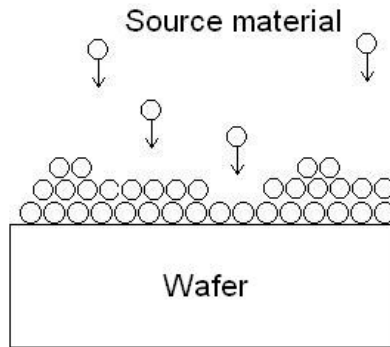
Figure 11. Schematic of the additive deposition process (Liu, 2011).

In sputtering deposition, the source material is called a target and is physically bombarded with a flux of inert gas ions in a vacuum chamber at a pressure of 0.1-10Pa. The vacuum is to avoid the interruption with the air molecules. The atoms or molecules from the target are ejected and deposited onto the wafer. Nearly any inorganic material can be sputtered. Sputtering is a favored method in MEMS for deposition at low temperatures ($<150^oC$) for thin metal films such as aluminum, titanium, chromium, tungsten, Al/Si and Ti/W alloys, amorphous silicon, and piezoelectric ceramics (Maluf and Williams, 2004).

Another common method in deposition is Chemical-Vapor Deposition (CVD). In this process, a chemical reaction is initiated near the heated surface of the wafer in a controlled atmosphere, resulting in a deposition of the reacted species on the wafer. In contrast to sputtering, CVD is a high temperature process ($>300^oC$). Common thin films deposited by CVD included polysilicon, silicon oxides and nitrides (Maluf and Williams, 2004).

I.1.3.2 Photolithography

The purpose of photolithography is to produce fine features on the wafer surface. The process involves depositing a layer of photoresist material, which is a photo-sensitive chemical, on the wafer surface, then exposing this layer to light through a mask which contains the pattern

to be made on the photoresist. This process is illustrated in Fig.12 ((Maluf and Williams, 2004).

The patterned photoresist layer then can be used in deposition or etching processes to create the

desired features. The layer of photoresist is then removed and what is left is the desired feature

on the wafer surface.
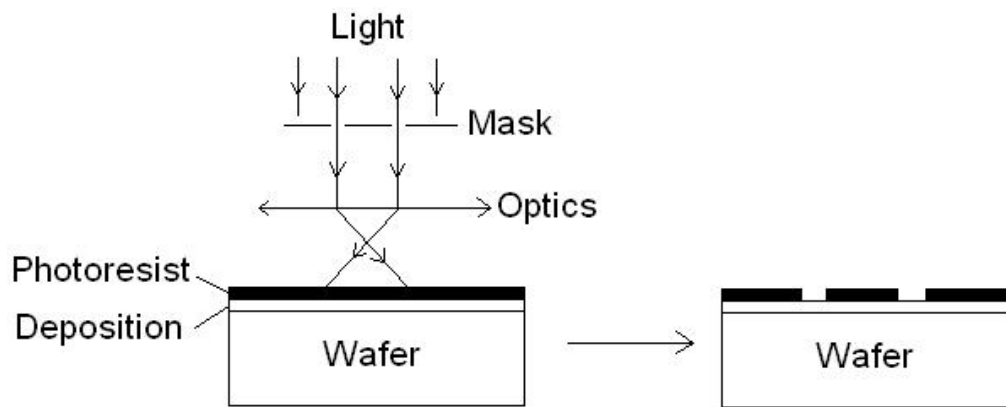
Figure 12. Schematic of the photolithography process (Maluf and Williams, 2004).

I.1.3.3 Etching

Etching techniques can be divided into two techniques: wet etching and dry etching. Wet

etching is a technique to remove material by wet chemical reaction. The selectivity of the etching

against photoresist material, substrate material, and deposited material is a crucial issue in

MEMS design and fabrication. In reality, the etching chemical can affect any material that it

contacts. An etching process with two windows A and B is illustrated in Fig. 13 (Liu, 2011).

Ideally, the etch rate on the thin film deposition should be much higher than the etch rate on the

photoresist mask. The etch rate in different window sizes can also be different. However, at the

end of the etching process, the thin film in each window should be completely removed and the

mask's thickness is reduced in a small amount. Moreover, although the vertical etching is of

interest, the etching can also remove material in lateral direction. The extent of the lateral etch

during the process time is called undercut. The undercut obviously affects the precision of the

desired feature (Liu, 2011).
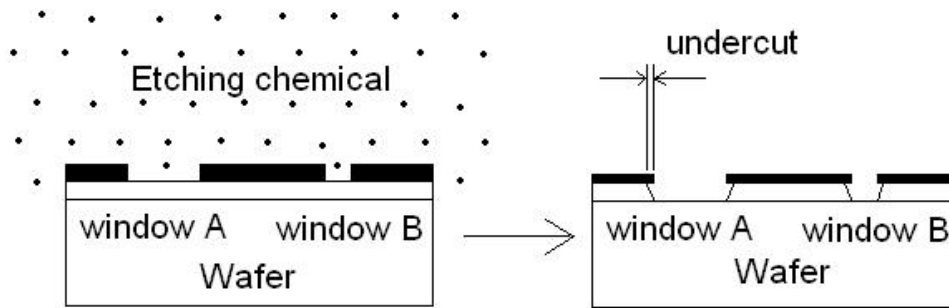
Figure 13. Schematic of the wet etching process (Liu, 2011).

Dry etching, or plasma etching, gets its name because it does not involve wet chemical.

In plasma etching, gas species are broken up by the electric field into active gaseous radicals that

are electrically charged and can react with the wafer chemically. Moreover, because of the

electric field, the charge radicals are also accelerated to high speed and interact with the wafer

physically. Thus both the chemical and physical removal processes can happen at the same time.

In general, the physical etching is more directional and hence anisotropic, whereas the chemical

etching is more isotropic and material selective (Liu, 2011).

I.1.3.4 Doping

Another common process in micro fabrication is doping, which is a process of planting

dopant atoms into the host semiconductor lattice in order to change the electrical and also

mechanical characteristics of the material. The dopant atoms can further diffuse from a high-

concentration to low-concentration regions under thermal activation; the process is called

thermal diffusion. The concentration of the doped material at a location depends on the time of

the doping process, the distance from the surface, and the temperature at which the doping is

implemented. The doping process for a selected region is illustrated in Fig. 14 (Liu, 2011).
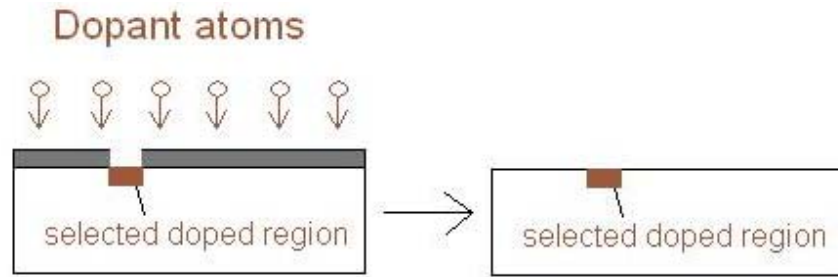
Figure 14. Schematic of the doping process (Liu, 2011).

Unfortunately, the doping process can only be performed on the top surfaces of the wafer, and the high temperature encountered in consequent steps in the fabrication process can cause a redistribution of the dopant atoms and change the electrical characteristics of the material (Liu, 2011).

I.2. Flexural beam theory

The configuration of the micro resonator in this project is a cantilever. Therefore, this section reviews the classical analysis of a flexural cantilever which derives the mode shapes and the modal frequencies of the beam. Damping is ignored in this analysis. Fig. 15 is a schematic of a flexural beam on which a distributed load $f(x, t)$ is applied.
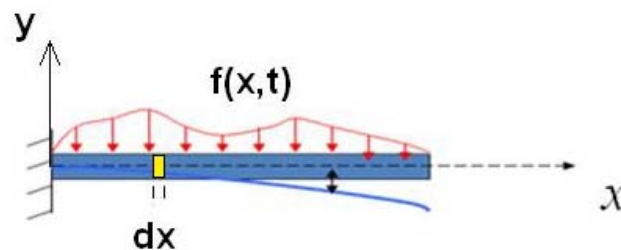
Figure 15. Flexural beam under distributed load.

Newton second law in vertical direction for a small element dx of the beam yields the governing differential equation of the motion of the beam in vertical direction

$$\rho A \frac{\partial^2 y}{\partial t^2} + \frac{\partial^2}{\partial x^2}(EI \frac{\partial^2 y}{\partial x^2}) = f(x,t). \tag{1}$$

where ρ is the mass density of the beam, A is the cross sectional area, E is the Young's modulus of the material of the beam, and I is the area moment of inertia along z axis (going out of the page in Fig. 15). To solve Eq. 1, we assume that the displacement function of the beam $y(x, t)$ is separable in space and time, which is

$$y(x,t) = Y(x)e^{i\omega t}. \tag{2}$$

$Y(x)$ is the amplitude of the vibration at different location on the beam, ω is the angular frequency at which the beam is vibrating. Substituting Eq. 2 into Eq. 1 and assuming that there is no applied force, we obtain

$$\frac{d^4}{dx^4}Y(x) - \beta^4 Y(x) = 0 \tag{3}$$

with

$$\beta^4 = \omega^2 \frac{\rho A}{EI}. \tag{4}$$

The solution of Eq. 3 has the form

$$Y(x) = C_1 \sin \beta x + C_2 \cos \beta x + C_3 \sinh \beta x + C_4 \cosh \beta x, \tag{5}$$

where $Y(x)$ is the mode shape of the vibrating beam. The constants C_1, C_2, C_3, and C_4 are solved by using the boundary conditions of the beam. For a fixed-free cantilever beam there are four boundary conditions applied: at the fixed end, the displacement and slope of the beam are zero, and at the free end, the moment and shear force are zero

At $x=0$
$$y(x,t) = 0 \text{ and } \frac{\partial y(x,t)}{\partial x} = 0 \tag{6 a}$$

At $x=L$
$$\frac{\partial^2 y(x,t)}{\partial x^2} = 0 \text{ and } \frac{\partial^3 y(x,t)}{\partial x^3} = 0 \tag{6 b}$$

Using the boundary conditions given by Eqs 6a and 6b we can solve for the modal shape

28

function of a cantilever beam and the natural frequency for each mode. Theoretically for a continuous system like the cantilever beam there is an infinite number of modes and thus infinite number of natural frequencies, with the first, or fundamental, mode at the lowest frequency. However, because higher modes require much higher energy to excite and are harder to detect, we are interested only in the first several modes. Their natural frequencies are as follows (Rao, 2004)

$$f_i = \frac{\beta_i^2}{2\pi L^2} \sqrt{\frac{EI}{\rho A}} \quad (i = 1, 2, \cdots)$$ (7)

,

Table 1. Constants for resonant frequencies at the first 6 modes (Rao, 2004).

β_1	β_2	β_3	β_4	β_5	β_6
1.875	4.694	7.855	10.996	14.137	17.279

where β_i are constants that are numerically solved, L is the length of the beam, ρ is the mass density of the beam, A is the cross sectional area, E is the Young modulus of the material of the beam, and I is the area moment of inertia along z axis.

At a given excitation frequency, vibration of the beam is a superposition of all the modes. When the excitation frequency is close to the natural frequency of a particular mode, resonance will occur and the displacement of that particular mode will be dominant. Thus, once the natural frequency for each mode is known, we can excite the beam at those frequencies to observe the beam's displacement at each mode.

I.3. Q-factor

In resonance, one expression for Quality factor (Q-factor) is the ratio of the resonant frequency to the frequency bandwidth of half-maximum amplitude. It can be understood by first

introducing the expression for the steady-state response amplitude for a forced oscillation (Gorman, 2002)

$$x_0(\omega) = \frac{F_0}{m[(\omega_0{}^2 - \omega^2)^2 + 4(\omega\delta)^2]^{1/2}} \,, \tag{8}$$

where Fo is the amplitude of the applied force, m is the mass, ω_0 is the natural angular frequency, ω is the angular frequency of the applied force, and $\delta = \zeta\omega_0$, where ζ is the damping ratio. The plot of the response amplitude is shown in Fig. 16.
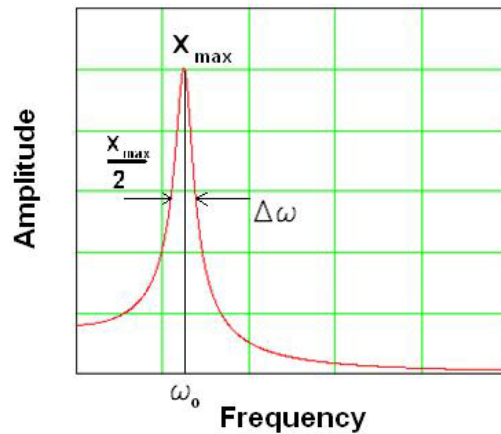
Figure 16. Amplitude response vs. applied frequency.

It can be shown from Eq. 8 that the length of the half-maximum amplitude bandwidth is 2δ (Gorman, 2002). The Quality factor can be described as a ratio of the resonant frequency to the half-maximum amplitude bandwidth (Gorman, 2002)

$$Q = \frac{\omega_0}{\Delta\omega} = \frac{\omega_0}{2\delta} = \frac{1}{2\zeta} \,. \tag{9}$$

The expression in Eq. 9 shows that the higher the Q-factor, the higher is the peak amplitude, and the narrower is the bandwidth, which means the more sensitive is the vibrating body to that resonant frequency. Also from Eq. 9, because the overall damping ratio is just the sum of the damping ratio of each type of damping, we have

30

$$\frac{1}{Q} = \frac{1}{Q_{TED}} + \frac{1}{Q_{Anchor}} + \frac{1}{Q_{Air}} + \frac{1}{Q_{Surface}} + \frac{1}{Q_{other}} \ . \tag{10}$$

Equation 10 shows that the overall Q-factor will be smaller than each Q-factor caused by each damping mechanism. Thus, the damping mechanism that has the smallest Q will have the most significant impact on the overall Q.

Q-factor can also be calculated in different ways, leading to alternate expressions for the Q-factor. Another definition of the Q-factor is the ratio of the total amount of stored energy to lost energy, which is the work done to maintain oscillation, in one radian (Gorman, 2002). The energy lost in one radian can be found by the integral over one cycle of oscillation and then divide that amount by 2π.

$$\Delta W_{lost} = \frac{1}{2\pi} \oint \sigma d\varepsilon \ , \tag{11}$$

where σ and ε are stress and strain. The energy stored can be found by the integral from zero to maximum strain

$$\Delta W_{stored} = \int_0^{\pi/2} \sigma d\varepsilon \ . \tag{12}$$

Thus the Q-factor is

$$Q = \frac{\Delta W_{stored}}{\Delta W_{lost}} = \frac{\int_0^{\pi/2} \sigma d\varepsilon}{\frac{1}{2\pi} \oint \sigma d\varepsilon} \ . \tag{13}$$

Another expression for the Q-factor is in terms of the complex natural frequency of the oscillation (Gorman, 2002). The general equation of motion for a vibrating body, assuming zero applied force

$$m\ddot{x} + b\dot{x} + kx = 0 \ , \tag{14}$$

where m, b, k are equivalent mass, equivalent damping constant, and equivalent spring constant.

For oscillation with $x = Xe^{\gamma t}$, where γ is the complex natural frequency, Eq.14 gives

$$m\gamma^2 + b\gamma + k = 0. \tag{15}$$

Solve for the complex frequency

$$\gamma = \frac{b}{2m} \pm i\sqrt{\frac{k}{m}}. \tag{16}$$

Hence, now the Q-factor can be written in terms of the complex frequency as

$$Q = \frac{1}{2}\frac{|Im(\gamma)|}{|Re(\gamma)|} = \frac{1}{2}\frac{2m\omega_0}{b} = \frac{1}{2\zeta}. \tag{17}$$

The expressions of Q in Eqs 9, 13, and 17 are all equivalent. The individual contributions to Q-factor are discussed below.

I.3.1. Thermoelastic damping

Unfortunately, damping is an unavoidable mechanism. Zener was the first one who proved the existence of internal friction in solids and calculated the damping (Zener, 1937 and 1938).   There are many sources of damping, for example, electronics damping, air damping, anchor damping, residual gas damping, etc. Among all these damping, thermal elastic damping (TED) has been identified as the most important loss in micro-resonators (Duwel et al. 2002). TED occurs in any thermal-elastic solid that is subjected to cyclic stress, which causes strain field as long as the thermal expansion coefficient is non-zero, and consequently the temperature field based on the law of thermodynamics. As a temperature gradient exists, heat conduction occurs. This is an irreversible flow of heat because of the coupling of the stress-strain relationship to heat flow in material. This gives rise to the increase in entropy and consequently to the dissipation of vibration energy (Hao et al. 2009). It has been shown that when the period of

cyclic stress decreases, the rate of mechanical energy loss increases and thus TED increases (Pryputniewicz, 2006).

Thermal elastic damping was first discussed and calculated by Zener based on the extension of Hooke's law. The thermalelastic damping for a flexural mode beam resonator is

$$Q_{TED}^{-1} = \frac{E\alpha^2 T_0}{C_v} \frac{\omega\tau}{1+(\omega\tau)^2},$$ (18)

with

$$\tau = \frac{C_v t^2}{k\pi^2},$$ (19)

where E is Young's modulus, α is the linear coefficient of thermal expansion, T_0 is the original temperature, ω is the resonance frequency, C_v is the specific heat per meter cubic volume, t is the thickness of the beam element and k is the thermal conductivity.

From the Eq.18, we can see that there is a damping peak at $\omega = \frac{1}{\tau}$; when $\omega \gg \frac{1}{\tau}$ or $\omega \ll \frac{1}{\tau}$, the damping is the minimum.

Later a more accurate equation for TED of a thin beam was derived by Lifshitz and Roukes (Lifshitz and Roukes, 2000) based on the Euler-Bernoulli beam theory. Lifshitz's equation is more sophisticated in that it takes into account the fact that the resonance frequency has a small dependence on the Q factor (Chandorkar et al. 2009). The equation for TED is

$$Q^{-1} = \frac{E\alpha^2 T_0}{C_v} \left[\frac{6}{\xi^2} - \frac{6}{\xi^3} \frac{\sinh(\xi)+\sin(\xi)}{\cosh(\xi)+\cos(\xi)}\right],$$ (20)

with

$$\xi = h\sqrt{\frac{\omega C_v}{2k}}, \tag{21}$$

where E, α, T_0, ω, C_v, h and k are the same parameters as described previously.

In comparison with Lifshitz's equation, Zener's equation overestimates TED by 2% at low frequencies for $\xi < \pi/\sqrt{2}$ and underestimates by a maximum of 20% as $\xi \to \infty$ (Prabhakar and Vengallatore, 2008). Both Zener's and Lifshitz's relations, Eqs 18 and 20 respectively, are only applicable for beams with rectangular cross-sections, with length to thickness ratio greater than 40, and where only one thermal mode is coupled to the mechanical mode. The maximum error in Zener's and Lifshitz's relations can exceed 80% for doubly clamped beams with length to thickness ratio less than 10 (Prabhakar and Vengallatore, 2008). For beams with more complex geometries, for example, with openings or slots, multi-thermal modes are coupled to the mechanical mode (Candler et al. 2006). Prabhakar derived a formula to predict TED for short beams with aspect ratio less than 10. Prabhakar also derived the equation for TED in hollow and slotted microresonators by dividing the beam into a number of convenient sub-regions, summing up the work lost in each sub-region as the total work lost. By definition, the magnitude of TED is (Prabhakar and Vengallatore, 2009).

$$Q_{TED}^{-1} = \frac{1}{2\pi}\frac{\sum_{j=1}^{n}\Delta W_j}{\sum_{j=1}^{n}W_j}, \tag{22}$$

where n is the number of sub-regions; ΔW_j is the work lost per cycle due to TED in sub-region j, W_j is the peak strain energy stored within region j during a cycle of vibration.

I.3.2. Anchor Damping

When a cantilever beam vibrates, elastic waves can dissipate into the mounting medium through attachment points. This is known as anchor damping and can have a significant effect

based on the dimensions of the beam. Assuming a fixed-free prismatic cantilever beam, the damping ratio due to energy dissipation through fixed attachment point can be calculated by (Hosaka et al, 1994)

$$\xi_{anchor} = 0.23 \times \frac{t^3}{L^3},$$ (23)

where, t is the thickness and L is the length of the cantilever, respectively. From this relationship the Q-factor related to anchor damping can be calculated as

$$Q_{anchor} = 2.17 \times \frac{t^3}{L^3}.$$ (24)

I.3.3. Air damping

An additional source of damping is produced fro the interaction of the micro cantilever and the surrounding medium. This form of damping is termed air damping or gas damping and can be quite large depending on the pressure of the medium. Air damping can be broken down into three regions, depending on the pressure of the medium (Yang et al, 2004):

1) Viscous damping region, where the air or gas medium acts as a viscous fluid.

2) Molecular region, where the interaction of individual molecules with the surface of the beam is responsible for damping.

3) Intrinsic region, where air damping is negligible.

The values for which these regions begin and end depend on several factors such as beam dimensions and type of fluid. The authors found that for sub-micron sized beams the viscous region began to dominate at a pressure level of 6 mbar and the molecular region began at 10^{-2} mbar, for pressure levels below 10^{-2} mbar, damping was negligible (Yang et al, 2004).

I.3.4. Surface damping

As the dimensions of the cantilever approaches the nanoscale, surface damping becomes dominate. Surface damping is a surface effect and thus becomes quite large as the ratio of surface area to volume increases. Surface damping is caused by absorbates or flaws on the surface of the cantilever. The surface layer will not store vibrational energy, however it does dissipate the energy leading to damping (Yasumara et al, 2000). The Q-factor related to surface damping is given by (Yang et al, 2004)

$$Q_{surface} = \frac{wt}{2\delta(3w+t)} \frac{E}{E_{ds}}, \tag{25}$$

where w is the width of the cantilever, t is the thickness of the cantilever, E is the elastic modulus of the cantilever, δ is the thickness of the absorbate layer or coating, and E_{ds} is the dissipation value of the Young's modulus of the surface layer.

The authors found that in sub-micron cantilever beams surface damping dominated and the Q-factor was largely a function of surface damping, particularly as the ratio of the surface area to volume increased (Yang et al, 2004).

I.3.5. Material Properties and Q-factor

Micro-cantilevers are typically made of silicon, silicon nitride, or silicon oxide (Vashist, 2007). From both Zener's and Lifshitz's relations, Eqs.18 and 20 respectively, we can see that material mechanical properties have direct effects in the Q-factor. Previous work has been done in varying the concentration of boron in boron-doped SiGe epitaxial materials in calculating the Q-factor of MEMS gyros. The presence of Ge in Si would bring great advantages in device machining and material processing. However, Ge would reduce the thermal conductivity due to phonon scattering (Duwel et al. 2002). The result shows that boron-diffused silicon, where the

boron concentration is approximately 10^{21} molecules per cubic centimeter has the highest Q

factor, followed by the SiB epi. A detailed comparison of materials mechanical properties and Q-

factor can be found in Table 2.

Table 2. Material and device parameters used in TED calculations.

The notation "Int" refers to a linear interpolation between the silicon and germanium values, based on the alloy composition (Duwel et al. 2002).

Quantity	Symbol	Units	SiB epi	SiGeB 2%	SiGeB 23%	SiGeB 30%	B-diff	Si Value	Ge Value
Thermal Coefficient of Expansion	α	1/°C	2.57E-06	2.65E-06	3.33E-06	3.55E-06	2.59E-06	2.59E-06	5.80E-06
reference			Si value	Int	Int	Int	[21]	[17],[18]	[18]
Modulus	E	N/m²	1.69E+11	1.68E+11	1.54E+11	1.49E+11	1.69E+11	1.69E+11	1.03E+11
reference			Si value	Int	Int	Int	Si value	[18]	[18]
Density	ρ	kg/m³	2.33E+03	2.39E+03	3.02E+03	3.24E+03	2.33E+03	2.33E+03	5.35E+03
reference			Si value	Int	Int	Int	Si value	[17]	[18]
Specific Heat	$C_{sp}=C_v/\rho$	J/(K*kg)	7.00E+02	7.05E+02	6.23E+02	5.95E+02	7.00E+02	7.13E+02	3.20E+02
reference			Si value	Int	Int	Int	Si value	[20]	
Thermal Conductivity	K	J/(K*s*m)	80	10.67	5.71	5.52	80.00	1.56E+02	58.61
reference			[22,16]	[22,16]	[22,16]	[22,16]	[22,16]	[18],[20]	[18]
Time Constant	τ	s	9.00E-08	7.62E-07	1.40E-06	1.54E-06	7.44E-08		
Beam Width	b	m	6.60E-06	6.90E-06	6.48E-06	6.60E-06	6.00E-06		
Resonant Frequency	$f=\omega/2\pi$	Hz	12,851	13,327	10,357	10,785	12,361		
Thermoelastic Q value	Q_{TED}		6.70E+05	7.48E+04	4.07E+04	3.30E+04	8.29E+05		

To obtain the desired material properties on Q-factor, both Zener's and Lifshitz's

relations, Eqs.18 and 20 respectively, show that different material properties have different effect

in the Q-factor. It is important to know which properties affect Q-factor the most, and thus focus

on optimizing those specific properties. A plot showing how the Q-factor changes as each

material property changes is prepared in MathCad as shown in Fig. 17. From the plot, we can tell

that the coefficient of thermal expansion α and Young's modulus E have negative effects in the

Q-factor, while the density ρ and thermal conductivity k have positive effects in the Q-factor.

The effect of specific heat c_p is not noticeable. Among all these investigated material properties,

coefficient of thermal expansion α has the greatest effect, followed by the thermal conductivity k

and Young's modulus E. So materials with low coefficient of thermal expansion and Young's modulus but high thermal conductivity are desirable.

The decision for material selection must be made carefully while taking into consideration compatibility with silicon technology, desirable electromechanical properties, and low values of residual stresses (Srikar, 2003). We are going to follow Ashby's approach in material selection for the micro-cantilever beam (Ashby, 1999). The first step of this approach is to acquire ranges of values for many classes of materials. From Fig. 17, we know that we need the class of materials with very low to zero coefficient of thermal expansion. So ceramics is the best class of materials. Once the class of the material is chosen, we will narrow the choices down to a few materials and will need to know the values of their material properties in greater precision. At this point, material properties like Young's modulus, density, specific heat, Poisson's ratio and coefficient of thermal expansion can be obtained from bulk materials. Because the physical origins of these properties lie at the atomic scale, these properties thus can be expected to be the same as those of bulk materials. However, other properties like thermal conductivity and yield strength are affected by length scales and processing parameters. Therefore, experimental data are needed for these properties (Srikar, 2003). In the class of ceramics, we continue to look for specific materials with low coefficient of thermal expansion, low Young's modulus, and high thermal conductivity.
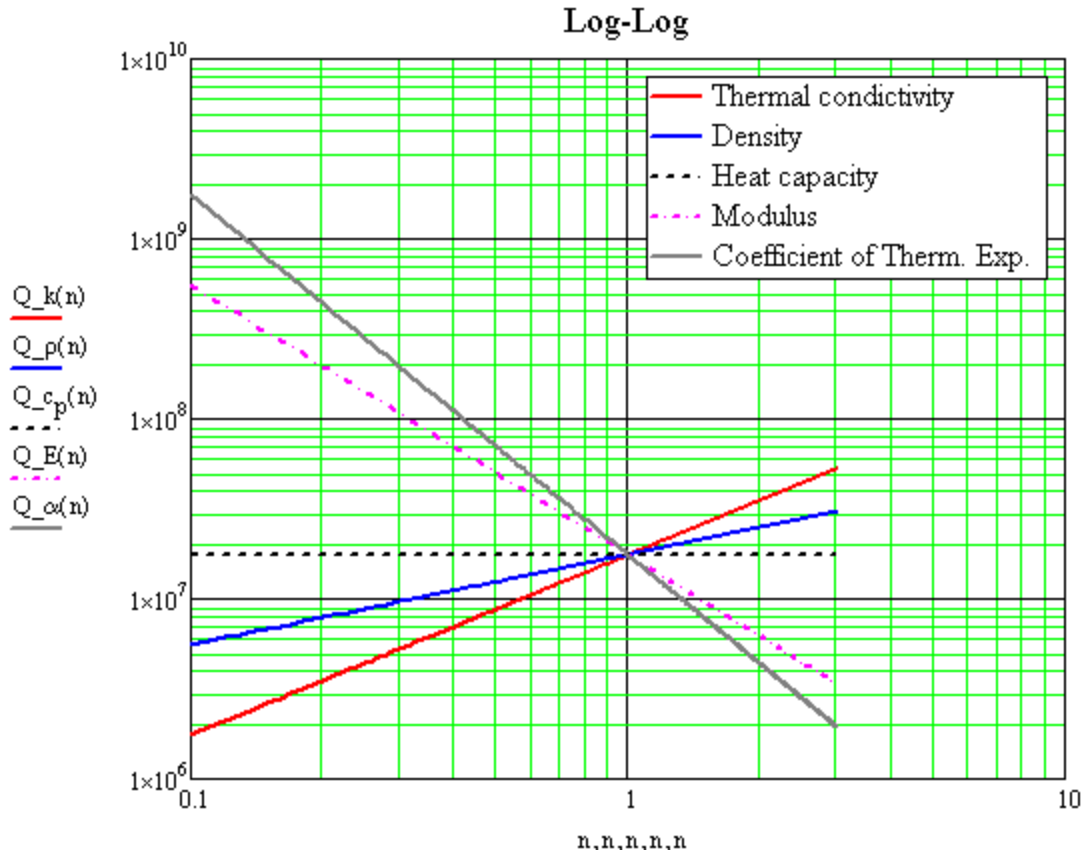
Figure 17. A log-log plot for Q-factor vs. material properties generated from MathCad.
"n" is the number used to multiply by the nominal value. Each material property ranges from
0.1*(nominal value) to 3*(nominal value).

I.3.6. Geometry and Q-factor

Research has been done to investigate novel geometry that is intended to disrupt the heat
flow in order to alter the Q-factor. It has been proposed to make slots through the width of the
beam to disrupt the heat flow along the thickness (Candler *et al*., 2006). They also investigated in
the impact of the slots location on the TED-related Q-factor. Prabhakar and Vengallatore (2009)
also presented an analytical framework to compute TED in general micro resonator containing
discontinuities in form of slots.

In Candler's work, they designed beams with slots of various sizes at different locations,
created simulations for their slotted beams and compared them with the experimental results and

Zener's theory. Their beams are clamped-clamped. Beams without slots were also studied to determine the locations of slots that have the greatest impact. Figure 18 is the simulation of the beam without slots with temperature profile which is in black and white gradient (Candler et al., 2006).
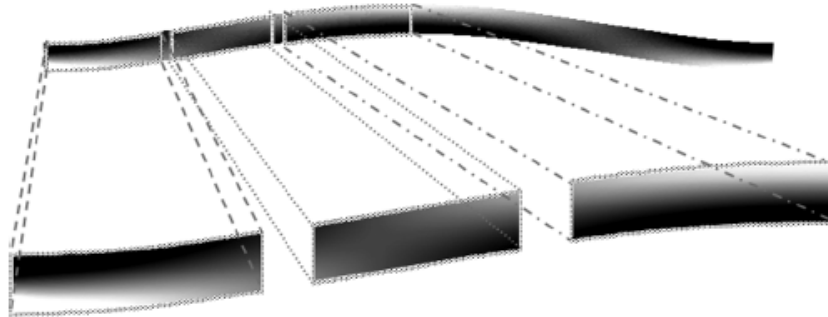
Figure 18. Temperature profile of a slotted beam; note the increased temperature gradient near the end and center of the beam (Candler et al., 2006).

It has been reasoned that due to higher strain gradient near the anchors and the middle of the beam, the temperature gradient at those locations are higher than that at different locations of the beam. The temperature gradient causes the heat flow, which is the energy loss mechanism of TED. Thus, the slots at those locations should have the greatest impact. This intuition is confirmed by their results. Figure 19 is an illustration of the actual slots that are made in their beams (Candler et al., 2006).
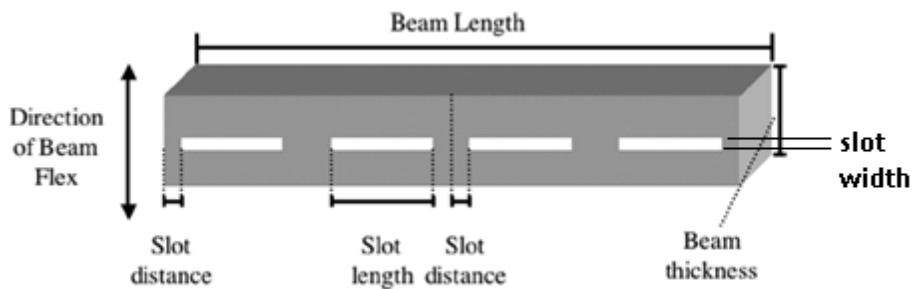
Figure 19. Schematic of the slotted beam (Candler et al., 2006).

Figures 20 and 21 are the results for slots which have length 1/10 and 1/6 of the beam length. The slot width is 1 micron while the beam thickness is 12 micron and the beam length is 400 micron (Candler et al., 2006).
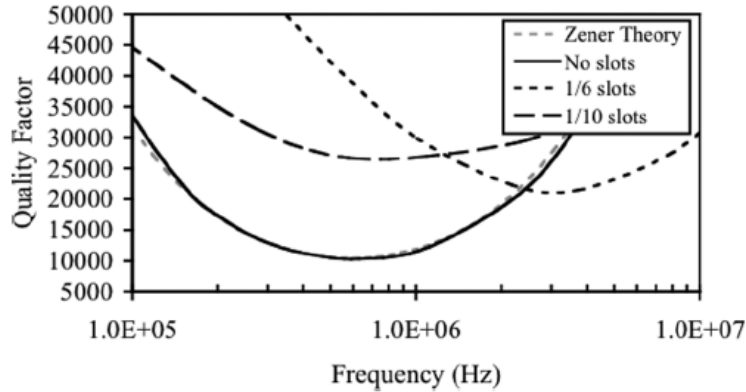
Figure 20. Results for no slots, slot length = 1/6 beam length, slot length = 1/10 beam length, and Zener's analytical solution (Candler et al., 2006).
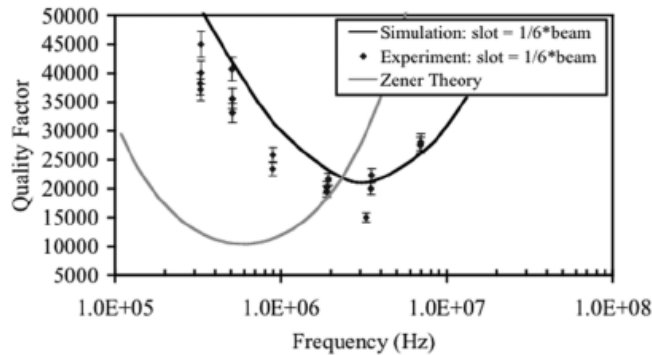
Figure 21. Experimental results of beams with 4 slots, the same thickness, and varying length compared to simulation and analytical results (Candler *et al*., 2006).

Candler *et al.(2006)* have come up with several meaningful conclusions:

- Most importantly, in slotted beam the mechanical mode can couple to more than one thermal mode. This is reasonable, because with the slotted beam, in addition to the temperature gradient in the direction of the thickness of the beam, temperature gradient in other directions can become significant. Thus, simplified Zener's Eq.18   as in Eq. 1 which includes only one thermal mode no longer satisfactorily predicts the Q-factor for

slotted beams, as shown in Fig. 20, as the experimental results do not match the Zener's results. However, simplified Zener's Eq.18   is still a fair approximation for clamped-clamped unslotted beam, as shown also in Fig. 20.

- There is a frequency shift of the minimum Q between the slotted beam and unslotted beam, which is shown in Fig. 20. This shift is caused by the shifting from coupling with the initial thermal mode to the coupling with higher frequency thermal mode of the slotted beam. Thus multiple thermal modes are affecting the Q-factor.

- The minimum Q-factor of the slotted beam is different from that of the unslotted ones. Candler *et al. (2006)* explained that because the slots weaken the coupling between the mechanical mode with the initial thermal mode, while the increased coupling with higher frequency mode is not enough to compensate for the reduction in coupling with the initial thermal mode. Therefore, minimum Q-factor is increased with the addition of slots, as shown in Fig. 20.

- Finally, the Q-factor for the slotted beam is worse than the slotted beam in some frequency regimes, which is also shown in Figs 20 and 21. While the minimum Q-factor in the slotted beam increases, it is not higher than that of the unslotted beam at all frequencies, especially at higher frequencies. The reason, as explained by Candler *et al.(2006)*, is that the slotted beam is partially coupled with higher frequency thermal modes.

II. Facilities

In order to carry out these objectives, a combination of analytical, computational, and experimental instruments were used in combination with a detailed uncertainty analysis as follows.

42

II.1. Michelson Interferometer

A schematic of the Michelson Interferometer that was used to measure the frequencies of the beam vibration is shown in Fig. 22.
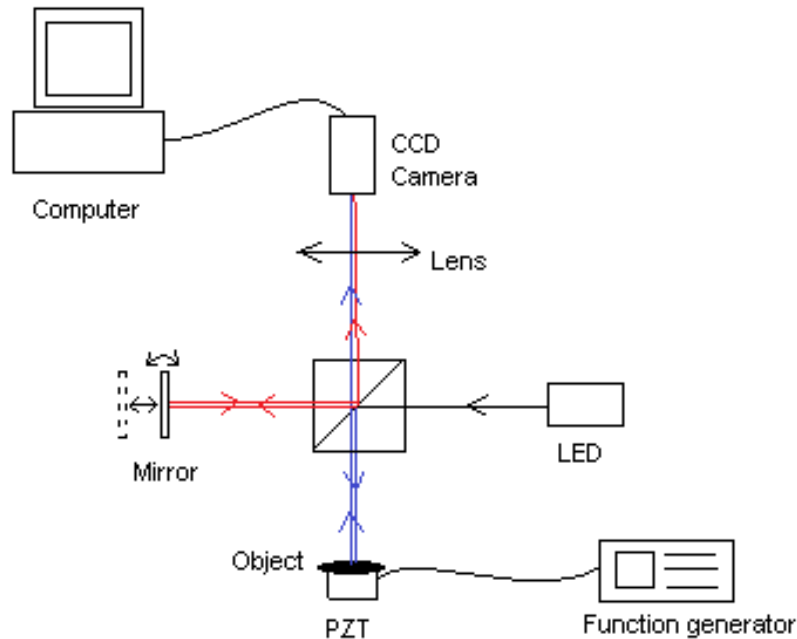
Figure 22. Schematic of a Michelson Interferometer.

In Fig. 22, light from the LED, whose intensity can be controlled by the amount of supplied current, is divided into two perpendicular beams by a beam splitter: the reference beam which goes to a mirror, and the object beam which illuminates the micro cantilever. The beam is shaken by a piezoelectric transducer (PZT). The voltage amplitude and vibration frequency applied to the PZT are controlled by a function generator. The reference beam, which is reflected by the mirror, and the object beam, which is reflected by the object, are then combined again at the beam splitter and interfere with each other. The interference is recorded as a time average holography by a CCD (Charge-Coupled Device) camera and sent to a computer.

To characterize the interference, we need to take into account that light is an electromagnetic wave. Based on literature, let $\mathbf{F_0}$(x, y, z) be the value of the light field that is reflected by the cantilever beam at rest (Pryputniewicz, 1985)

$$\boldsymbol{F_0}(x,y,z) = \boldsymbol{A_0}(x,y,z)\exp(i\phi_0(x,y,z)). \tag{26}$$

The displacement of the cantilever beam is a function of time, and for a cosinusoidal excitation, the displacement of the cantilever beam can be expressed as

$$\boldsymbol{L_t}(x,y,z,t) = \boldsymbol{L_0}(x,y,z)\cos(\omega t). \tag{27}$$

This displacement causes a temporal change in the phase of the light field reflected by the object. This shift in phase, Ω_t(x, y, z, t) can be calculated by the dot product between the sensitivity vector $\mathbf{K}$(x, y, z) and the displacement vector $\mathbf{L_t}$

$$\Omega_t(x, y, z, t) = \mathbf{K}(x, y, z)\mathbf{L_t}(x, y, z, t), \tag{28}$$

where

$$\boldsymbol{K}(x,y,z) = \boldsymbol{K_2}(x,y,z) - \boldsymbol{K_1}(x,y,z), \tag{29}$$

with $\mathbf{K_1}$(x, y, z) and $\mathbf{K_2}$(x, y, z) being the illumination and observation propagation vectors representation. They are unit vectors in space and in our Michelson interferometer are in the directions of the beams which come to and reflect from the micro cantilever surface. Thus the magnitude of this sensitivity vector is maximum in this case.

The new light field reflected from the cantilever beam, after the change in phase is applied, is

$$\boldsymbol{F_v}(x,y,z) = \boldsymbol{A_0}(x,y,z)\exp(i\phi_0(x,y,z) + i\Omega_t(x,y,z,t)). \tag{30}$$

44

Meanwhile, the value of the light field of the reference beam which is reflected from the mirror is

$$F_r(x, y, z) = A_r(x, y, z)\exp(i\phi_r(x, y, z)). \tag{31}$$

The mirror is adjusted and then kept fixed so that the lens is in focus on both the mirror and the cantilever beam before exciting the beam. Thus the reference beam is fixed and is a representation of the light field of the beam reflected from the cantilever beam at rest. Thus the resulting light field now has the following form, with the phase of the beam at rest is cancelled by the reference beam

$$F(x, y, z) = A_0(x, y, z)\exp(i\Omega_t(x, y, z, t)). \tag{32}$$

The camera does not record the instantaneous value of this interference field but rather the average value over the exposure time T, which is given by

$$F_{avg}(x, y, z) = \lim_{T\to\infty} \frac{A_0(x, y, z)}{T} \int_0^T \exp(i\Omega_t(x, y, z, t))dt. \tag{33}$$

Taking into account that the time-dependent part of the phase change $\Omega_t(x, y, z, t)$ is a sinusoidal function, the above integral is equivalent to

$$F_{avg}(x, y, z) = A_0(x, y, z)J_0[\Omega_t(x, y, z)]. \tag{34}$$

With J_0 being the zero order Bessel function of the first kind. Because the camera records the intensity of the light field, which is proportional to the square of the value of the light field, the observed intensity in the image is

$$I_m(x, y, z) = I_0(x, y, z)J_0{}^2[\Omega_t(x, y, z)]. \tag{35}$$

The plot of the zero order Bessel function of the first kind is shown in Fig. 23.
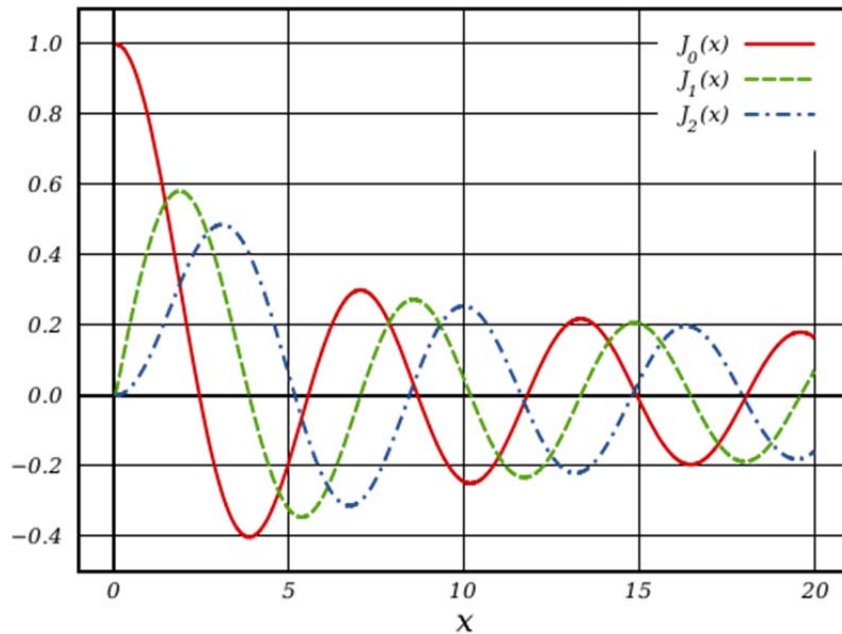
Figure 23. Zero, first, and second order Bessel functions of the first kind.

From Fig. 23, it is clear that the pattern to be observed in the camera image is a fringe pattern. Also, according to Eqs 28 and 35, the intensity is brightest at the locations where the displacement is zero. Thus the brightest area on the image represents the nodes of the vibrating cantilever beam. Therefore, the mode of vibration is identified by counting the number of brightest spots on the image of the cantilever beam. In addition, it is shown that an area of the cantilever beam reaches maximum displacement when the number of fringes over that area is maximum, because more peaks of the Bessel function will be included as the displacement increases. Thus, in order to find the correct resonant frequencies, we need to look for the frequency that gives the most fringes at a given vibration mode.

II.2. Laser Doppler Vibrometer

A Polytec OFV-502 Laser Doppler Vibrometer (LDV) was used to measure the velocity of resonators as a function of time. A LDV is used to measure vibration displacement or velocity

of a fixed point. It is based on the Doppler-effect, measuring the frequency shift of back-scattered light from the vibrating surface. The frequency shift due to the Doppler effect is given by

$$f_D = 2 \times \frac{v}{\lambda}, \tag{36}$$

where v is the velocity of the moving object and λ is the laser wavelength (Polytec, 2011). By measuring the Doppler shift, the velocity and displacement of the object can be calculated using the wavelength of the laser.

The optical arrangement of a heterodyne vibrometer is shown in Fig. 24 (Johansmann et al., 2005). The laser beam is divided into two beams by a Polarizing Beam Splitter (PBS), one being the measurement beam and the other a reference beam. A Quarter Wave Plate (QWP) rotates the polarization of the back-reflected light 90 degrees, then a second PBS guides it to the detector. The reference beam goes through an acousto-optic modulator, or Brag Cell (BC) inducing a frequency shift onto the reference beam. Finally the two beams are combined and two photo detectors (PD) to receive twice the signal power and remove the DC component. If the object is stationary, the PD will see only the BC reference frequency ω_c. When the object is in motion, the PD will detect an increase in frequency when the object moves away from the beam and a decrease in frequency when the object moves towards the beam. This method allows not only velocity but direction to be determined (Johansmann et al., 2005). Polytec vibrometers are capable of attaining a resolution of 2 nm (Polytec, 2011).
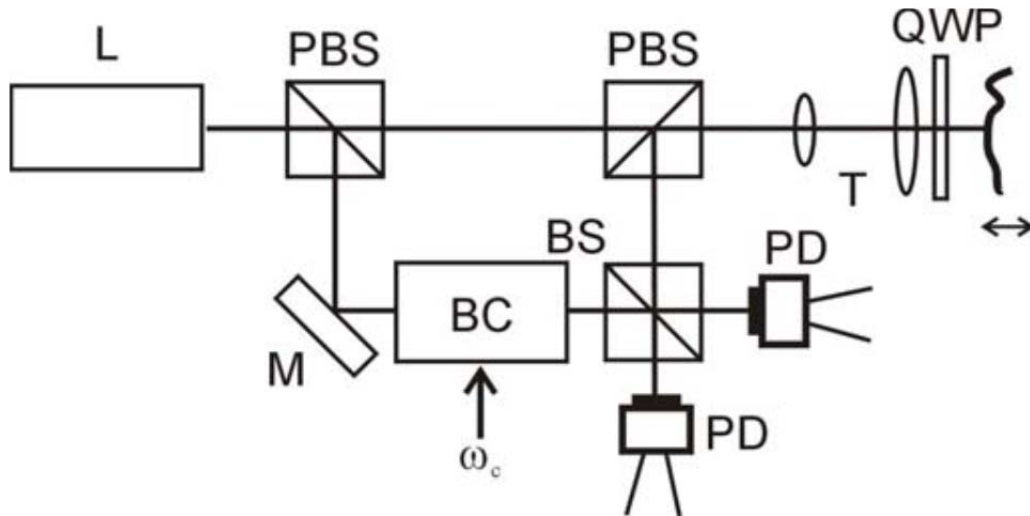
Figure 24. Schematic of a heterodyne vibrometer (Johansmann et al., 2005).

II.3. MathCad

Mathcad 15.0 was used for analytical solutions. MathCad is a software package which enables engineers to easily perform, document and share calculation and design results. MathCad allows variables and equations to be input and solved in an easy manner. This allows for the convenient changing of parameters without the hassle of resolving equations. Additionally results can be displayed graphically (PTC, 2011).

II.4. COMSOL

COMSOL 3.5a was used for designing beams with different geometries, calculating Q-factor, obtaining temperature and stress distributions etc. COMSOL is a Finite Element Analysis (FEA) software package for modeling various physics and engineering problems including coupled phenomena such as thermoelasticity (COMSOL Multiphysics, 2011).

III. Methodology

Since the Q-factor is comprised of several different contributors, each of these must be considered in analyzing the Q-factor of a resonant sensor. Q-factor is comprised of anchor

damping, air damping, TED, and surface damping. In general, anchor losses are small as compared to other loss mechanisms in the resonator. Air damping is relatively small since these micro-cantilever resonators are operated in vacuum. TED is a volumetric phenomenon and is most prominent when the dimensions of the cantilever are in microscale. As the size of the cantilever approaches the nanoscale, TED becomes less dominant. Surface damping is a surface effect and becomes dominant as the ratio of surface area to volume becomes large. As the cantilever approaches the nanoscale, surface damping begins to dominate.

For these reasons it is important to focus on the surface damping effect as the current trend is to build smaller and smaller sensors. Many sensors require a coating to function and these coatings can have a substantial negative impact of the surfaced damping of the resonators. In addition to the effect of surface damping on bare resonators, the effect of coating material and thickness is investigated.

In order to investigate the impact of surface damping on the Q-factor of uncoated and coated beams an Analytical, Computational, and Experimental Solutions methodology was carried out. Through a combination of analytical and computational analysis, combined with experimental results, the effect of surface damping on the Q-factor was investigated.

III.1. Sample Selection

In order to facilitate the experimental testing it was determined the best samples would be Atomic Force Microscopy (AFM) probes. These are cantilever beams manufactured in differing geometries. Tipless AFM probes were chosen to simplify the analytical and computational computations. It was determined through analytical analysis that depending on the geometry, differing damping mechanisms can dominate the Q-factor. Silicon was chosen for the material

due to its widespread use in the MEMS industry. By keeping the material properties constant, the effect of surface damping could better be investigated.

Individual damping values for uncoated, tipless Silicon AFM probes available from Applied Nanostructures were calculated using the manufacturer supplied nominal dimensional values. In addition material properties of Silicon were obtained from Granta's CES EduPack 2011 software, the dimensions and material properties of the available AFM probes are listed in Table 3 (Granta, 2011).

Table 3. Dimensions of potential samples.

ID	thickness [μ]	width [μ]	length [μ]
SHOCON	1	43	225
SICON	2.5	40	450
FORT	3	30	225
ACT	4.5	35	125
ACL	8.5	40	225
ACST	2.5	25	150

Table 4. Properties of single-crystal silicon.

Single-crystal Silicon		
Property	Units	Value
Young's modulus	Gpa	165
Density	kg/m^3	2330
Coefficient of thermal expansion	$10^{-6}K^{-1}$	2.6
poisson' ratio		0.27
Heat capacity	J/kg*K	690
Thermal conductivity	W/m*K	160

Equation 20 was used to calculate TED with the values from Table 4. It was found that as the surface area to volume ratio became small, TED began to dominate the damping. The Ted is plotted as a function of thickness for the probes available from Applied Nanostructures in Fig.26.

50

Note as the thickness increases, the Q-factor decreases, indicating an increase in damping as the thickness increases. This makes sense since TED is a volumetric phenomenon and thus increases as the ratio of surface area to volume decreases.
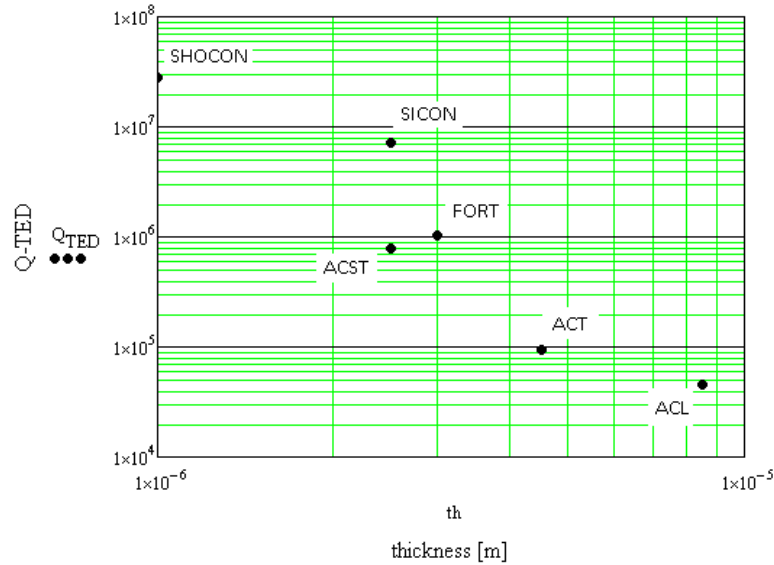
Figure 25. Q-factor due to TED plotted as a function of thickness.

Equation 24 was used to calculate anchor losses with the values from Table 3. It was found that, similar to TED, as the surface area to volume ratio became small, the anchor losses became quite large. The Q-factor associated with anchor damping is shown in Fig. 27, plotted as a function of thickness. Note as the thickness increases, the Q-factor decreases, indicated an increase in damping due to anchor losses as the thickness increases. This makes sense since for a larger cross-sectional area the anchor makes up a larger portion of the cantilever.
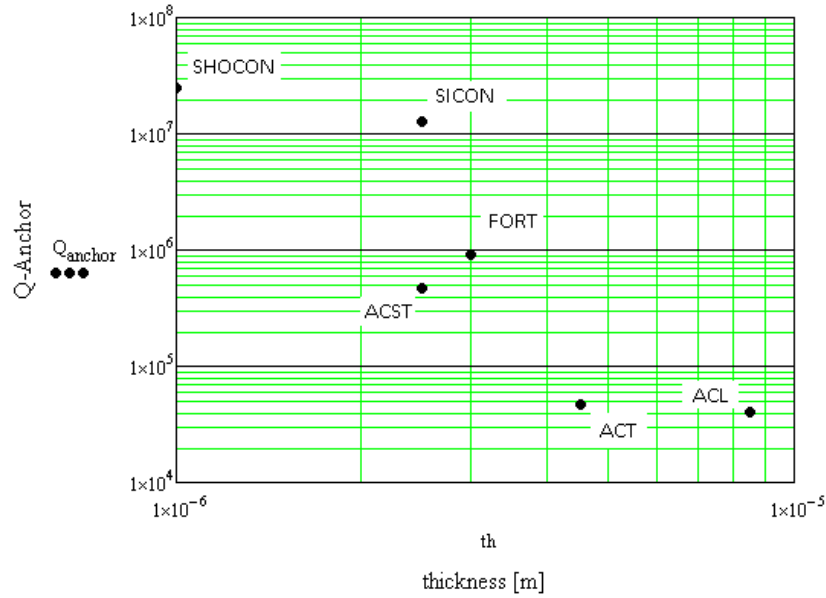
Figure 26. Q-factor due to anchor loss plotted as a function of thickness.

Equation 25 was used to calculate surface losses with the values from Table 3 along with the value of δE_{DS} reported by Hao et al. (2003). It was found that as the surface area to volume ratio became large, surface damping became dominant. The Q-factor associated with surface damping is shown in Fig. 28, plotted as a function of thickness. Note as the thickness decreases, the Q-factor decreases, indicated an increase in damping due to surface losses as the thickness decreases. This makes sense since surface damping is a surface phenomenon and thus increases as the ratio of surface area to volume increases.
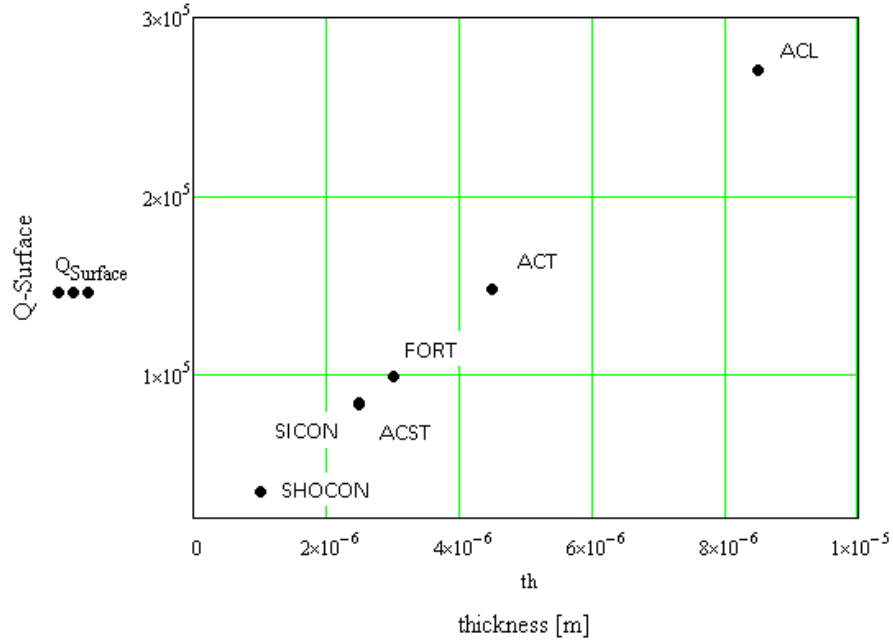
Figure 27. Q-factor due to surface damping plotted as a function of thickness.

Using Eq. 10 the expected Q-factor for each probe can be calculated. The Q-factor is plotted as a function of thickness in Fig. 29. Note the value of Q-factor for the thickest and thinnest beams is smallest, while the maximum value is at a thickness of around 3 microns. For this reason, the FORT and SICON probes were chosen for analysis. Additionally, the SHOCON probe was chosen because of the large amount of surface damping present in this probe. The ACL probe was also chosen due to the large TED and anchor damping predicted to be exhibited from this probe.
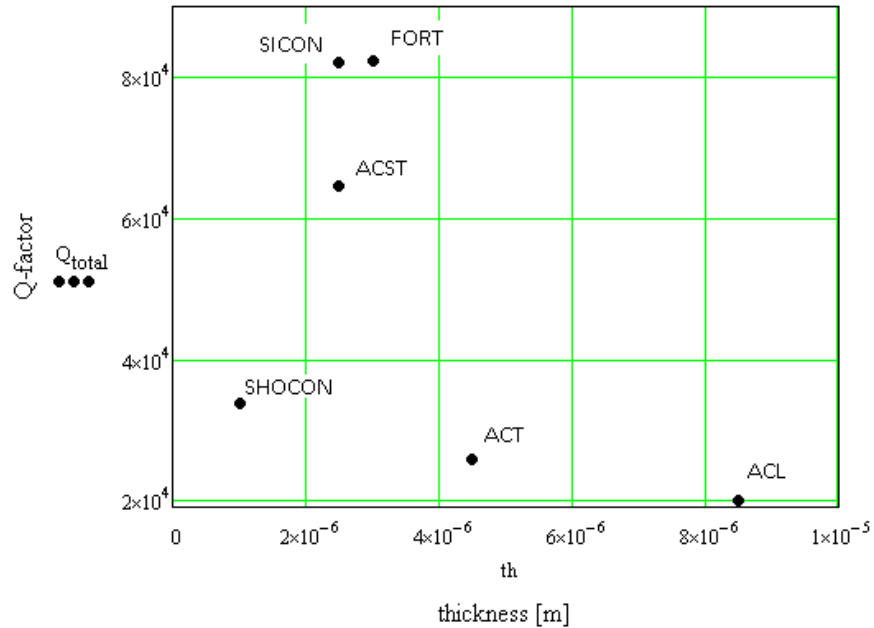
Figure 28. Q-factor plotted as a function of thickness.

In addition to the uncoated probes, coated probes were required for analysis. Aluminum is a common coating for AFM probes and is available in different thicknesses. Beams coated on both sides and only on one side were chosen for this study and are listed in Table 5. In addition to the Aluminum coated beams, it was decided to coat the uncoated beams with an AuPd mixture. It was decided to focus on the effect the increased mass had on the Q-factor of the beams. The properties of the AuPd mixture and Aluminum are listed in Table 6 and were obtained from Granta's CES EduPack 2011 (Granta, 2011). Note the modulus is similar, but the much greater density of the AuPd mixture.

Table 5. Dimensions of Al coated beams.

Aluminum coated Silicon probes				
thickness [µ]	width [µ]	length [µ]	coating thickness [nm]	# of sides coated
2	50	450	5	1
2	50	450	5	2
2	50	450	10	1
2	50	450	20	1
2	50	450	30	2

Table 6. Material properties of Al, Au, PD, and AuPd mixture.

Property	Units	Al	Au	Pd	AuPd mixture
Young's modulus	Gpa	71	78.5	121	87
Density	kg/m^3	2700	19300	12.05	15442
Coefficient of thermal expansion	$10^{-6}K^{-1}$	23.5	14	11.5	13.5
poisson' ratio		0.34	0.42	0.39	0.41
Heat capacity	J/kg*K	935	130	245	153
Thermal conductivity	W/m*K	244	312	73.5	264.3

III.2. Analytical solution

The analytical solutions for TED were carried out using the both the relation proposed by Zener and the relation proposed by Lifshitz, Eqs 18 and 20, respectively. The dimensional values will be measured and the material properties of Silicon listed in Table 4 will be used. Due to the small size of the beam it is not feasible to measure the thickness of every beam. However, the thickness can be calculated with the relation

$$t = \sqrt{\frac{\rho\left(\frac{2f_n \pi L^2}{\beta_n^2}\right)^2}{\frac{E}{12}}} , \qquad (37)$$

where ρ is the density, f_n is nth the resonant frequency, L is the length of the beam, E is the elastic modulus, and β_n is the nth modal proportionality constant for a fixed-free cantilever beam (note this corresponds to the resonant frequency used).

In order to insure all resonators were tested at a frequency far away from their characteristic damping frequency, the characteristic damping frequency was calculated for each beam. The characteristic damping frequency is defined as follows

$$F_0 = \frac{\pi k}{2\rho C_p t^2} \,, \tag{38}$$

where k is the thermal conductivity, ρ is the density, C_p is the heat capacity, and t is the thickness of the cantilever (Pryputniewicz, 2007). TED as a function of relative frequency, actuation frequency divided by characteristic damping frequency, is shown below in Fig. 30. TED is maximum at the characteristic damping frequency and all tests should be performed far away from this frequency in order to avoid biased results.
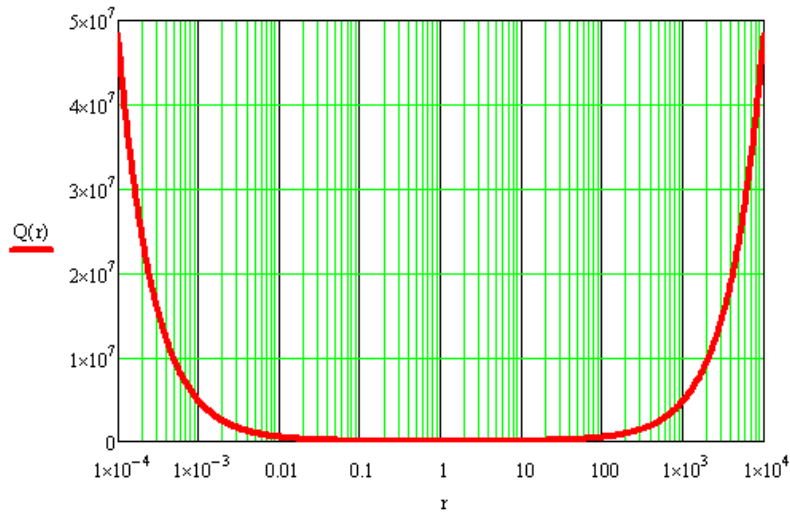
Figure 29. Q-factor as a function of relative frequency (Pryputniewicz, 2006).

The results of the calculations for characteristic damping frequency along with relative frequency for the chosen samples assuming actuation in the first bending mode are listed in Table 7. Note all values except the ACL sample lie within the 0.0001 to 0.01 range. This suggests that TED for the ACL sample will be quite large.

Table 7. Characteristic damping frequencies and relative frequencies of selected samples.

Sample	F_0 [MHz]	F [Hz]	F/F_0
Coated	34.49	13621	0.0004
SICON	59.91	10813	0.0002
SHOCON	153.5	24910	0.0002
FORT	22.92	75268	0.0033
ACL	3.49	169210	0.0485

Anchor Damping will be calculated using Eq. 24 along with the measured dimensions of the beam. All tests will be conducted in a vacuum level of at least 10^{-4} mbar, so air damping can be ignored. Surface damping can be calculated with Eq. 25, assuming δ and E_{ds} are known. In our case, for the uncoated beams neither δ nor E_{ds} are known. For these beams we can use the experimentally obtained value of Q-factor along with the calculated value of TED and anchor damping to calculate $Q_{surface}$ and δE_{ds} utilizing Eqs.10 and 25, respectively. In the case of the coated beams, δ is known, so E_{ds} can be calculated.

III.3. Computational solution

The analytical equations to calculate the TED-related Q-factor proposed by Zener and Lifshitz are derived using a simple rectangular beam model. Although the beam samples used in this project can be approximated as a simple rectangular beam, it is still preferable to develop a finite element model to analyze the real geometry of the beam as well as to facilitate future analysis with various geometries.

In finite element model, the Q-factor can be calculated by using the expression of Q as a ratio of the real part and the imaginary part of the complex frequency

$$Q = \frac{1}{2} \frac{|Re(\omega)|}{|Im(\omega)|}.$$

(39)

The complex frequency can be found by solving for the eigenvalues of the multiple degrees of freedom system (the finite element cantilever beam). In terms of the eigenvalue $\gamma = i\omega$ the Q-factor in Eq. 39 can be rewritten as

$$Q = \frac{1}{2} \frac{|Im(\gamma)|}{|Re(\gamma)|}.$$

(40)

According to Gorman (2002), to establish the eigenvalue problem, the coupled thermoelastic and heat transfer differential equations need to be obtained. Gorman has derived the coupled equations from stress-strain equation for isotropic materials and Fourier's law for heat conduction.

III.3.1. The coupled thermoelastic and heat transfer equations

The constitutive stress-strain relationship for an isotropic thermoelastic solid is (Gorman, 2002)

$$\sigma_{ij} = C_{ijkl}\varepsilon_{kl} - \frac{\alpha \Delta T}{(1-2\nu)} \delta_{ij},$$

(41)

where σ_{ij} is the stress tensor, C_{ijkl} is the 6x6 stiffness matrix, ε_{kl} is the strain tensor, α is the thermal expansion coefficient, ΔT is the temperature variation from the initial temperature, ν is the Poisson ratio, and δ_{ij} is the Kronecker delta. By definition, $\delta_{ij} = 1$ when i=j, and $\delta_{ij} = 0$ when i≠j. The repeated suffix notations k and l denote the summation over all values of k and l. Eq. 41 is for a infinitesimally small stress cube, and can be expanded into simplified matrix form

$$
\begin{bmatrix} \sigma_1 \\ \sigma_2 \\ \sigma_3 \\ \sigma_4 \\ \sigma_5 \\ \sigma_6 \end{bmatrix} = \begin{bmatrix} \lambda+2\mu & \lambda & \lambda & 0 & 0 & 0 \\ \lambda & \lambda+2\mu & \lambda & 0 & 0 & 0 \\ \lambda & \lambda & \lambda+2\mu & 0 & 0 & 0 \\ 0 & 0 & 0 & \mu & 0 & 0 \\ 0 & 0 & 0 & 0 & \mu & 0 \\ 0 & 0 & 0 & 0 & 0 & \mu \end{bmatrix} \begin{bmatrix} \varepsilon_1 \\ \varepsilon_2 \\ \varepsilon_3 \\ \varepsilon_4 \\ \varepsilon_5 \\ \varepsilon_6 \end{bmatrix} - (3\lambda+2\mu)\Delta T \begin{bmatrix} \alpha \\ \alpha \\ \alpha \\ 0 \\ 0 \\ 0 \end{bmatrix} \tag{42}
$$

where the first three entries of the stress and strain vectors are normal components, and the last three are shear components, and λ and μ are Lamé coefficients

$$
\lambda = \frac{E}{1+v}\left(\frac{v}{1-2v}\right) \text{ and } \mu = \frac{E}{2(1+v)}. \tag{43}
$$

By substituting the force balance equation and the strain-displacement relationship into Eq. 42, we obtain the first of the two coupled equations (Gorman, 2002)

$$
\rho\frac{\partial^2 \vec{u}}{\partial t^2} - \mu\nabla^2\vec{u} - (\lambda+\mu)\vec{\nabla}(\vec{\nabla}\cdot\vec{u}) + \frac{\alpha E}{(1-2v)}\vec{\nabla}T = 0 , \tag{44}
$$

where $\vec{u}$ is the displacement vector of a small stress cube in the cantilever beam

$$
\vec{u} = (u_x, u_y, u_z) , \tag{45}
$$

$$
\vec{u} = \left(\frac{\partial^2 u_x}{\partial x^2} + \frac{\partial^2 u_x}{\partial y^2} + \frac{\partial^2 u_x}{\partial z^2}, \frac{\partial^2 u_y}{\partial x^2} + \frac{\partial^2 u_y}{\partial y^2} + \frac{\partial^2 u_y}{\partial z^2}, \frac{\partial^2 u_z}{\partial x^2} + \frac{\partial^2 u_z}{\partial y^2} + \frac{\partial^2 u_z}{\partial z^2}\right), \tag{46}
$$

$$
\vec{\nabla}(\vec{\nabla}\cdot\vec{u}) = \text{grad}(\text{div}\,\vec{u}) , \tag{47}
$$

$$
\vec{\nabla}T = \left(\frac{\partial T}{\partial x}, \frac{\partial T}{\partial y}, \frac{\partial T}{\partial z}\right). \tag{48}
$$

The second of the two coupled equations is derived from the heat conduction equation at a point (x, y, z) in the cantilever beam. Fourier's law gives

$$
T\frac{dS}{dt} = k\nabla^2 T . \tag{49}
$$

For an isotropic linear thermoelastic solid, the entropy per unit volume is given by (Comsol, 2011)

$$S = \rho C_p ln\frac{T}{T_0} + \alpha(\sigma_1 + \sigma_2 + \sigma_3) \,. \tag{50}$$

Substituting Eq. 49 into Eq. 48 and linearize the resulting equation, and then convert stress into displacement using strain-displacement relationship, we obtain the second coupled equation (Gorman, 2002)

$$k\nabla^2 T - \rho C_p \frac{\partial T}{\partial t} - \frac{\alpha E T_0}{(1-2v)}\vec{\nabla} \cdot \left(\frac{\partial \vec{u}}{\partial t}\right) = 0. \tag{51}$$

Thus we obtained two coupled equations, and they are rewritten as followed

$$\rho\frac{\partial^2 \vec{u}}{\partial t^2} - \mu\nabla^2\vec{u} - (\lambda + \mu)\vec{\nabla}(\vec{\nabla} \cdot \vec{u}) + \frac{\alpha E}{(1-2v)}\vec{\nabla}T = 0, \tag{52}$$

$$k\nabla^2 T - \rho C_p \frac{\partial T}{\partial t} - \frac{\alpha E T_0}{(1-2v)}\vec{\nabla} \cdot \left(\frac{\partial \vec{u}}{\partial t}\right) = 0. \tag{53}$$

Equation 51 is a vector equation and is equivalent to three scalar equations corresponding to three components of each vector. By assuming that the temperature function and the displacement function can be separable in terms of position and time, we can bring the eigenvalue γ into the coupled equations

$$\vec{u}(x, y, z, t) = \vec{u}(\text{x}, \text{y}, \text{z})e^{\gamma t} \text{ and } T(x, y, z, t) = T(x, y, z)e^{\gamma t}. \tag{54}$$

The eigenvalue can be solved for by using commercial finite element analysis software.

III.3.2. Using COMSOL Multiphysics to solve for the resonant frequencies and Q-factor

The problem of calculating the TED-related Q-factor is common, COMSOL has a built in function for calculating the Q-factor using the theory mentioned above. The beam model is created by using the Damped Eigenfrequency application mode coupled with the Heat Transfer

application mode in COMSOL. Figure 25 shows the boundary conditions used in our beam and the material properties in Table 4 were used in the model.
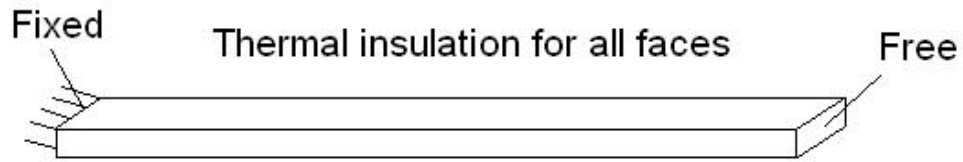
Figure 30. Boundary conditions of beam model.

.

III.4. Experimental solution

The experimental setup used to investigate the beams is shown below in Fig. 31 (Klempner et al., 2009). The sample is mounted to a 1 inch diameter Al disk with a cyanoacrylate adhesive. It is placed inside the vacuum chamber and is mounted to a steel disk attached to five piezoelectric actuators driven by a TTi TGA1442 40 MHz Arbitrary Waveform Generator. The setup can utilize interchangeable interferometer modules or the LDV.
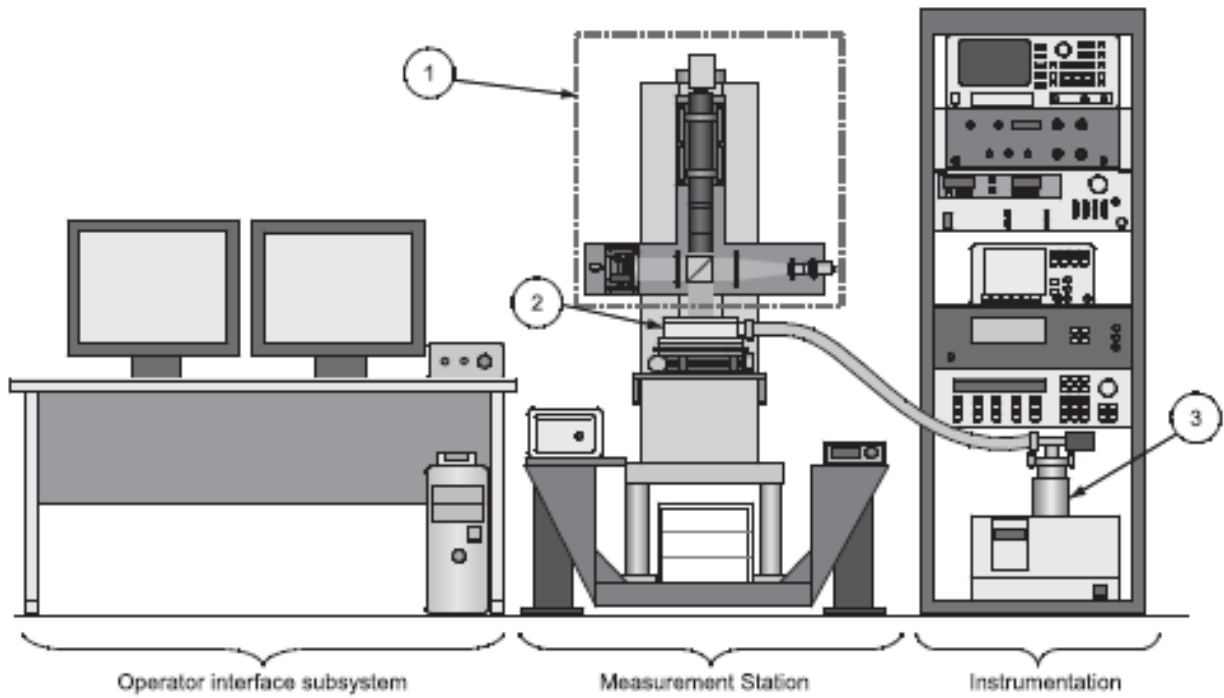
Figure 31. Schematic of measurement setup: (1) Interchangeable Interferometer modules, (2) Vacuum chamber, (3) Vacuum pump (Klempner et al., 2009).

The dimensions of the beams provided to us by the manufacturer are only nominal value, and the tolerances associated with them, especially the thickness, make our analytical results less accurate. Therefore, we decided to measure the dimensions of the beam ourselves instead of using the provided nominal values. Using a microscope and micro-positioner system, we are able to measure the dimensions of the beam as shown in Fig. 32.
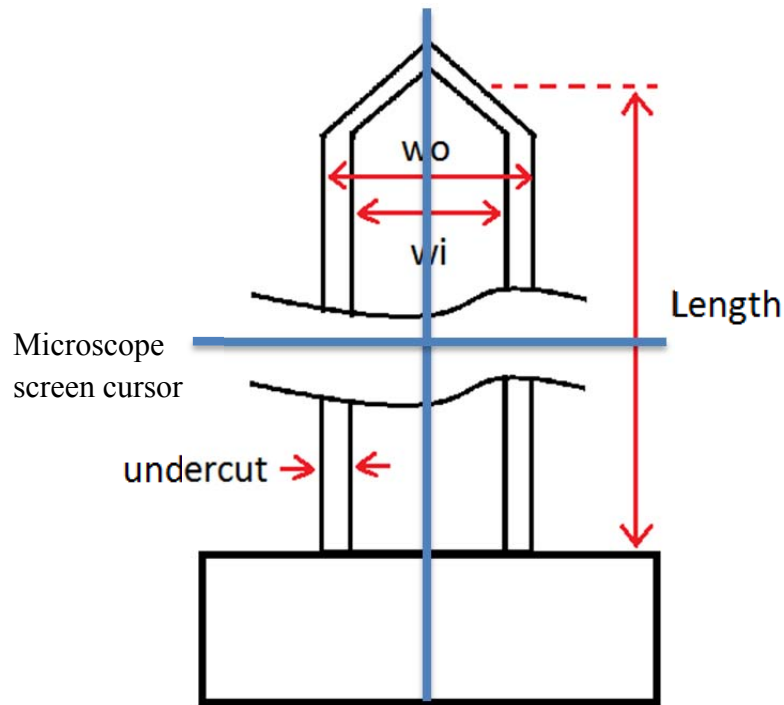
Figure 32. Schematic of cantilever beam.

We position the beam as parallel to the screen cursor as possible and displace the beam to measure its length and widths. The positioner is able to displace the beam with 0.5µm accuracy, so we assume a 1µm accuracy in our dimensions measurement (we need to catch 2 edges to get a dimensions), providing that the beam's dimensions are even. The undercut shows up as the inner width and outer width of the beam, so we use the average of the two for the width in our calculation. Figure 33 shows the setup used for obtaining dimensions. A cantilever beam can be seen on the monitor in the middle, on the right is the didital readout from the Nikon Measurescope MM-11which is on the left.

Figure 33. The measurement setup used for determining dimensions of the cantilevers.

III.4.1. Interferometry

We need to measure the resonant frequency as accurate as possible to improve the uncertainty in our thickness calculation as well as Q-factor calculation. We can achieve a high accuracy of the resonant frequency with the Michelson Interferometry system. As discussed in section II.1, the beam's amplitude of vibration is maximum when the number of fringes is maximum. However, as the excitation frequency approaches the resonant frequency, the amplitude of the beam can be so high that the beam can be broken, which did happen to us in some cases. Thus we need to continue to decrease the excitation voltage amplitude, while at the same time adjusting a smaller fraction of a kHz in the function generator to get the highest number of fringes again. Using this technique we can obtain resonance to an accuracy of one tenth of a Hertz (the limit of the function generator) with the excitation voltage as small as 5mV. This technique is illustrated in Fig. 34.
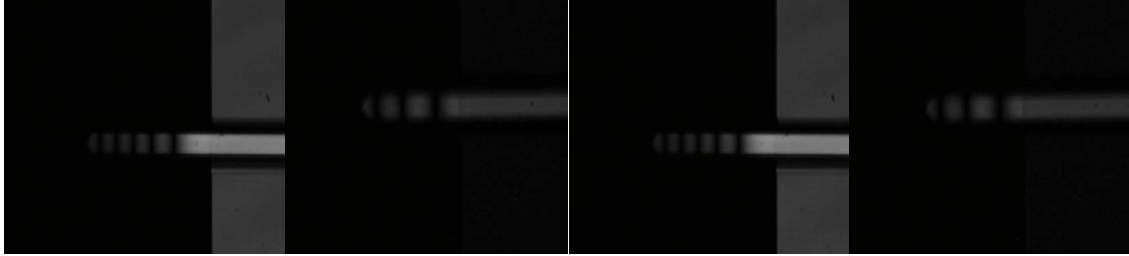
Figure 34. From left to right: maximum fringes obtained at one digit of excitation frequency, reduce excitation amplitude, move to next digit, reduce amplitude again.

III.4.2. Laser Doppler Vibrometry

To calculate the Q-factor of our samples, a LDV was utilized to perform ringdown tests. The LDV is mounted in place of the interferomic module shown in Fig. 31. The test consists of vibrating the probe with our piezoelectric shaker actuated by the waveform generator. The laser of the LDV is positioned onto the beam. The LDV outputs a Voltage as a function of time proportional to velocity.

It was decided the best location for taking velocity measurements would be the very tip of the beams, since the testing would take place in the first bending mode. The location of the laser on the beam is shown in Fig. 35 (Appnano, 2012).
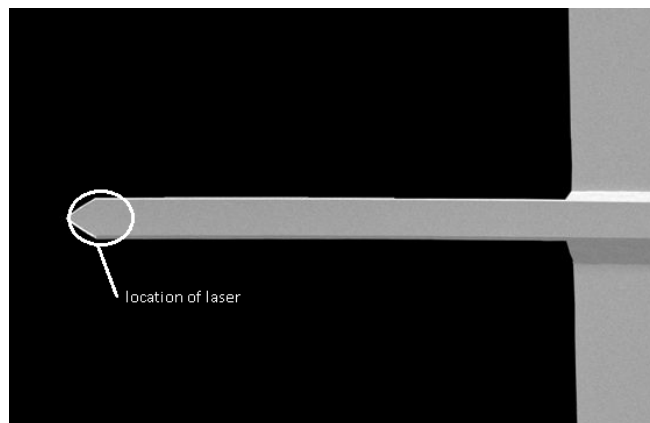
Figure 35. Image of a cantilever beam with laser location indicated by circle (Appnano, 2012).

65

To aid in finding the tip of the beam a Pixelink 6.6 Megapixel CCD camera with an Edmund Optics 1X telocentric lens was used to locate the base of the beam. The angular orientation of LDV head was adjusted to maximize the signal as indicated by the signal level gauge on the LDV unit. Once the signal was maximized the beam was moved with an X-Y positioner. The edge of the beam could be located because the signal would fall off when the laser was no longer on the beam since the flat black surface below the beam did not reflect enough of the laser to obtain a signal. This was repeated until the tip of the beam was reached.

Once the tip of the beam was located the piezoelectric shaker was turned on at a value close to the estimated resonant frequency of the beam. The output of the LDV was monitored on an Agilent Technologies DS06012A 100 MHz 2 GSa/s oscilloscope and the frequency of the signal generator was adjusted until the beam reached resonance. This was determined to be at the point of maximum velocity. Once resonance was reached, the signal generator was turned off and the output of the LDV was recorded with the oscilloscope at a sample rate ten times the actuation frequency of the beam. From this relationship the Q-factor of the beam can be calculated as described in the next section.

There was concern over the effect that the position of the laser on the beam would have on the results of the experiments. Since a range of angles of the head relative to the beam will saturate the signal meter on the LDV, there was no way to insure the angle would be the same for every test. Additionally the laser cannot be placed exactly on the tip of the beam, but approximately on the tip. In order to investigate these variables, a beam was tested under normal conditions to get a baseline. The test was repeated after moving the laser 25% of the length of the beam toward the base and then again after moving the beam 50% of the length of the beam towards the base.

The beam was then reset to the baseline position and the angle of the LDV head was adjusted. The angle was increased to the maximum value in one direction to the point just before the signal was lost and the test run. Following this the head was adjusted on an axis perpendicular to the first to the point just before the signal was lost. Additionally, since the test is being repeated under identical test conditions, these results can be used as a measure of precision of the experimental setup.

Another variable worth investigating is the frequency at which the test is performed. The testing is performed at the resonant frequency of the cantilever. Theoretically, there are an infinite number of resonant frequencies of the beam, however we are limited to the first six or seven modes due to the limitations of our equipment. The most convenient mode to test is the first, but to determine if this variable was significant, seven resonant frequencies were tested on a single beam under similar test conditions. The mode shapes were further investigated with Michelson interferometry.

In order to eliminate the effect of air damping on the Q-factor of the beams, all tests were conducted in a vacuum greater than 10^{-5} mbar. In order to insure that the air damping was negligible, tests were conducted on a beam at pressures ranging from atmospheric to 6.3 x $^{10-6}$ mbar.

III.4.3. Extracting Q-factor from the ring-down test

The LDV data of the decaying velocity of the beam can be used to extract the damping ratio, which is directly related to the Q-factor. The equation for the decaying velocity is

$$v = V_0 e^{-\zeta \omega t} , \tag{55}$$

where V_0 is the initial velocity, ζ is the damping ratio, and ω is the angular frequency (rad/s). To

extract ζ, we need to generate the envelope curve of the decaying data. Thus we decided to import the data into MATLAB and run an algorithm to record all the positive peak data points and fit an exponential curve to those positive peak data points. Please see Appendix II. for the MATLAB algorithm. The fitting gave us two parameters p1 and p2 of the exponential equation

$$\text{peaks} = p_1 e^{p_2 t} . \tag{56}$$

The equation is plotted with the original decaying data, as shown in Fig. 36, to verify the accuracy of the obtained p1 and p2. It is not unusual that the obtained p1 and p2 does not yield an accurate envelope curve. The reason we identified is that the data recorded may be too early that they include the time before the decaying happens or too late that they include mainly the noise. Therefore, we need to trim the raw data that we obtain from the oscilloscope until p1 and p2 yield the most accurate envelope curve. The region in the recorded data that we usually trim is shown in Fig. 36. An example of a final curve fitting is shown in Fig. 37.
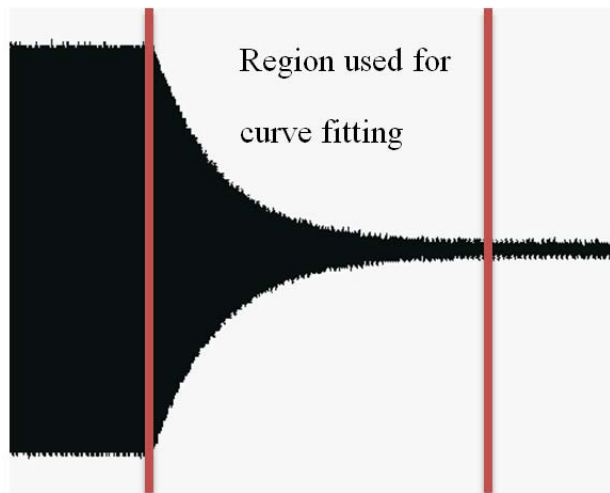
Figure 36. Region of ring-down curve used for analysis.
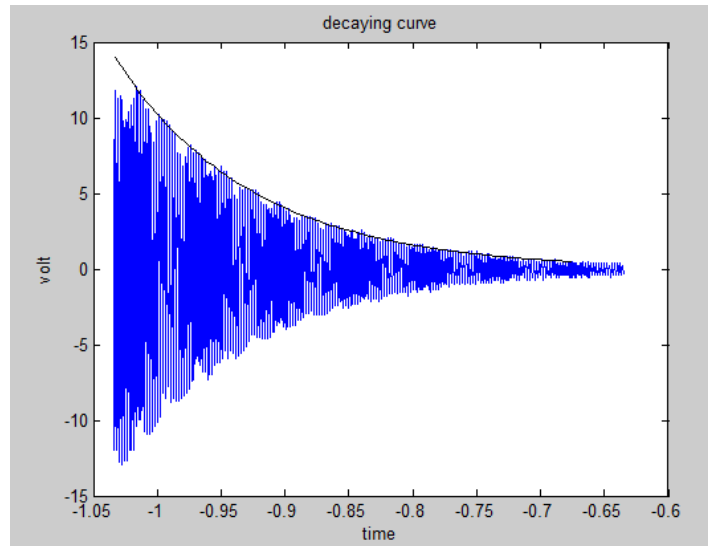
Figure 37. Ringdown curve shown with curve-fit.

Since we excited all the beams at a known forced frequency (their first resonant frequency), we can back-calculate the damping ratio

$$\zeta = -\frac{p_2}{\omega}.$$

(57)

Here we have assumed that after switching off the excitation signal, the beam will continue to vibrate at the same frequency as the excitation frequency. This may not be always accurate since the damping can change the frequency of a freely vibrating beam. However, we have verified our assumption by running a Fast Fourier Transform (FFT) of the decaying data and the peak of the FFT curve is right at the excitation frequency. The Q-factor is calculated from the damping ration by the equation

$$Q = \frac{1}{2\zeta}.$$

(58)

III.5. Uncertainty analysis

In order to determine the uncertainty of the results of this project, Root Sum of the Squares (RSS) uncertainty analysis will be conducted. The process begins by identifying the

69

phenomenological equation. The uncertainty can then be calculated as follows:

$$\delta Q = \sqrt{\sum_{i=1}^{n} \left(\frac{\partial Q}{\partial v_i} \delta v_i \right)^2}, \tag{59}$$

where Q is the phenomenological equation consisting of n variables, v_i is the ith variable of the phenomenological equation, and δv_i is the uncertainty of the ith variable.

IV. Results

IV.1. LDV precision

The results of the laser position study are displayed in Table 8. The sample was an uncoated SHOCON beam and the tests were done with the same pressure, amplitude, and frequency. Position one corresponds to the baseline position. Positions two and three are at locations laser 25% of the length of the beam toward the base and 50% of the length of the beam towards the base, respectively. Positions four and five correspond to the angles just before the signal was lost. The mean value of Q-factor was determined to be 44,824. The standard deviation is 1,908 or 4.3% of the mean Q-factor. The precision of our experimental measurements can be considered to be 4.3 %.

Table 8. Results from lower position study.

Laser Position Study (1 x 43 225 μm uncoated SHOCON)					
f [Hz]	A [mV]	P [mbar]	Q	Sa rate	position
24010.5	5	3.00E-06	46,227	200	1
24009.6	5	3.00E-06	42,256	200	2
24009.9	5	3.00E-06	47,666	200	3
24009.2	5	3.00E-06	43,707	200	4
24010.1	5	3.00E-06	44,264	200	5

mean Q-factor	44,824
standard deviation	1,908

The results of the frequency investigation are shown in Table 9. The Q-factor was calculated for the first seven modes of an uncoated SICON beam. Note this beam was soaked in acetone in order to remove it from the mounting disk. When retested the Q-factor was drastically reduced. Investigation revealed a layer of glue had beam deposited on the surface of the beam as the acetone evaporated resulting in increased damping. Although additional damping is present in this beam, the results of this study on the effect of mode on the Q-factor can still be considered reliable. The mean value of Q-factor was calculated to be 13,706 with a standard deviation of 3,265. This is a relatively high value, however note the extremely low Q-value for the seventh mode. The frequency is getting closer to the characteristic damping frequency at this point, the relative frequency for the seventh mode is 0.02, which explains the higher TED in this mode. When the seventh mode data point is ignored, the standard deviation is 1,277, a much more reasonable value. Considering this, it was decided to conduct the remaining tests in the first bending mode.

Table 9. Results of mode study.

Mode Study (2.5 x 40 x 450 μm uncoated SICON					
f [Hz]	A [mV]	P [mbar]	Q	Sa rate	mode
1219480.0	600	5.40E-06	6,250	5000	7
875262.0	3000	4.60E-06	16,474	10000	6
587372.0	200	5.40E-06	13,731	10000	5
356100.0	30	4.60E-06	15,622	2500	4
182140.9	50	4.60E-06	15,886	1000	3
65436.0	40	4.60E-06	15,175	500	2
10613.0	40	4.60E-06	12,807	200	1

mean Q-factor	13,706
standard deviation	3,265

The results for the resonant frequency obtained from LDV were also compared to the results obtained from Michelson interferometry. The results are shown in Table 10. The correlation was excellent, not the small percentage difference between the two methods.

Table 10. Resonant frequencies obtained from Michelson Interferometry and LDV.

sample	f LDV [Hz]	f Michelson [Hz]	mode	diff [%]
SICON 1	10778.30	10778.55	1	0.00232
SICON 1	24129.50	24129.00	2	0.00207
SICON 1	67088.65	67089.00	3	0.00052
SICON 2	10612.95	10613.35	1	0.00377
SICON 2	65436.00	65440.50	2	0.00688
SICON 2	182140.90	182155.00	3	0.00774
SICON 2	356100.00	356120.00	4	0.00562
SICON 2	587372.00	587390.50	5	0.00315
SICON 2	875262.00	875280.00	6	0.00206
SICON 2	1219480.00	1219450.00	7	0.00246

The results of the mode study for the SICON beam obtained from Michelson interferometry are shown in Fig. 38. In the image of the first mode, the relative size of the distance between the fringes coincides with a displacement from the reference plane. In this case, the distance between fringes decreases steadily from the base towards the tip of the beam, indicating the first bending mode. In the remaining images, the fringes correlate to areas of the beam displaced from the reference plane. The white areas indicates areas on the reference plane and are the nodes. Note the third mode has a combination of bending and torsion. This is assumed to arise due to a slight non-symmetry in the beam, causing a torsional mode and a bending mode to fall within close proximity to each other in the frequency range.

72
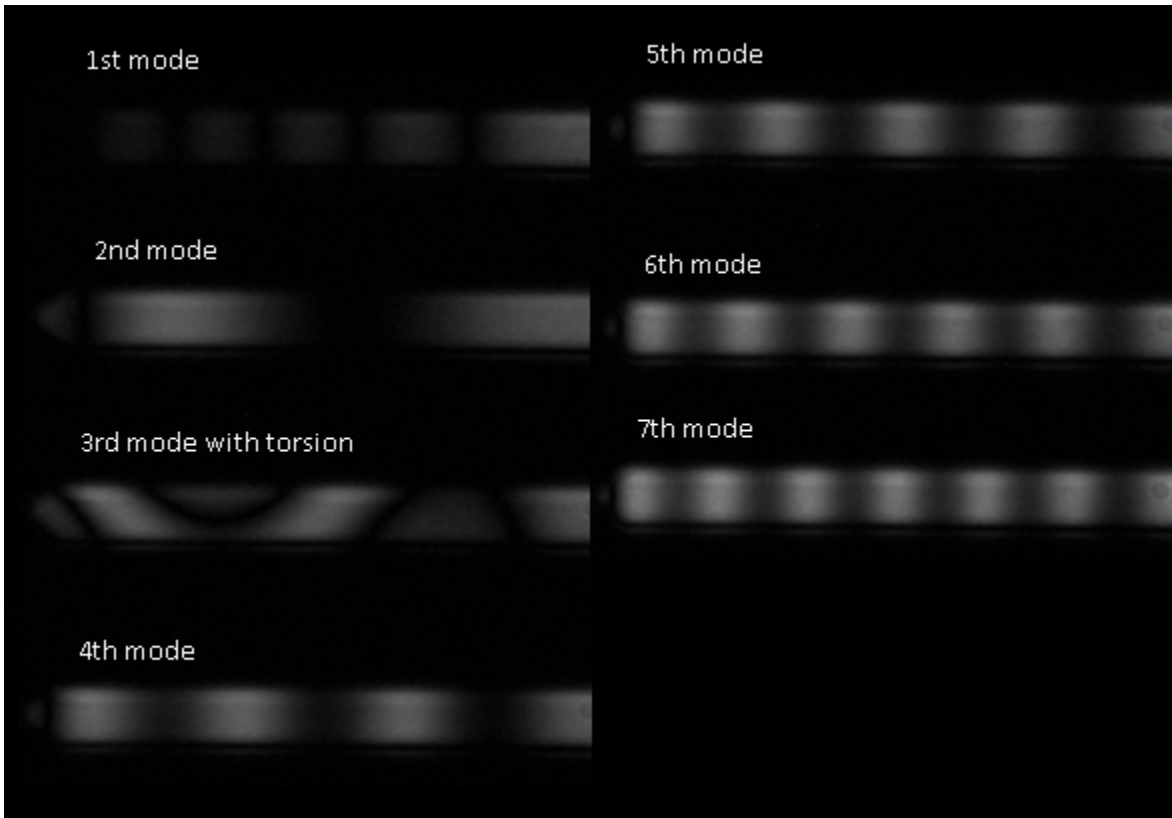
Figure 38. Images of fringe patterns obtained from Michelson Interferometry.

The results of the air pressure study are shown below in Table 11. Note the large effect air damping has on the Q-factor at atmospheric pressure. The effect of air damping gradually decreases until it becomes negligible at 6.3×10^{-6} mbar.

Table 11. Results of air damping study.

Air damping Study (2 x 40 x 450 Al coated sample)			
f [Hz]	A [mV]	P [mbar]	Q
14010.00	6000	1.00E+03	47
14190.00	2000	8.60E+01	148
14210.00	2000	1.00E+01	198
14210.00	500	1.00E+00	593
14210.00	50	1.00E-01	5,187
14211.00	50	4.00E-02	11,334
14211.00	50	1.40E-02	21,782
14211.00	50	1.60E-04	32,787
14210.30	10	5.40E-05	34,803
14210.20	10	2.50E-05	37,154
14210.35	10	6.30E-06	39,704

The results are displayed graphically in Fig. 39. The three regions of air damping are noticeable in this plot, the viscous damping region from to 10 mbar to 1 bar, the molecular damping region, from 10^{-4} mbar to 10 mbar, and the intrinsic region below 10^{-4} mbar. These data illustrate that air damping is negligible as long as the air pressure is below 10^{-5} mbar.
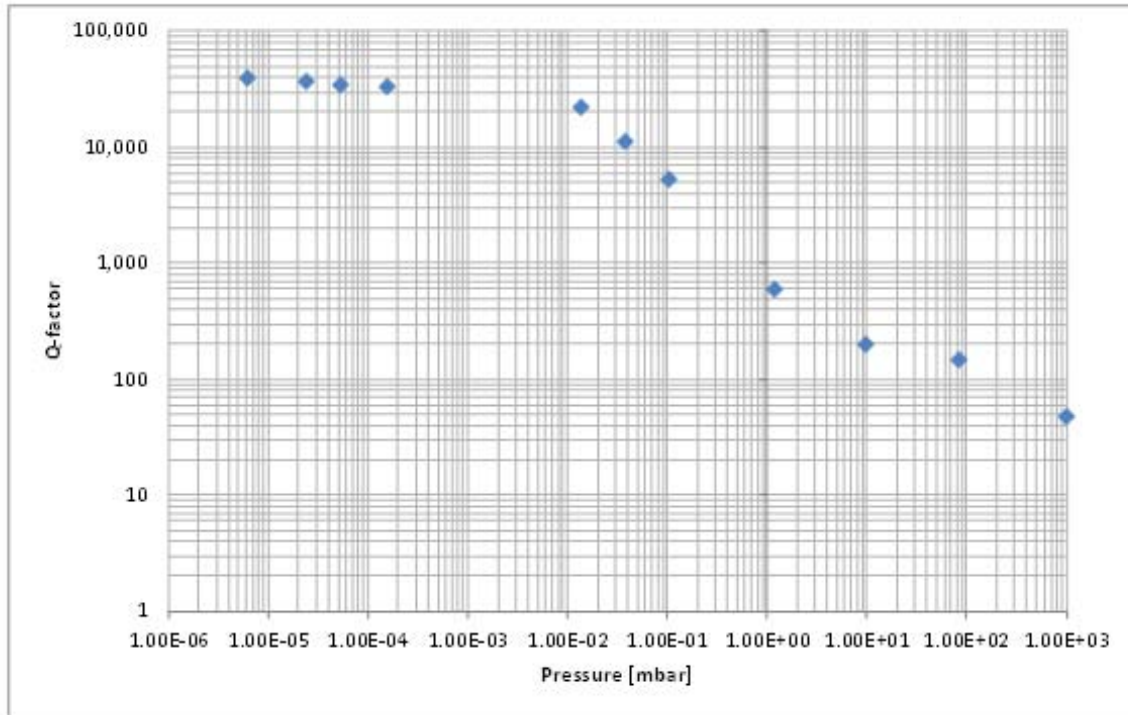
Figure 39. Q-factor plotted as a function of air pressure.

The resonant frequency is also affected by the air pressure. The resonant frequency as a function of air pressure is shown in Fig. 40. Note that there is a large effect above 10 mbar, however below 10 mbar there is little effect on the resonant frequency.
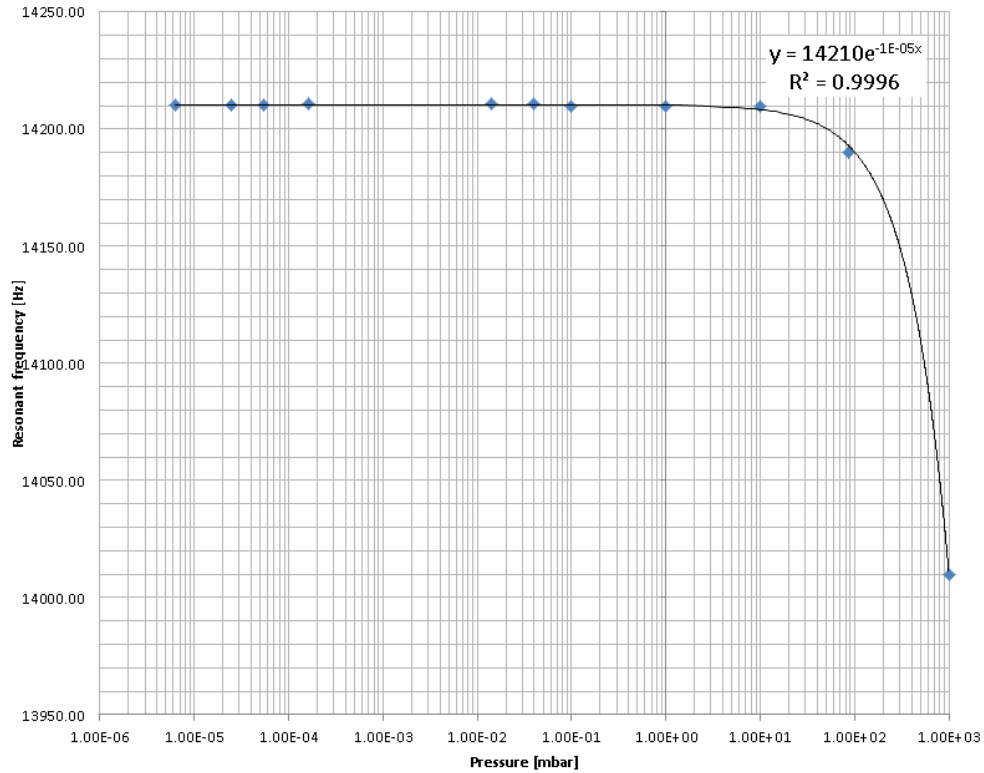
Figure 40. Resonant frequency as a function of air pressure.

IV.2. Analytical results

The results of the analytical calculations for individual contributions to Q-factor are listed in Table 12 along with measured values of width, length, and resonant frequency. Note the thickness was calculated with Eq. 37 using the resonant frequency along with the dimensions in Table 12 and the properties of Silicon listed in Table 4.

Table 12. Analytical results.

sample	ref #	width [µm]	length [µm]	thickness [µm]	frequency [Hz]	$Q_{TED\ Zener}$ x 10^{-6}	$Q_{TED\ Lifshitz}$ x 10^{-6}	Q_{anchor} x 10^{-6}	$\%_{diff}\ Q_{zener}$ vs $Q_{Lifshitz}$
SICON 1	10	45.8	446.0	1.614	11049.8	26.17	26.51	45.86	1.28
SICON 2	14	45.0	447.0	1.582	10778.3	27.95	28.31	49.08	1.27
SICON 3	17	44.5	446.0	1.550	10609.7	29.56	29.95	51.81	1.30
SHOCON 1	11	43.4	231.0	1.008	25730.0	28.80	29.18	26.14	1.30
SHOCON 2	15	44.5	229.0	0.924	23987.0	36.81	37.29	33.12	1.29
SHOCON 3	18	42.5	233.3	1.036	25912.0	27.10	27.46	24.85	1.31
SHOCON 4	22	43.5	231.5	0.945	24010.4	35.14	35.60	31.96	1.29
FORT 1	12	29.5	213.5	2.610	77967.0	1.42	1.44	1.19	1.25
FORT 2	16	28.5	213.0	2.235	67085.2	2.25	2.28	1.88	1.32
FORT 3	25	30.5	214.5	2.662	78785.1	1.35	1.37	1.14	1.32
FORT 4	23	30.0	214.3	2.605	77235.3	1.44	1.46	1.21	1.30
ACL 1	19	40.5	232.0	6.869	169209.5	0.0998	0.1011	0.0907	1.32
5nm Al	13	45.0	447.0	1.976	13469.2	14.32	14.51	25.15	1.31
5nm Al	26	47.0	449.8	2.070	13931.0	12.62	12.79	22.31	1.33
5nm x 2 Al	21	48.3	449.5	2.289	15428.6	9.32	9.44	16.46	1.30
5nm x 2 Al	27	47.5	451.0	2.052	13736.0	13.03	13.20	23.09	1.29
10 nm Al	9	46.0	451.5	2.127	14210.0	11.72	11.87	20.78	1.26
10 nm Al	28	47.5	449.5	2.144	14452.0	11.34	11.49	20.02	1.31
10 nm Al	29	48.0	449.0	2.181	14730.0	10.75	10.90	18.97	1.38
20 nm Al	20	46.0	448.0	2.169	14713.5	10.89	11.03	19.17	1.27
20 nm Al	30	46.3	449.5	2.144	14450.0	11.34	11.49	20.03	1.31
20 nm Al	31	46.3	448.5	2.008	13596.0	13.74	13.92	24.21	1.29
30nm x 2 Al	24	45.8	450.8	1.650	11056.5	25.03	25.36	44.33	1.30
30nm x 2 Al	32	46.8	450.8	1.742	11675.0	21.27	21.55	37.66	1.30
30nm x 2 Al	33	46.0	451.5	1.741	11628.0	21.38	21.66	37.93	1.29

The Q-factor related to TED was calculated utilyzing both Eqs 18 and 20, respectivly. The results are very similar, with the Zener equation slightly underpredicting the value of Q-factor slightly in most instances. The difference however was only 1.3 %.

The effect of TED appears to decrease with decreasing dimensions of the beams. The Q-factor related to TED was plotted as a function of the surface area to volume ratio in Fig. 41. The data was plotted in two groups based on length, the first with a length of about 450 µm and the second with a length of around 225 µm. Note the strong relationship between the surface area to volume ratio and Ted. As the ratio increases, the effect of TED becomes insignificant. Notice the excellent fit of the trendline and the nonlinear behavior of the TED with a change in the surface

area to volume ratio. Also, as the length of the cantilever beam becomes longer the data points are shifted to the left. This suggests that increasing the length of the cantilever causes the effect of increasing the surface area to volume ratio to become more pronounced.
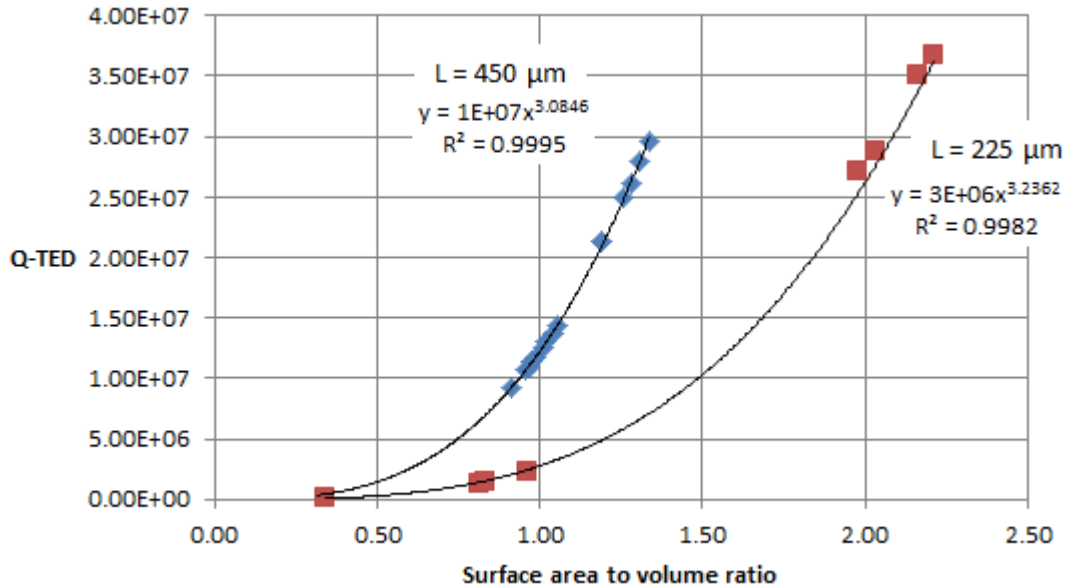
Figure 41. Q-factor related to TED vs. surface area to volume ratio.

Also note there is a size effect on the anchor damping of the samples. In order to see the effect the geometry has on anchor damping, the Q-factor related to anchor damping was plotted as a function of the thickness to length ratio in Fig. 42. Note the strong nonlinear relationship between the anchor damping and the thickness to length ratio. As the thickness to length ratio increases, the anchor damping becomes significant. This indicates that a longer, thinner beam will have less damping due to anchor losses.
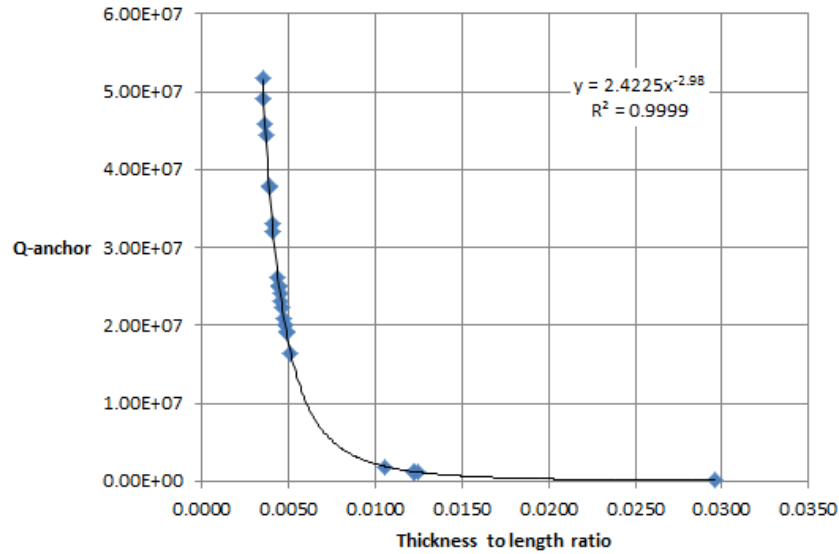
Figure 42. Q-factor related to anchor damping vs. thickness to length ratio.

IV.3. Computational results

Thermoelastic damping and resonate frequencies for different beams are simulated with COMSOL. The thickness of each beam is obtained from Eq. 37 using experimental resonant frequency. The other dimensions for each beam are from measurements using optical microscopy. Figure 44 shows displacement of SICON vibrating at different modes. The black and white images are from experimentation while the color images are from simulations. As Fig. 43 shows, the red area represents the maximum displacement while the blue area represents the minimum displacement within each beam.

Figure 43. Correspondence of color to displacement in COMSOL results.
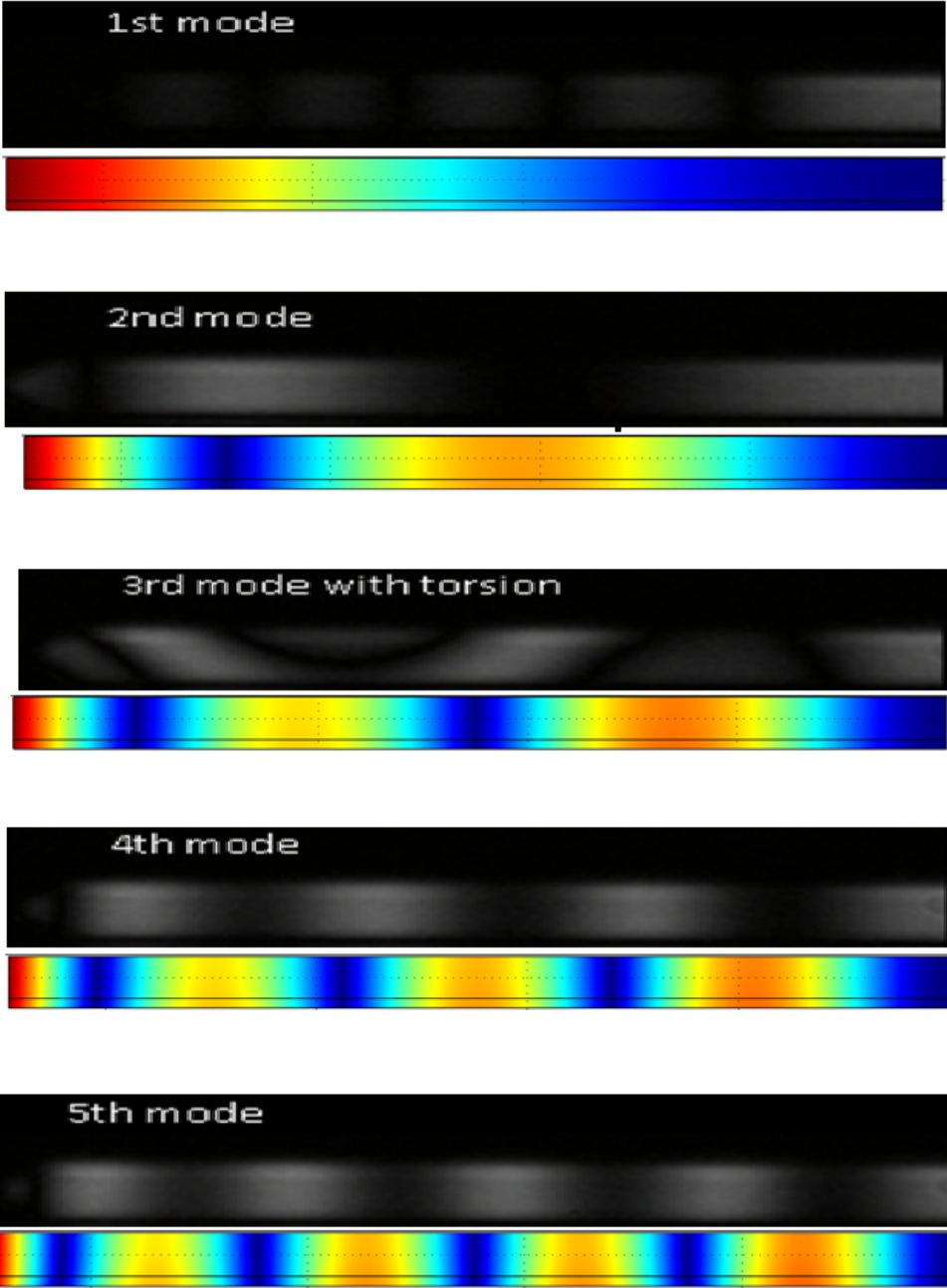
Figure 44. Vibrating SICON at different modes along with computational results.

Experimental result match computational result at each mode expect at the 3rd mode, where there is torsion in the experimental result. This torsion may be caused by non-symmetry over the width in the beam. However, it is assumed to be symmetric in computational modeling.

SHOCON 1st mode

FORT 1st mode
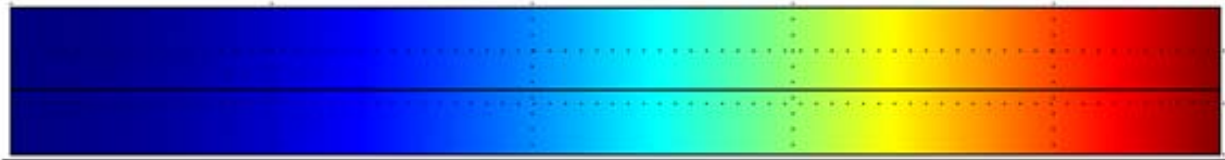
ACL 1st mode

2μmX42μmX450μm 1st mode

Figure 45. Computational results for samples at their first mode.

Table 13. Results of computational study.

Name	Nominal TxWxL (μm)	L1 (μm)	L2 (μm)	w1 (μm)	w2 (μm)	t (μm)	Q1(TED)-comp	Q1(TED)-Analy	f1(Hz)-comp	f1(Hz)-Exp
SICON	2.5x40x450	433.50	458.50	40.17	49.00	1.550	9.459E+06	2.995E+07	1.065E+04	1.061E+04
SHOCON	1x43x225	219.00	243.00	43.40	43.40	1.008	2.904E+07	2.918E+07	2.598E+04	2.573E+04
FORT	3x30x225	206.00	222.50	23.50	36.50	2.605	5.557E+05	1.460E+06	7.720E+04	7.724E+04
ACL	8.5x40x225	219.00	245.00	25.00	57.00	6.690	4.741E+04	1.011E+05	1.660E+05	1.692E+05
Coated	2x40x450	434.00	460.00	42.00	43.00	1.976	1.559E+07	1.451E+07	1.354E+04	1.347E+04

Table 14. Comparison of analytical to computational results for SICON sample.

Name	f2	Q2(TED)	f3	Q3(TED)	f4	Q4(TED)	f5	Q5(TED)
SICON-comp	6.673E+04	1.560E+06	1.869E+05	6.246E+05	3.665E+05	3.815E+05	6.063E+05	2.684E+05
SICON-Analy	6.544E+04	4.838E+06	1.821E+05	1.728E+06	3.561E+05	8.816E+05	5.874E+05	5.334E+05

Table 13 compares resonant frequencies from computational and experimental methods, and Q-factors in terms of TED from computational and analytical methods. The computational results for displacements along the beams are pictured in Fig. 45. For SHOCON and the 2 μm x 40 μm x 450 μm beam, Q-factors are very close for both methods. However, Q-factors are quite different for the other beams. It is because these beams are not rectangular in shape as assumed in the analytical analysis, but have different widths at the top and at the bottom. In analytical method, beams are assumed to be prismatic beams, therefore, the Q-factors are overestimated. This also explains the difference of Q-factor from both methods in Table 14. In Table 14, resonant frequencies for each beam from computational and experimental methods are not very close to each other. This difference may be explained by the assumptions made in computational method, for example, symmetry of the beam over its width.

IV.4. Experimental results

The measured Q-factors for the uncoated beams ordered from AppNano are listed in Table 15 together with the results for other beams. Again, the uncoated beams are SICON, SHOCON, FORT and ACL. It should be noted that, although the beams are labeled uncoated, the surfaces of these beams are covered by a layer of Silicon oxide whenever they are exposed to the air. This Silicon oxide layer, having an amorphous structure, also has a detrimental effect on the Q-factor of the beam similar to the metal coating layers.

From Table 15, we can see that the measured Q-factors for the beams SICON, SHOCON are fairly consistent. The variation in the Q-factors is partially due to the inevitable variation in

the beams dimensions and surface conditions. The FORT type has an outlier, with a value for Q-factor of 31,680, but we could not come up with a reasonable explanation for this variation. Unfortunately, 3 out of 4 ACL beams were damaged, the thickest among the uncoated beams, so we only have one data point for this type of beam.

Table 15. Experimental results.

sample	width [µm]	length [µm]	thickness [µm]	frequency [Hz]	$Q_{measured}$	Q_{coated}	$Q_{surface}$	δE_{ds} [kg/s2]	$E_{ds\,Al}$ [Mpa]	$E_{ds\,AuPd}$ [Mpa]
SICON 1	45.8	446.0	1.614	11049.8	103,690	7,354	104,300	0.42		198.7
SICON 2	45.0	447.0	1.582	10778.3	111,850		112,600	0.38		
SICON 3	44.5	446.0	1.550	10609.7	99,550		100,100	0.42		
SHOCON 1	43.4	231.0	1.008	25730.0	55,000	2,733	55,220	0.50		342.9
SHOCON 2	44.5	229.0	0.924	23987.0	57,627		57,820	0.44		
SHOCON 3	42.5	233.3	1.036	25912.0	50,706		50,900	0.56		
SHOCON 4	43.5	231.5	0.945	24010.4	44,154	2,185	44,270	0.59		402.3
FORT 1	29.5	213.5	2.610	77967.0	105,170	7,455	125,400	0.56		311.4
FORT 2	28.5	213.0	2.235	67085.2	31,680		32,680	1.84		
FORT 3	30.5	214.5	2.662	78785.1	120,270		149,200	0.48		
FORT 4	30.0	214.3	2.605	77235.3	108,340	5,196	129,600	0.54		457.2
ACL 1	40.5	232.0	6.869	169209.5	32,540		101,900	1.72		
5nm Al	45.0	447.0	1.976	13469.2	63,857	7,758	64,300	0.84	167.2	217.4
5nm Al	47.0	449.8	2.070	13931.0	78,000		78,760	0.72	143.0	
5nm x 2 Al	48.3	449.5	2.289	15428.6	43,235	7,216	43,550	1.43	142.8	256.5
5nm x 2 Al	47.5	451.0	2.052	13736.0	40,000		40,190	1.39	138.9	
10 nm Al	46.0	451.5	2.127	14210.0	39,704		39,910	1.45	144.9	
10 nm Al	47.5	449.5	2.144	14452.0	39,000		39,210	1.49	148.7	
10 nm Al	48.0	449.0	2.181	14730.0	38,600		38,820	1.53	152.7	
20 nm Al	46.0	448.0	2.169	14713.5	21,735		21,800	2.70	135.1	
20 nm Al	46.3	449.5	2.144	14450.0	24,500		24,580	2.37	118.5	
20 nm Al	46.3	448.5	2.008	13596.0	22,000		22,050	2.48	123.9	
30nm x 2 Al	45.8	450.8	1.650	11056.5	3,686	2,755	3,687	12.21	203.4	147.3
30nm x 2 Al	46.8	450.8	1.742	11675.0	4,800		4,802	9.89	164.8	
30nm x 2 Al	46.0	451.5	1.741	11628.0	4,680		4,682	10.14	168.9	

Ignoring these data points, the experimental data agrees with the theoretical calculations mentioned previously. To illustrate this, the Q-factor as a function of thickness was plotted for the experimental values along with the theoretical values in Fig. 46. In this figure, the black dots are the theoretical values and the red X's represent the experimental results. Note the SICON, FORT, and ACL beams are all shifted to the right. This is due to the difference between the actual thickness and the nominal thickness for these beams. Additionally, the theoretical data

points are all lower than the experimental. This is due to the estimation used for the value of δE_{ds} in Eq. 25.
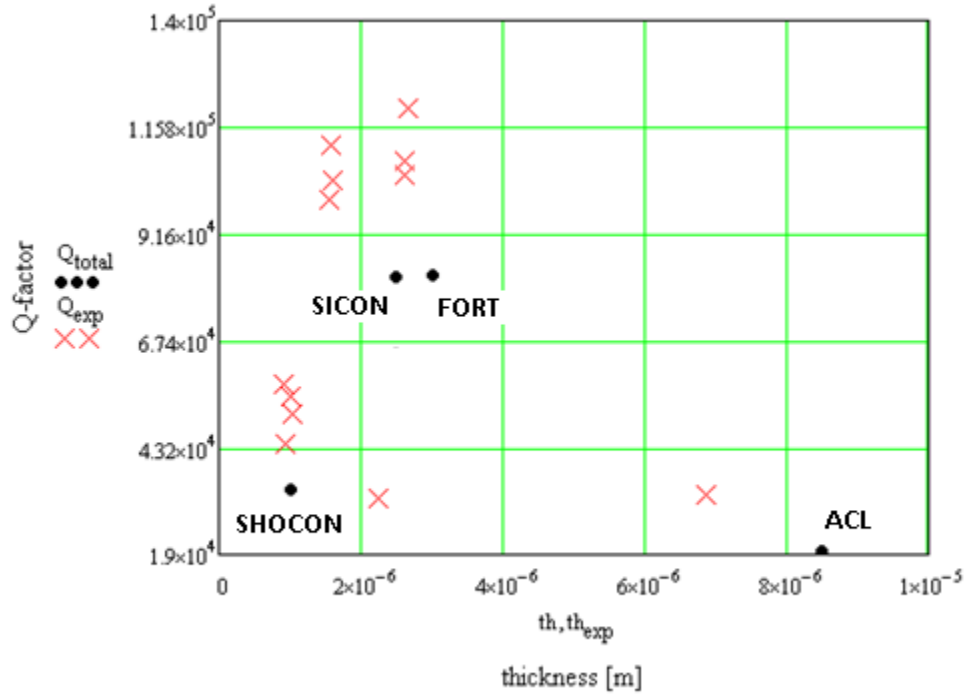
Figure 46. Predicted analytical results plotted with experimental results based on original assumptions.

The theoretical values were recalculated with the actual dimensions of the beam along with the value of δE_{ds} in Table 15. The Q-factor as a function of thickness was plotted for the experimental values along with the newly calculated theoretical values in Fig. 47. As in Fig. 46, the black dots are the theoretical values and the red X's represent the experimental results. Note there is a better agreement between the theoretical and the experimental results.
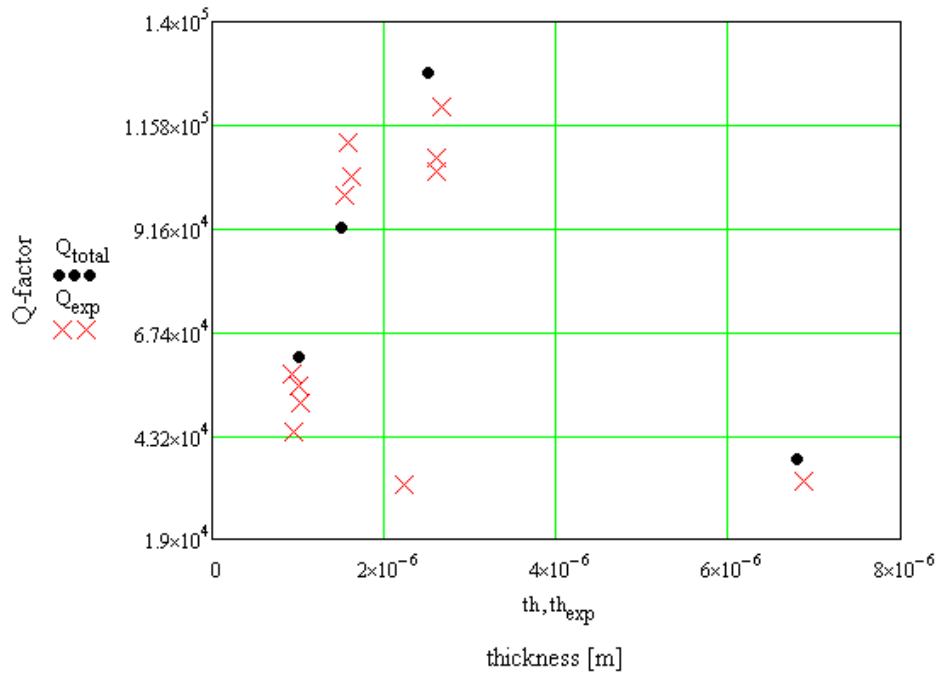
Figure 47. Predicted analytical results plotted with experimental results utilizing actual beam dimensions and δEds from Table 15.based on original assumptions.

In order to better understand the effect geometry has on surface damping, the Q-factor related to surface damping is plotted in Fig. 48 as a function of surface area to volume ratio. The surface damping increases linearly with the surface area to volume ratio.
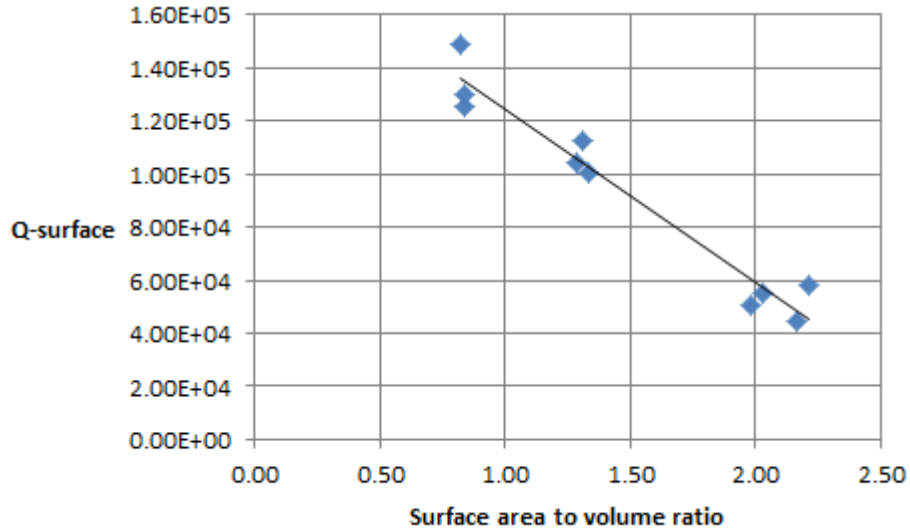
Figure 48. Q-factor related to surface damping plotted vs. surface to volume ratio.

The results for the calculation of the dissipation term for surface damping are listed in Table 16. For the uncoated beams, the dissipation term, E_{ds}, could not be calculated because it is a function of the absorbate layer thickness layer. The thickness of this layer is unknown, however a value can be calculated with the thickness of this layer included in this term. This term is δE_{ds} and it has units of kg/s^2. There were two data points that were considered outliers and eliminated, these were the FORT 2 sample and the ACL 1 sample. Ignoring these data points the mean value of δE_{ds} is 0.488 kg/s^2. The standard deviation of these data is 0.066 kg/s^2, or 14%.

Table 16. Mean and standard deviation for Eds .

	Uncoated	Al	AuPd
	δE_{ds} [kg/s2]	E_{ds} [Mpa]	E_{ds} [Mpa]
mean	0.488	150.2	291.7
standard deviation	0.066	21.3	99.3

For the coated samples, E_{ds} could be calculated because the coating thickness was known. The mean value of E_{ds} for the Al coated beams was 150.2 MPa. The standard deviation in these data is 21.3 MPa, 14 % of the mean. The value of E_{ds} for the Au/Pd coated beams was significantly higher than that for the Al coated beams, with a mean value of 291.7 MPa. The standard deviation of these data is 99.3. At 34% of the mean, this is a relatively large standard deviation. This large standard deviation is due to the large level of uncertainty in the coating thickness.

Refering to Table 6, note that the Young's modulus of AL is similar to the Young's modulus of the AuPd mixture. In contrast the density of the AuPd is over seven times greater than the density of the Al. E_{ds} for the AuPd mixture was twice as large as for the Al coating, qualitatively it can be seen that the mass properties of the coating have a large effect on damping in this case.

IV.5. Effect of geometry on total Q-factor

With the value of δE_{ds} known for uncoated single-crystal Silicon and the analytical models verified, a further investigation into the effect of geometry on the Q-factor can be carried

out. In respect to geometry alone Q-factor is a function of three variable, thickness, width , and length. It is difficult to graphically illustrate a function of three variables. In order to graphically illistrate the relationship between geometry and Q-factor, the following is substituted into Eq. 10

$$L = nw , \qquad (60)$$

where n is the length to width aspect ratio. With this substitution, Q-factor can be plotted as a function of thickness and width for:
$$n = 1,2,3, ...$$

Using the properties for single-crystal Silicon from Table 4, the experimentally derived value of δE_{ds} from Table 16, and $n = 5$, Q-factor as a function of width and thickness is plotted in Fig.49. Note there is a maximum Q-factor of around 250,000 on this plot.
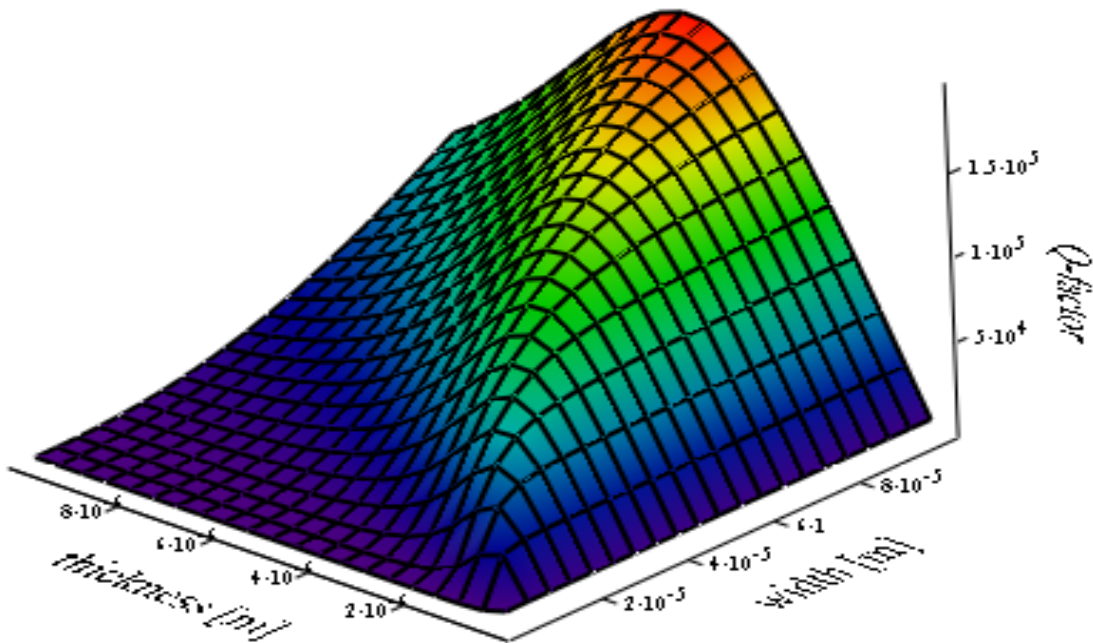
Figure 49. Q-factor as a function of thickness and width for n = 5 for a 4.5 μm x 100 μm x 500 μm beam.

In order to further investigate the effect of length, Q-factor as a function of thickness and width, with n = 10, is plotted in Fig. 50. Note the maximum values have shifted to the left, indicating a thicker beam is required for maximum Q-factor. Note the maximum value of Q-factor is about 400,000 on this plot, which corresponds to a beam 7 μm x 100 μm x 1000 μm.
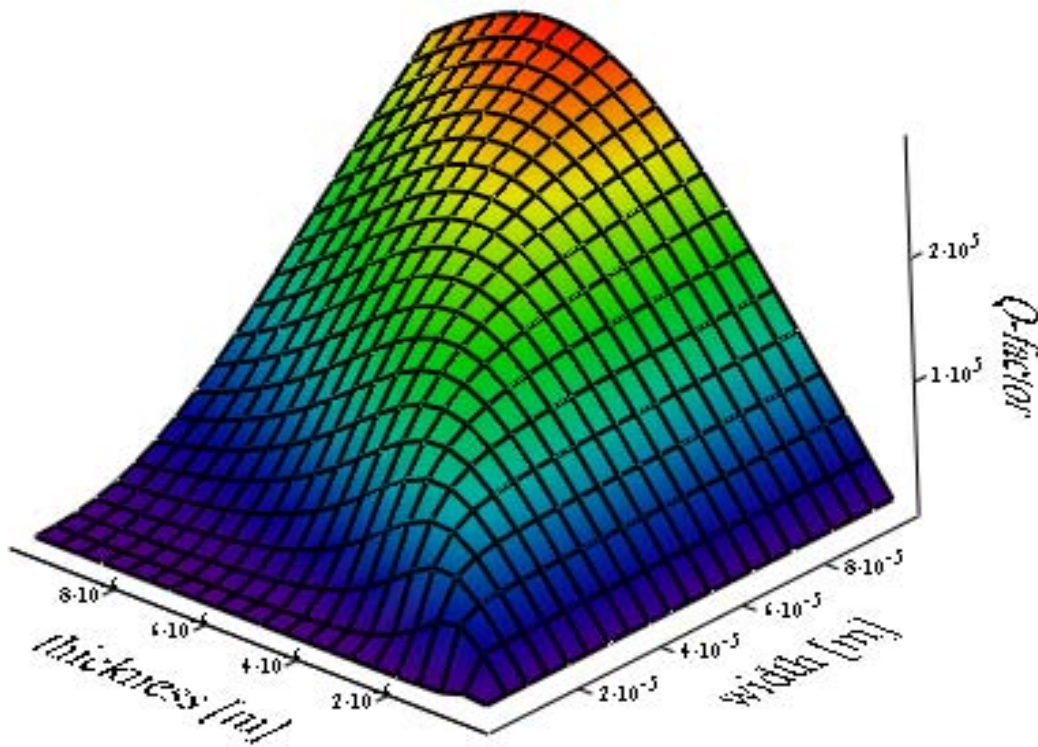
Figure 50. Q-factor as a function of thickness and width for n = 10.

Q-factor as a function of thickness and width, with n = 20, was plotted in Fig. 51 Note the maximum values have shifted even farther to the left, indicating an even thicker beam is required for maximum Q-factor. Note the maximum value of Q-factor about 700,000 on this

plot, which corresponds to a beam 10 μm x 100 μm x 2000 μm. This beam is into the millimeter level for length and there will come a point where the length to thickness ratio is so large the beam can no longer support its own weight.
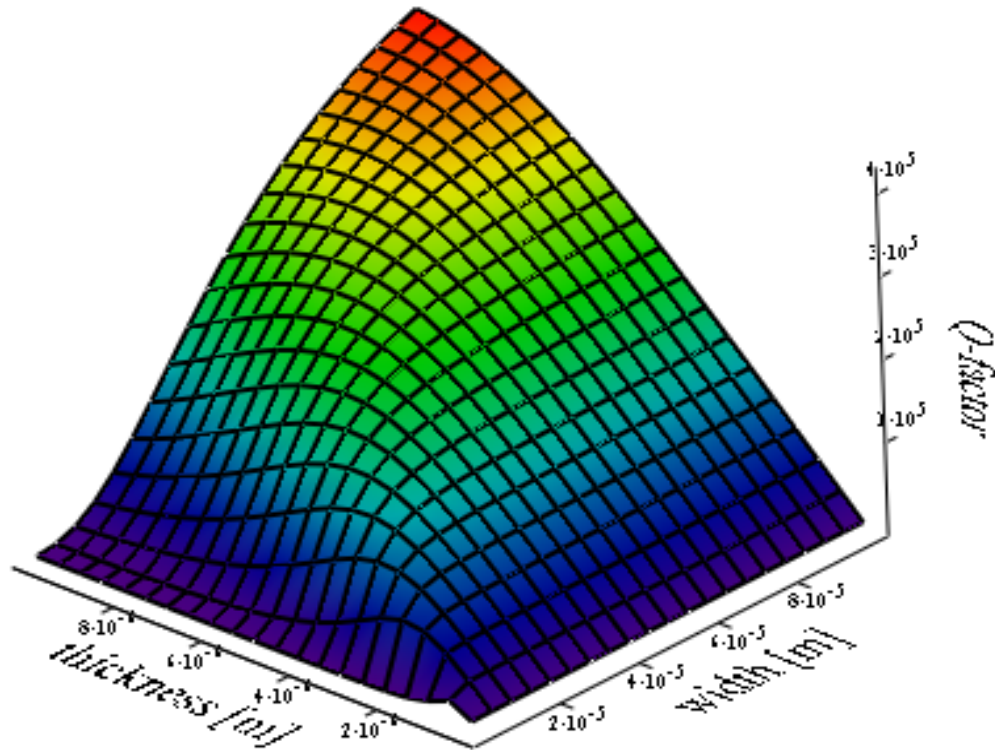
Figure 51. Q-factor as a function of thickness and width for n = 20.

IV.6. Uncertainty

A detailed uncertainty analysis was performed using the values listed in Table 17. The results of the uncertainty analysis are listed as a percentage of the parameter value in Table 18, the actual values are listed in Appendix I. The technique of calculating thickness using the measured resonant frequency of beam proved to be quite effective. The uncertainty of the

thickness using this technique was only about 2.3%. The uncertainty in the anchor damping was

reasonable at about 7%.

Table 17. Values used for uncertainty calculations.

Parameter	Value	Units	Parameter	Value	Units
temperature	1	K	Poisson's ratio	0.03	
length	1	μm	heat capacity	23	J/kg*K
width	1	μm	thermal conductivity	10	W/m*K
Young's modulus	6.3	Gpa	frequency	0.5	Hz
coefficient of thermal expansion	0.1	K^{-1}	density	50	kg/m^3

The TED damping uncertainty was relatively high at about 13%. Comparing the Lifshitz

equation to Zener's equation, the results obtained using the Lifshitz equation suffered slightly

less uncertainty. Upon further inspection, the largest contributor to this uncertainty is the value

for coefficient of thermal expansion which accounts for 33.4% of the uncertainty. The next

largest contributor was thickness, which accounted for 25.3% of the overall uncertainty. This is

despite the fact that the uncertainty in the thickness was only 2.3%. This illustrates the large

effect thickness has on TED. The other large contributors were thermal conductivity and

Young's modulus, accounting for 22.1 % and 18.4% of the overall uncertainty, respectively.

Table 18. Results of uncertainty analysis.

sample	%δt [%]	%δQTED Zener [%]	%δQTED Lifshitz [%]	%δQanchor [%]	%δQsurface [%]	%δδEds [%]	%ΔEds [%]	%ΔEds AuPd [%]
SICON 1	2.2	13.3	12.6	6.7	4.3	6.2		36.2
SICON 2	2.2	13.3	12.0	6.7	4.3	6.3		
SICON 3	2.2	13.3	12.6	6.7	4.3	6.1		
SHOCON 1	2.4	13.5	12.2	7.2	4.3	6.2		36.2
SHOCON 2	2.4	13.5	13.4	7.2	4.3	6.2		
SHOCON 3	2.3	13.5	12.7	7.2	4.3	6.3		
SHOCON 4	2.3	13.5	12.4	7.2	4.3	6.2		36.2
FORT 1	2.4	13.6	13.6	7.3	5.3	7.0		36.3
FORT 2	2.4	13.6	13.6	7.3	4.4	6.3		
FORT 3	2.4	13.6	13.6	7.3	5.6	7.1		
FORT 4	2.4	13.6	13.5	7.3	5.3	6.9		36.2
ACL 1	2.3	13.5	13.5	7.2	20.7	21.2		
5nm Al	2.2	13.3	12.0	6.7	4.3	6.2	20.9	36.3
5nm Al	2.2	13.3	13.3	6.7	4.3	6.2	20.9	
5nm x 2 Al	2.2	13.3	12.6	6.7	4.3	6.2	20.9	36.3
5nm x 2 Al	2.2	13.3	12.1	6.7	4.3	6.2	20.9	
10 nm Al	2.2	13.3	13.3	6.7	4.3	6.1	20.9	
10 nm Al	2.2	13.3	15.1	6.7	4.3	6.2	20.9	
10 nm Al	2.2	13.3	12.0	6.7	4.3	6.2	20.9	
20 nm Al	2.2	13.3	12.0	6.7	4.3	6.1	20.9	
20 nm Al	2.2	13.3	13.4	6.7	4.3	6.2	20.9	
20 nm Al	2.2	13.3	13.3	6.7	4.3	6.1	20.9	
30nm x 2 Al	2.2	13.3	12.6	6.7	4.3	6.2	20.9	41.3
30nm x 2 Al	2.2	13.3	12.0	6.7	4.3	6.1	20.9	
30nm x 2 Al	2.2	13.3	12.5	6.7	4.3	6.1	20.9	

There was a large amount of uncertainty in calculations involving the coatings. The uncertainty in the calculation of the dissipation term for Aluminum was 20.9%. This was due to the uncertainty in the coating thickness, which accounted for 91.3% of the overall uncertainty of the calculation. This corresponds well with the standard deviation in the calculation of dissipation term for Aluminum which was around 15%.

There was a larger amount of uncertainty in the calculation of the dissipation term for the Gold and Palladium mixture, which had an uncertainty of between 36.2% and 41.3%. The uncertainty in coating thickness accounted for 97.1% of the overall uncertainty. This was due to

an even larger uncertainty in the coating thickness due to the application process of the Gold and Palladium mixture. This uncertainty explains the standard deviation in the experimental results for the calculation of the dissipation term for the Gold and Palladium mixture which was around 34%.

V. Conclusions

In conclusion, the importance of geometry has been clearly illustrated. There is a geometry which minimizes the contributions of all forms of damping in combination and thus leads to maximum Q-factor. For maximum Q-factor, Fig. 50 clearly illustrates the optimum geometry which should be used. Additionally, at this point TED becomes much more pronounced and a material should be chosen which would minimize TED based on Fig. 17. In the case of the nanoscale sensor, surface damping becomes the dominant loss mechanism and therefore must be minimized. In this size range, absorbates on the surface must be minimized. Additionally, if a coating is required, one with minimum density and stiffness should be chosen.

VI. References

Appnano. Product information sheet. Retrieved 2/21, 2012, from http://www.appnano.com/products/silicon/

Arecco, D., &Worcester Polytechnic Institute. Mechanical Engineering Department. (2003). *Analysis and preliminary characterization of a MEMS cantilever-type chemical sensor.*Retrieved from http://www.wpi.edu/Pubs/ETD/Available/etd-0511104-150948/unrestricted/arecco.pdf

Ashby, M. F. (1999). *Materials selection in mechanical design*. Oxford, U.K: Butterworth-Heinemann.

Candler, R. N., Duwel, A., Varghese, M., Chandorkar, S. A., Hopcroft, M. A., Woo-Tae Park, et al. (2006). Impact of geometry on thermoelastic dissipation in micromechanical resonant beams. *Microelectromechanical Systems, Journal of, 15*(4), 927-934.

Chandorkar, S. A., Candler, R. N., Duwel, A., Melamud, R., Agarwal, M., Goodson, K. E., et al. (2009). Multimode thermoelastic dissipation. *Journal of Applied Physics, 105*(4), 043505-043505-13.

COMSOL Multiphysics, "Thermoelastic Damping in a MEMS Resonator," *COMSOL Multiphysics Library*. Retrieved 9/21, 2011, from http://www.comsol.com/products/multiphysics/

Duwel, A., Weinstein, M., Gorman, J., Borenstein, J., & Ward, P. (2002). Quality factors of MEMS gyros and the role of thermoelastic damping. Paper presented at the *Micro Electro Mechanical Systems, 2002. the Fifteenth IEEE International Conference on,* 214-219.

Elwenspoek, M., & Wiegerink, R. J. (2001). *Mechanical microsensors*. Berlin ; New York: Springer.

Feynman, R. P. (1992). There's plenty of room at the bottom [data storage]. *Microelectromechanical Systems, Journal of, 1*(1), 60-66.

Gad-el-Hak, M. (2002). *The MEMS handbook*. Boca Raton, Fla.: CRC Press.

Gorman, J. P., & Massachusetts Institute of Technology. Dept. of Materials Science and Engineering. (2002). *Finite element model of thermoelastic damping in MEMS* Retrieved from http://dspace.mit.edu/handle/1721.1/8458

Granta CES EduPack 2011 (2011), Product information page. Retrieved 11/12, 2011, from http://www.grantadesign.com/education/overview.html

Hao, Z., Xu, Y., & Durgam, S. K. (2009). A thermal-energy method for calculating thermoelastic damping in micromechanical resonators. *Journal of Sound and Vibration, 322*(4-5), 870-882. doi:10.1016/j.jsv.2008.12.005

Hao, Z., Xu, Y., & Durgam, S. K. A thermal-energy method for calculating thermoelastic damping in micromechanical resonators. (2009). *Journal of Sound and Vibration, 322*(4-5), 870-882.

Hao, Z., Erbil, A., & Ayazi, F. (2003). An analytical model for support loss in micromachined beam resonators with in-plane flexural vibrations. *Sensors and Actuators A: Physical, 109*(1–2), 156-164. doi:10.1016/j.sna.2003.09.037

Hao Z, "Thermoelastic Damping in Flexural-Mode ring gyroscopes." *Proc. ASME Intl. Mech. Eng. Congress and Exposition*, Orlando, Florida USA, 2005.

Hosaka, H., Itao, K., & Kuroda, S. (1995). Damping characteristics of beam-shaped micro-oscillators. *Sensors and Actuators A: Physical, 49*(1–2), 87-95.

Johansmann, M., Siegmund, G., Pineda, M., Targeting the limits of laser Doppler vibrometry, in: Proceedings of the IDEMA 2005, Tokyo, Japan, 2005, pp. 1–12.

Jinling Yang, Ono, T., & Esashi, M. (2002). Energy dissipation in submicrometer thick single-crystal silicon cantilevers. *Microelectromechanical Systems, Journal of, 11*(6), 775-783.

Klempner, A. R., Marinis, R. T., Hefti, P., & Pryputniewicz, R. J. (2009). Experimental determination of the Q-factors of microcantilevers coated with thin metal films. *Strain, 45*(3), 295-300.

Korvink, J. G., Paul, O., Knovel Electronics & Semiconductors Library, SpringerLink ebooks - Engineering, & Books 24x7. (2006). *Mems*. Norwich, NY; Heidelberg, Germany: W. Andrew Pub.; Springer. Retrieved from http://AU4SB9AX7M.search.serialssolutions.com/?V=1.0&L=AU4SB9AX7M&S=JCs&C=TC0000072509&T=marc&tab=BOOKS

Lange, D., Brand, O., & Baltes, H. (2002). *CMOS cantilever sensor systems: Atomic force microscopy and gas sensing applications*. Berlin ; New York: Springer.

Lee, J. H., Hwang, K. S., Park, J., Yoon, K. H., Yoon, D. S., & Kim, T. S. (2005). Immunoassay of prostate-specific antigen (PSA) using resonant frequency shift of piezoelectric nanomechanical microcantilever. *Biosensors and Bioelectronics, 20*(10), 2157-2162.

Lifshitz R, and Roukes M, "Thermoelastic damping in micro- and nanomechanical systems,"*Physical Review B, Condensed Matter Physics*, vol. 61, No. 8, pp. 5600-5609, 1999.

Liu, C. (2011). *Foundations of MEMS* (2nd ed.). Upper Saddle River, N.J.: Prentice Hall.

Maluf, N., Williams, K., & Books24x7, I. (2004). *An introduction to microelectromechanical systems engineering, second edition* (2nd ed.). Boston: Artech House.

Polytec. *Vibrometer product overview.* Retrieved 9/21, 2011, from http://www.polytec.com/us/products/vibration-sensors/

Prabhakar, S., & Vengallatore, S. (2008). Theory of thermoelastic damping in micromechanical resonators with two-dimensional heat conduction. *Microelectromechanical Systems, Journal of, 17*(2), 494-502.

Prabhakar, S., & Vengallatore, S. (2009). Thermoelastic damping in hollow and slotted microresonators. *Microelectromechanical Systems, Journal of, 18*(3), 725-735.

Pryputniewicz R, Pryputniewicz E, "TED-based Q-factors of MEMS resonators," *Proc. 33rd Annual Symp. and Exhibition of Internat. Microelectronics and Packaging Soc. (IMAPS)*, Boston, MA, pp. 184-195, 2006.

Pryputniewicz R, "Holographic and Finite Element Studies of Vibrating Beams," *Proc. Optics in Engineering Measurement*, Cannes, France, vol. 599, pp. 54-62, Dec. 1985.

Pryputniewicz, E. J., & Pryputniewicz, R. J. (2006). TED based Q-factors of MEMS resonators. *Proceedings of the 33Rd Annual Symposium and Exhibition of IMAPS-NE,* Boxboro, MA. 184-195.

PTC. Product information page. Retrieved 9/21, 2011, from http://www.ptc.com/products/mathcad/ .

Sandeep Kumar Vashist. (2007). A review of microcantilevers for sensing applications.

Srikar, V. T., & Spearing, S. M. (2003). Materials selection in micromechanical design: An application of the ashby approach. *Microelectromechanical Systems, Journal of, 12*(1), 3-10.

Vashist, S. (2007). A review of Microcantilevers for sensing applications. *Nanotechnology Online, Journal of.* Retrieved 3/12, 1012 from http://www.azonano.com/article.aspx?ArticleID=1927.
.

Weinberg, M. S., & Kourepenis, A. (2006). Error sources in in-plane silicon tuning-fork MEMS gyroscopes. *Microelectromechanical Systems, Journal of, 15*(3), 479-491.

Yang, J., Ono, T., Esashi, M. (2002). Energy dissipation in submicrometer thick single-crystal silicon cantilevers. *Microelectromechanical Systems, Journal of, 11*(6), 775-783.

Yasumura, K. Y., Stowe, T. D., Chow, E. M., Pfafman, T., Kenny, T. W., Stipe, B. C., et al. (2000). Quality factors in micron- and submicron-thick cantilevers. *Microelectromechanical*

Systems, Journal of, 9(1), 117-125.

Zener Clarence. (1937). Internal friction in solids: I. theory of internal friction in reeds. *Physical Review, 52*, 230-235.

Zener Clarence. (1938). Internal friction in solids: II. general theory of thermalelastic internal friction. *Physical Review, 53*, 90-99.

Appendix I. Uncertainty Values

sample	δt [nm]	δQ_{TED} Zener x10^{-6}	δQ_{TED} Lifshitz x10^{-6}	δQ_{anchor} x10^{-6}	$\delta Q_{surface}$ x10^{-3}	$\delta\delta E_{ds}$ [kg/s2]	ΔE_{ds} [Mpa]	ΔE_{ds} AuPd [Mpa]
SICON 1	36.00	3.48	3.34	3.08	4.5	0.026		72.0
SICON 2	35.27	3.72	3.40	3.30	4.9	0.024		
SICON 3	34.56	3.93	3.78	3.48	4.3	0.026		
SHOCON 1	23.69	3.89	3.57	1.87	2.4	0.031		124.3
SHOCON 2	21.73	4.97	4.98	2.38	2.5	0.027		
SHOCON 3	24.31	3.66	3.48	1.78	2.2	0.035		
SHOCON 4	22.20	4.75	4.41	2.29	1.9	0.036		145.8
FORT 1	62.04	0.19	0.19	0.09	6.7	0.039		112.9
FORT 2	53.15	0.30	0.31	0.14	1.5	0.116		
FORT 3	63.23	0.18	0.19	0.08	8.4	0.034		
FORT 4	61.88	0.19	0.20	0.09	6.9	0.037		165.7
ACL 1	157.10	0.01	0.01	0.01	21.1	0.364		
5nm Al	44.07	1.91	1.74	1.69	2.8	0.052	35.0	78.9
5nm Al	46.14	1.68	1.70	1.50	3.4	0.044	29.9	
5nm x 2 Al	51.04	1.24	1.19	1.11	1.9	0.088	29.9	93.1
5nm x 2 Al	45.74	1.73	1.59	1.55	1.7	0.086	29.1	
10 nm Al	47.42	1.56	1.58	1.40	1.7	0.089	30.3	
10 nm Al	47.81	1.51	1.74	1.35	1.7	0.092	31.1	
10 nm Al	48.62	1.43	1.31	1.28	1.7	0.094	32.0	
20 nm Al	48.35	1.45	1.33	1.29	0.9	0.166	28.3	
20 nm Al	47.80	1.51	1.54	1.35	1.1	0.146	24.8	
20 nm Al	44.78	1.83	1.85	1.63	1.0	0.152	25.9	
30nm x 2 Al	36.78	3.33	3.20	2.98	0.2	0.751	42.6	60.9
30nm x 2 Al	38.83	2.83	2.59	2.53	0.2	0.608	34.5	
30nm x 2 Al	38.88	2.84	2.70	2.55	0.2	0.623	35.3	

Appendix II. Matlab code

```matlab
%% Calculate damping
% 10/21/2011
%%
% Get date from excel file
clear; clc;close all;
[decay]=xlsread('');
[rdecay,cdecay]=size(decay);
volt=decay(3:rdecay,2);time=decay(3:rdecay,1);f=decay(3,3);
volt_avg=mean(volt);
volt=volt-volt_avg;%shift the curve to center about x axis
figure(1)
plot(time,volt);xlabel('time');ylabel('volt');title('decaying curve');
hold on;
%% Find peaks and calculate Q
%% find peaks
peaks=[0];ptime=[0];
for i=2:(size(decay)-4) %check with rdecay
    if volt(i-1,1)<=volt(i,1)&&volt(i,1)>=volt(i+1,1)&&volt(i,1)>0
        peaks=[peaks; volt(i,1)];
        ptime=[ptime; time(i,1)];
    end
end
peaks(1)=[];ptime(1)=[];
plot(ptime, peaks,'r');hold on
%% refine peak (execute this cell until rpeaks stops decreasing)
clear j
[rpeaks, cpeaks]=size(peaks);
iteration=0;
%while iteration<1000;
for j=2:rpeaks-1
    [rpeaks, cpeaks]=size(peaks);
    if j<rpeaks
        if peaks(j-1)>peaks(j)&&peaks(j)<=peaks(j+1)
            peaks(j)=[];
            ptime(j)=[];
        end
    end
%end
iteration=iteration+1;
end
%%
 plot(ptime, peaks,'g'); hold on


 % [f, spectrum, peakFreq]=fftVib(volt, time);
```

100

```
%%
%frequency
%determine time between peaks
P=zeros(P);
for k=1:numel(ptime)-1;
    P(k)=ptime(k,1)-ptime(k+1,1);
end
f0=abs(1/mean(P));


%% calculate Q
peaks_ln=log(peaks);
p=polyfit(ptime,peaks_ln,1);
fit=exp(p(2))*exp(p(1)*ptime);
plot(ptime,fit,'black');
%damping ratio
w1=f*2*pi;%Hz, first mode
z1=-p(1)/w1;
Q1=1/(2*z1)
```

Appendix III. MathCad calculations

The following analysis is done based the assumption that the resonance frequency = frequency of

oscillation

$\Delta n := 0.01$

$n := 0.1, 0.1 + \Delta n .. 3$

$b := 42 \cdot 10^{-6} \, m$

$E := 167.5 \cdot 10^{9} \, Pa$

$L := 442 \cdot 10^{-6} \, m$

$\rho := 2330 \, kg/m^{3}$

$h := 1.7 \cdot 10^{-6} \, m$

$\alpha := 2.6 \cdot 10^{-6} / K$

$T_0 := 25 + 273$ K

$c_p := 700$ J/kg-K

$\beta_1 := 1.875$

$k := 130$ W/m-K

$$f_n := \frac{\beta_1^2 \cdot \sqrt{\dfrac{3 \cdot E \cdot h^2}{\rho}}}{12 \cdot \pi \cdot L^2}$$

resonance freq.

$$f_n = 1.192 \times 10^4$$

$$f_o := \frac{\pi \cdot k}{2 \cdot \rho \cdot c_p \cdot h^2}$$

characteristic freq.

$$\Gamma := \frac{E \cdot \alpha^2 \cdot T_0}{4 \cdot \rho \cdot c_p}$$

$$\Lambda := 2 \cdot \left(\frac{f_o \cdot f_n}{f_o^2 + f_n^2} \right)$$

$$Q := \frac{1}{2 \cdot \Gamma \cdot \Lambda}$$

$$Q = 1.757 \times 10^7$$

$$Q\_k(n) := \frac{2 \cdot \sqrt{3} \cdot \pi^4 \cdot L^4 \cdot (k \cdot n)^2 + \dfrac{\sqrt{3} \cdot E \cdot \rho \cdot c_p^2 \cdot h^6 \cdot \beta_1^4}{6}}{\pi^2 \cdot E \cdot L^2 \cdot T_0 \cdot \alpha^2 \cdot h^2 \cdot (k \cdot n) \cdot \beta_1^2 \cdot \sqrt{\dfrac{E \cdot h^2}{\rho}}}$$

102

$$Q\_E(n) := \frac{2\cdot\sqrt{3}\cdot\pi^4\cdot L^4\cdot k^2 + \dfrac{\sqrt{3}\cdot(E\cdot n)\cdot\rho\cdot c_p^{\,2}\cdot h^6\cdot\beta_1^{\,4}}{6}}{\pi^2\cdot(E\cdot n)\cdot L^2\cdot T_0\cdot\alpha^2\cdot h^2\cdot k\cdot\beta_1^{\,2}\cdot\sqrt{\dfrac{(E\cdot n)\cdot h^2}{\rho}}}$$

$$Q\_\rho(n) := \frac{2\cdot\sqrt{3}\cdot\pi^4\cdot L^4\cdot k^2 + \dfrac{\sqrt{3}\cdot E\cdot(\rho\cdot n)\cdot c_p^{\,2}\cdot h^6\cdot\beta_1^{\,4}}{6}}{\pi^2\cdot E\cdot L^2\cdot T_0\cdot\alpha^2\cdot h^2\cdot k\cdot\beta_1^{\,2}\cdot\sqrt{\dfrac{E\cdot h^2}{(\rho\cdot n)}}}$$

$$Q\_c_p(n) := \frac{2\cdot\sqrt{3}\cdot\pi^4\cdot L^4\cdot k^2 + \dfrac{\sqrt{3}\cdot E\cdot\rho\cdot(c_p\cdot n)^2\cdot h^6\cdot\beta_1^{\,4}}{6}}{\pi^2\cdot E\cdot L^2\cdot T_0\cdot\alpha^2\cdot h^2\cdot k\cdot\beta_1^{\,2}\cdot\sqrt{\dfrac{E\cdot h^2}{\rho}}}$$

$$Q\_\alpha(n) := \frac{2\cdot\sqrt{3}\cdot\pi^4\cdot L^4\cdot k^2 + \dfrac{\sqrt{3}\cdot E\cdot\rho\cdot c_p^{\,2}\cdot h^6\cdot\beta_1^{\,4}}{6}}{\pi^2\cdot E\cdot L^2\cdot T_0\cdot(\alpha\cdot n)^2\cdot h^2\cdot k\cdot\beta_1^{\,2}\cdot\sqrt{\dfrac{E\cdot h^2}{\rho}}}$$

103

Log-Log

Q_k(n)

Q_ρ(n)

Q_c_p(n)

Q_E(n)

Q_α(n)

n,n,n,n,n

Q vs k

Q_k(n)

Q

n,1

Q vs density

Q_ρ(n)

Q

n,1

104

Q vs Cp

$Q\_c_p(n)$

Q

Q vs E

$Q\_E(n)$

Q

Q vs alfa

$Q\_\alpha(n)$

Q
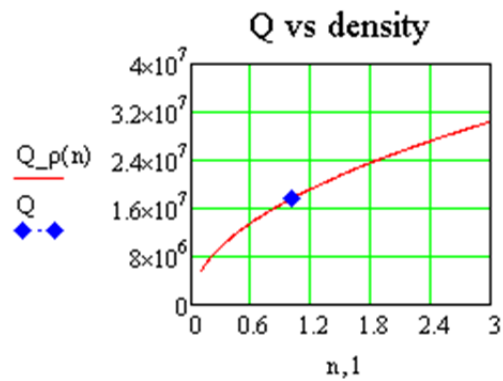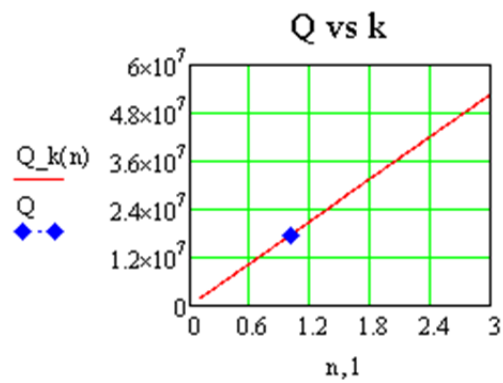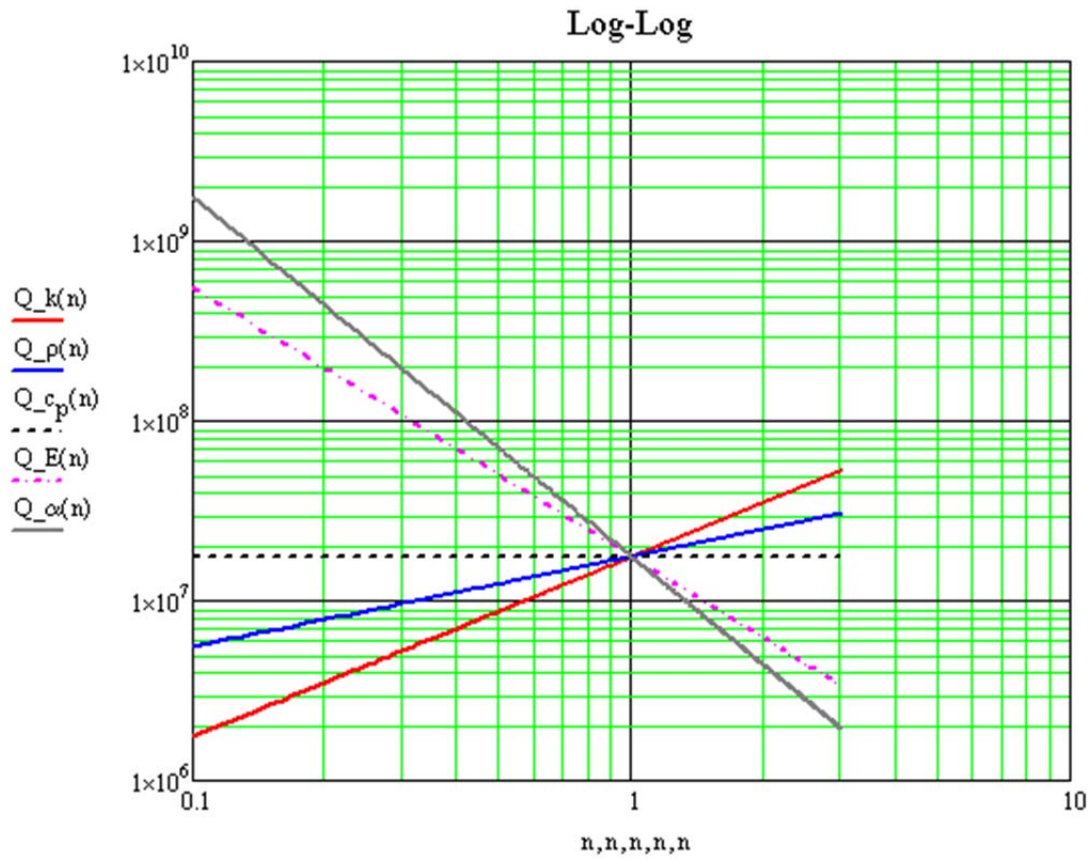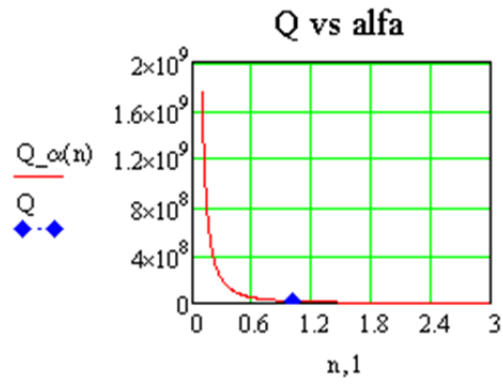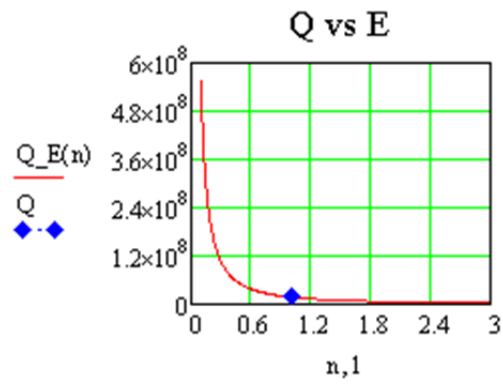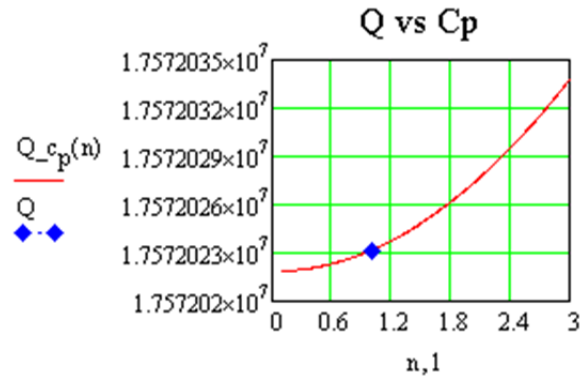
Input

mode coefficients for rectangular cantilever free-fixed

$\beta_1 := 1.875$ $\quad \beta_2 := 4.694$ $\quad \beta_3 := 7.855$ $\quad \beta_4 := 10.996$ $\quad \beta_5 := 14.137$ $\quad \beta_6 := 17.279$

Nominal Dimensions

30nm Al Coated   **SHOCUN**   **SICON**   **FORT**

$L_0 := 450\mu m$ $\quad L_1 := 225\mu m$ $\quad L_2 := 450\mu m$ $\quad L_3 := 225\mu m$

$t_0 := 2 \cdot \mu m$ $\quad t_1 := 1 \cdot \mu m$ $\quad t_2 := 2.5 \cdot \mu m$ $\quad t_3 := 3 \cdot \mu m$

$w_0 := 40\mu m$ $\quad w_1 := 43\mu m$ $\quad w_2 := 40\mu m$ $\quad w_3 := 30\mu m$

   ACT   **ACL**   **ACST**   **SiN**   **SiN**

$L_4 := 125\mu m$ $\quad L_5 := 225\mu m$ $\quad L_6 := 150\mu m$ $\quad L_7 := 50\mu m$ $\quad L_8 := 200\mu m$

$t_4 := 4.5 \cdot \mu m$ $\quad t_5 := 8.5 \cdot \mu m$ $\quad t_6 := 2.5 \cdot \mu m$ $\quad t_7 := 0.2 \cdot \mu m$ $\quad t_8 := 0.6 \cdot \mu m$

$w_4 := 35\mu m$ $\quad w_5 := 40\mu m$ $\quad w_6 := 25\mu m$ $\quad w_7 := 35\mu m$ $\quad w_8 := 40\mu m$

Material Properties

Properties for Si   Properties for SiN   Uncertainties for Properties for Si

$E_0 := 165.6 GPa$ $\qquad E_N := 290 GPa$ $\qquad T_0 := (273 + 25)K$ $\qquad \delta\alpha := 0.1\dfrac{\mu m}{m \cdot K}$

$\rho_0 := 2330 kg \cdot m^{-3}$ $\qquad \rho_N := 3200 kg \cdot m^{-3}$ $\qquad \delta L := 1\mu m$

$\qquad\qquad\qquad\qquad\qquad\qquad\qquad\qquad\qquad\qquad \delta t := 0.025\mu m$ $\qquad \delta v := 0.03$

$\alpha_0 := 2.6\dfrac{\mu m}{m \cdot K}$ $\qquad \alpha_N := 2.8\dfrac{\mu m}{m \cdot K}$ $\qquad \delta w := 1\mu m$ $\qquad \delta c_p := 23\dfrac{J}{kg \cdot K}$

$v := 0.27$ $\qquad\qquad v := 0.27$ $\qquad\qquad \delta E := 6.3 GPa$

$\qquad\qquad\qquad\qquad\qquad\qquad\qquad\qquad\qquad\qquad\qquad\qquad \delta k := 10\dfrac{W}{m \cdot K}$

$c_{p.0} := 691\dfrac{J}{kg \cdot K}$ $\qquad c_{p.N} := 691\dfrac{J}{kg \cdot K}$ $\qquad \delta\rho := 50 \cdot kg \cdot m^{-3}$ $\qquad \delta T := 1K$

$k_0 := 160\dfrac{W}{m \cdot K}$ $\qquad k_N := 26\dfrac{W}{m \cdot K}$ $\qquad \delta\beta := 0.0005$

$\qquad\qquad\qquad\qquad\qquad\qquad\qquad\qquad\qquad\qquad \delta f := 0.5 \cdot Hz$

$M := 28.97 \cdot 10^{-3} \cdot kg$ $\qquad\qquad$ molecular mass of air

$R := 8.314 \cdot 10^3 \cdot \dfrac{J}{K}$ $\qquad\qquad$ Gas constant

Measured Values

Air pressure in Pascals for air damping calculations

$P_1 := 1 \cdot 10^5 \cdot Pa$ $\quad P_4 := 1.2 \cdot 10^2 \cdot Pa$ $\quad P_7 := 1.4 \cdot Pa$ $\qquad P_{10} := 2.5 \cdot 10^{-3} \cdot Pa$

$P_2 := 8.6 \cdot 10^3 \cdot Pa$ $\quad P_5 := 1 \cdot 10^1 \cdot Pa$ $\quad P_8 := 1.6 \cdot 10^{-2} \cdot Pa$ $\quad P_{11} := 6.3 \cdot 10^{-4} \cdot Pa$

$P_3 := 1 \cdot 10^3 \cdot Pa$ $\quad P_6 := 4 \cdot Pa$ $\qquad\quad P_9 := 5.4 \cdot 10^{-3} \cdot Pa$

Dimensions

Beam 1A SICON

$L_{10} := 446 \cdot \mu m$ measured (avg)

$w_{10} := 45.8 \mu m$ measured (avg)

$f_{10} := 11049.8 \cdot Hz$ fn measured

$Q_{10} := 10369($

$Q_{Au10} := 7354$

Beam 1B SHOCON

$L_{11} := 231 \cdot \mu m$ measured (avg)

$w_{11} := 43.4 \mu m$ measured

$f_{11} := 25730 \cdot Hz$ fn measured

$Q_{11} := 55000$

$Q_{Au11} := 2733$

Beam 1C FORT

$L_{12} := 213.5 \cdot \mu m$ measured (avg)

$w_{12} := 29.5 \mu m$ measured (avg)

$f_{12} := 77967 \cdot Hz$ fn measured

$Q_{12} := 10517($

$Q_{Au12} := 7455$

Beam 1E 5 nm Al coating

$L_{13} := 447 \cdot \mu m$ measured (avg)

$w_{13} := 45 \mu m$ measured (avg)

$f_{13} := 13469.21 \cdot Hz$ fn measured

$Q_{13} := 63857$

$Q_{Au13} := 7758$

Beam 2A SICON

$L_{14} := 447 \cdot \mu m$ measured (avg)

$w_{14} := 45 \mu m$ measured (avg)

$f_{14} := 10778.3 \cdot Hz$ fn measured

$Q_{14} := 111850$

Beam 2B SHOCON

$L_{15} := 229 \cdot \mu m$ measured (avg)

$w_{15} := 44.5 \mu m$ measured

$f_{15} := 23987 \cdot Hz$ fn measured

$Q_{15} := 57627$

Beam 2C FORT

$L_{16} := 213 \cdot \mu m$ measured (avg)

$w_{16} := 28.5 \mu m$ measured (avg)

$f_{16} := 67085.2 \cdot Hz$ fn measured

$Q_{16} := 3168($

Beam 2E 10 nm Al coating

$L_9 := 451.5 \cdot \mu m$ measured (avg)

$w_9 := 46 \mu m$ measured (avg)

$f_9 := 14210 \cdot Hz$ fn measured

$Q_9 := 39704$

Beam 3A SICON

$L_{17} := 446 \cdot \mu m$ measured (avg)

$w_{17} := 44.5 \mu m$ measured (avg)

$f_{17} := 10609.7 \cdot Hz$ fn measured

$Q_{17} := 99550$

Beam 3B SHOCON

$L_{18} := 233.3 \cdot \mu m$ measured (avg)

$w_{18} := 42.5 \mu m$ measured

$f_{18} := 25912 \cdot Hz$ fn measured

$Q_{18} := 50706$

Beam 3D ACL

$L_{19} := 232 \cdot \mu m$ measured (avg)

$w_{19} := 40.5 \mu m$ measured (avg)

$f_{19} := 169209.5 \cdot Hz$ fn measured

$Q_{19} := 32540$

Beam 3E 20 nm Al coating

$L_{20} := 448 \cdot \mu m$ measured (avg)

$w_{20} := 46 \mu m$ measured (avg)

$f_{20} := 14713.5 \cdot Hz$ fn measured

$Q_{20} := 21735$

Beam 4A 5 nm x 2 Al coating

$L_{21} := 449.5 \cdot \mu m$ measured (avg)

$w_{21} := 48.3 \mu m$ measured (avg)

$f_{21} := 15428.6 \cdot Hz$ fn measured

$Q_{21} := 43235$

$Q_{Au21} := 7216$

Beam 4B SHOCON

$L_{22} := 231.5 \cdot \mu m$ measured (avg)

$w_{22} := 43.5 \mu m$ measured (avg)

$f_{22} := 24010.35 \cdot Hz$ fn measured

$Q_{22} := 44154$

$Q_{Au22} := 2185$

Beam 4C FORT

$L_{23} := 214.3 \cdot \mu m$ measured (avg)

$w_{23} := 30 \mu m$ measured (avg)

$f_{23} := 77235.3 \cdot Hz$ fn measured

$Q_{23} := 10834($

$Q_{Au23} := 5196$

Beam 4E 30 nm x 2 Al coating

$L_{24} := 450.8 \cdot \mu m$ measured (avg)

$w_{24} := 45.8 \mu m$ measured (avg)

$f_{24} := 11056.5 \cdot Hz$ fn measured

$Q_{24} := 3686$

$Q_{Au24} := 2755$

Beam 3C FORT

$L_{25} := 214.5 \cdot \mu m$ measured (avg)

$w_{25} := 30.5 \mu m$ measured (avg)

$f_{25} := 78785.1 \cdot Hz$ fn measured

$Q_{25} := 12027(0)$

5 nm   Al coating 02-1

$L_{26} := 449.8 \cdot \mu m$ measured (avg)

$w_{26} := 47 \mu m$ measured (avg)

$f_{26} := 13931 \cdot Hz$ fn measured

$Q_{26} := 7800(0)$

5 nm x 2   Al coating 01-2

$L_{27} := 451 \cdot \mu m$ measured (avg)

$w_{27} := 47.5 \mu m$ measured (avg)

$f_{27} := 13736 \cdot Hz$ fn measured

$Q_{27} := 4000(0)$

10 nm   Al coating 02-3

$L_{28} := 449.5 \cdot \mu m$ measured (avg)

$w_{28} := 47.5 \mu m$ measured (avg)

$f_{28} := 14452 \cdot Hz$ fn measured

$Q_{28} := 3900(0)$

10 nm   Al coating 01-3

$L_{29} := 449 \cdot \mu m$ measured (avg)

$w_{29} := 48 \mu m$ measured (avg)

$f_{29} := 14730 \cdot Hz$ fn measured

$Q_{29} := 3860(0)$

20 nm   Al coating 02-4

$L_{30} := 449.5 \cdot \mu m$ measured (avg)

$w_{30} := 46.25 \mu m$ measured (avg)

$f_{30} := 14450 \cdot Hz$ fn measured

$Q_{30} := 2450(0)$

20 nm   Al coating 01-4

$L_{31} := 448.5 \cdot \mu m$ measured (avg)

$w_{31} := 46.25 \mu m$ measured (avg)

$f_{31} := 13596 \cdot Hz$ fn measured

$Q_{31} := 2200(0)$

30 nm x 2   Al coating 01-5

$L_{32} := 450.75 \cdot \mu m$ measured (avg)

$w_{32} := 46.75 \mu m$ measured (avg)

$f_{32} := 11675 \cdot Hz$ fn measured

$Q_{32} := 480(0)$

30 nm x 2   Al coating 02-5

$L_{33} := 451.5 \cdot \mu m$ measured (avg)

$w_{33} := 46 \mu m$ measured (avg)

$f_{33} := 11628 \cdot Hz$ fn measured

$Q_{33} := 468(0)$

Preliminary Calculations

$$I(w, t) := \frac{1}{12} w \cdot t^3 \qquad A(w, t) := w \cdot t \qquad \text{Rectangular Cantilever Beam}$$

Thickness Calculation

$$t_\alpha(E, I, \rho, w, L, \beta, f) := \left[\frac{\left[\rho \cdot \left(\frac{f \cdot 2 \cdot \pi \cdot L^2}{\beta^2} \right)^2 \right]}{\frac{E}{12}} \right]^{\frac{1}{2}} \qquad \text{rectangular}$$

$$t_\beta(f, L, \beta, E, w1, w2, \rho) := f \cdot \frac{2\pi\, L^2}{\beta^2 \cdot \sqrt{\frac{E \cdot \left(w1^2 + 4 \cdot w1 \cdot w2 + w2^2 \right)}{18 \cdot \rho \cdot (w1 + w2)^2}}}$$

$$w1_{19} := 24.5 \cdot \mu m$$
$$w2_{19} := 56.5 \mu m \qquad \text{trapezoid}$$

$t_{\beta 19} := t_\beta\left(f_{19}, L_{19}, \beta_1, E_0, w1_{19}, w2_{19}, \rho_0 \right) = 6.869 \times 10^{-6}\, m$ ACL assuming trapezoidal shape

$t_9 := t_\alpha\left(E_0, I, \rho_0, w_9, L_9, \beta_1, f_9 \right) = 2.127 \times 10^{-6}\, m$ Beam 2E 10 nm Al coating

$t_{10} := t_\alpha\left(E_0, I, \rho_0, w_{10}, L_{10}, \beta_1, f_{10} \right) = 1.614 \times 10^{-6}\, m$ Beam 1A SICON

$t_{11} := t_\alpha\left(E_0, I, \rho_0, w_{11}, L_{11}, \beta_1, f_{11} \right) = 1.008 \times 10^{-6}\, m$ Beam 1B SHOCON

$t_{12} := t_\alpha\left(E_0, I, \rho_0, w_{12}, L_{12}, \beta_1, f_{12} \right) = 2.61 \times 10^{-6}\, m$ Beam 1C FORT

$t_{13} := t_\alpha\left(E_0, I, \rho_0, w_{13}, L_{13}, \beta_1, f_{13} \right) = 1.976 \times 10^{-6}\, m$ Beam 1E 5 nm Al coating

$t_{14} := t_\alpha\left(E_0, I, \rho_0, w_{14}, L_{14}, \beta_1, f_{14} \right) = 1.582 \times 10^{-6}\, m$ Beam 2A SICON

$t_{15} := t_\alpha\left(E_0, I, \rho_0, w_{15}, L_{15}, \beta_1, f_{15} \right) = 9.238 \times 10^{-7}\, m$ Beam 2B SHOCON

$t_{16} := t_\alpha\left(E_0, I, \rho_0, w_{16}, L_{16}, \beta_1, f_{16} \right) = 2.235 \times 10^{-6}\, m$ Beam 2C FORT

$t_{17} := t_\alpha\left(E_0, I, \rho_0, w_{17}, L_{17}, \beta_1, f_{17} \right) = 1.55 \times 10^{-6}\, m$ Beam 3A SICON

$t_{18} := t_\alpha\left(E_0, I, \rho_0, w_{18}, L_{18}, \beta_1, f_{18} \right) = 1.036 \times 10^{-6}\, m$ Beam 3B SHOCON

$t_{19} := t_\alpha\left(E_0, I, \rho_0, w_{19}, L_{19}, \beta_1, f_{19} \right) = 6.688 \times 10^{-6}\, m$ Beam 3D ACL

$t_{20} := t_\alpha\left(E_0, I, \rho_0, w_{20}, L_{20}, \beta_1, f_{20} \right) = 2.169 \times 10^{-6}\, m$ Beam 3E 20 nm Al coating

$$t_{21} := t_\alpha\left(E_0, I, \rho_0, w_{21}, L_{21}, \beta_1, f_{21}\right) = 2.289 \times 10^{-6}\, m$$ Beam 4A 5 nm x 2 Al coating

$$t_{22} := t_\alpha\left(E_0, I, \rho_0, w_{22}, L_{22}, \beta_1, f_{22}\right) = 9.45 \times 10^{-7}\, m$$ Beam 4B SHOCON

$$t_{23} := t_\alpha\left(E_0, I, \rho_0, w_{23}, L_{23}, \beta_1, f_{23}\right) = 2.605 \times 10^{-6}\, m$$ Beam 4C FORT

$$t_{24} := t_\alpha\left(E_0, I, \rho_0, w_{24}, L_{24}, \beta_1, f_{24}\right) = 1.65 \times 10^{-6}\, m$$ Beam 4E 30 nm x 2 Al coating

$$t_{25} := t_\alpha\left(E_0, I, \rho_0, w_{25}, L_{25}, \beta_1, f_{25}\right) = 2.662 \times 10^{-6}\, m$$ Beam 3C FORT

$$t_{26} := t_\alpha\left(E_0, I, \rho_0, w_{26}, L_{26}, \beta_1, f_{26}\right) = 2.07 \times 10^{-6}\, m$$ 5 nm   Al coating 26

$$t_{27} := t_\alpha\left(E_0, I, \rho_0, w_{27}, L_{27}, \beta_1, f_{27}\right) = 2.052 \times 10^{-6}\, m$$ 5 nm x 2   Al coating 27

$$t_{28} := t_\alpha\left(E_0, I, \rho_0, w_{28}, L_{28}, \beta_1, f_{28}\right) = 2.144 \times 10^{-6}\, m$$ 10 nm   Al coating 28

$$t_{29} := t_\alpha\left(E_0, I, \rho_0, w_{29}, L_{29}, \beta_1, f_{29}\right) = 2.181 \times 10^{-6}\, m$$ 10 nm   Al coating 29

$$t_{30} := t_\alpha\left(E_0, I, \rho_0, w_{30}, L_{30}, \beta_1, f_{30}\right) = 2.144 \times 10^{-6}\, m$$ 20 nm   Al coating 30

$$t_{31} := t_\alpha\left(E_0, I, \rho_0, w_{31}, L_{31}, \beta_1, f_{31}\right) = 2.008 \times 10^{-6}\, m$$ 20 nm   Al coating 31

$$t_{32} := t_\alpha\left(E_0, I, \rho_0, w_{32}, L_{32}, \beta_1, f_{32}\right) = 1.742 \times 10^{-6}\, m$$ 30 nm x 2   Al coating 32

$$t_{33} := t_\alpha\left(E_0, I, \rho_0, w_{33}, L_{33}, \beta_1, f_{33}\right) = 1.741 \times 10^{-6}\, m$$ 30 nm x 2   Al coating 33

Uncertainty in thickness

$$\delta t_\alpha(E, \rho, w, L, \beta, f, \delta E, \delta\rho, \delta w, \delta L, \delta\beta, \delta f) := \left[\left[\left(\frac{d}{dE} t_\alpha(E, I, \rho, w, L, \beta, f) \right) \cdot \delta E \right]^2 \ldots \\ + \left[\left(\frac{d}{d\rho} t_\alpha(E, I, \rho, w, L, \beta, f) \right) \cdot \delta\rho \right]^2 \ldots \\ + \left[\left(\frac{d}{dw} t_\alpha(E, I, \rho, w, L, \beta, f) \right) \cdot \delta w \right]^2 \ldots \\ + \left[\left(\frac{d}{dL} t_\alpha(E, I, \rho, w, L, \beta, f) \right) \cdot \delta L \right]^2 \ldots \\ + \left[\left(\frac{d}{d\beta} t_\alpha(E, I, \rho, w, L, \beta, f) \right) \cdot \delta\beta \right]^2 \ldots \\ + \left[\left(\frac{d}{df} t_\alpha(E, I, \rho, w, L, \beta, f) \right) \cdot \delta f \right]^2 \right]^{\frac{1}{2}}$$

$$\delta t_{\alpha 9} := \delta t_{\alpha}\left(E_0, \rho_0, w_9, L_9, \beta_1, f_9, \delta E, \delta\rho, \delta w, \delta L, \delta\beta, \delta f\right) = 4.742 \times 10^{-8} \, \text{m}$$

Beam 2E 10 nm Al coating

$$\delta t_{\alpha 10} := \delta t_{\alpha}\left(E_0, \rho_0, w_{10}, L_{10}, \beta_1, f_{10}, \delta E, \delta\rho, \delta w, \delta L, \delta\beta, \delta f\right) = 3.6 \times 10^{-8} \, \text{m}$$

Beam 1A SICON

$$\delta t_{\alpha 11} := \delta t_{\alpha}\left(E_0, \rho_0, w_{11}, L_{11}, \beta_1, f_{11}, \delta E, \delta\rho, \delta w, \delta L, \delta\beta, \delta f\right) = 2.369 \times 10^{-8} \, \text{m}$$

Beam 1B SHOCON

$$\delta t_{\alpha 12} := \delta t_{\alpha}\left(E_0, \rho_0, w_{12}, L_{12}, \beta_1, f_{12}, \delta E, \delta\rho, \delta w, \delta L, \delta\beta, \delta f\right) = 6.204 \times 10^{-8} \, \text{m}$$

Beam 1C FORT

$$\delta t_{\alpha 13} := \delta t_{\alpha}\left(E_0, \rho_0, w_{13}, L_{13}, \beta_1, f_{13}, \delta E, \delta\rho, \delta w, \delta L, \delta\beta, \delta f\right) = 4.407 \times 10^{-8} \, \text{m}$$

Beam 1E 5 nm Al coating

$$\delta t_{\alpha 14} := \delta t_{\alpha}\left(E_0, \rho_0, w_{14}, L_{14}, \beta_1, f_{14}, \delta E, \delta\rho, \delta w, \delta L, \delta\beta, \delta f\right) = 3.527 \times 10^{-8} \, \text{m}$$

Beam 2A SICON

$$\delta t_{\alpha 15} := \delta t_{\alpha}\left(E_0, \rho_0, w_{15}, L_{15}, \beta_1, f_{15}, \delta E, \delta\rho, \delta w, \delta L, \delta\beta, \delta f\right) = 2.173 \times 10^{-8} \, \text{m}$$

Beam 2B SHOCON

$$\delta t_{\alpha 16} := \delta t_{\alpha}\left(E_0, \rho_0, w_{16}, L_{16}, \beta_1, f_{16}, \delta E, \delta\rho, \delta w, \delta L, \delta\beta, \delta f\right) = 5.315 \times 10^{-8} \, \text{m}$$

Beam 2C FORT

$$\delta t_{\alpha 17} := \delta t_{\alpha}\left(E_0, \rho_0, w_{17}, L_{17}, \beta_1, f_{17}, \delta E, \delta\rho, \delta w, \delta L, \delta\beta, \delta f\right) = 3.456 \times 10^{-8} \, \text{m}$$

Beam 3A SICON

$$\delta t_{\alpha 18} := \delta t_{\alpha}\left(E_0, \rho_0, w_{18}, L_{18}, \beta_1, f_{18}, \delta E, \delta\rho, \delta w, \delta L, \delta\beta, \delta f\right) = 2.431 \times 10^{-8} \, \text{m}$$

Beam 3B SHOCON

$$\delta t_{\alpha 19} := \delta t_{\alpha}\left(E_0, \rho_0, w_{19}, L_{19}, \beta_1, f_{19}, \delta E, \delta\rho, \delta w, \delta L, \delta\beta, \delta f\right) = 1.571 \times 10^{-7} \, \text{m}$$

Beam 3D ACL

$$\delta t_{\alpha 20} := \delta t_{\alpha}\left(E_0, \rho_0, w_{20}, L_{20}, \beta_1, f_{20}, \delta E, \delta\rho, \delta w, \delta L, \delta\beta, \delta f\right) = 4.835 \times 10^{-8} \, \text{m}$$

Beam 3E 20 nm Al coating

$$\delta t_{\alpha 21} := \delta t_{\alpha}\left(E_0, \rho_0, w_{21}, L_{21}, \beta_1, f_{21}, \delta E, \delta\rho, \delta w, \delta L, \delta\beta, \delta f\right) = 5.104 \times 10^{-8} \, \text{m}$$

Beam 4A 5 nm x 2 Al coating

$$\delta t_{\alpha 22} := \delta t_{\alpha}\left(E_0, \rho_0, w_{22}, L_{22}, \beta_1, f_{22}, \delta E, \delta\rho, \delta w, \delta L, \delta\beta, \delta f\right) = 2.22 \times 10^{-8} \, \text{m}$$

Beam 4B SHOCON

$$\delta t_{\alpha 23} := \delta t_{\alpha}\left(E_0, \rho_0, w_{23}, L_{23}, \beta_1, f_{23}, \delta E, \delta\rho, \delta w, \delta L, \delta\beta, \delta f\right) = 6.188 \times 10^{-8} \, \text{m}$$

Beam 4C FORT

$$\delta t_{\alpha 24} := \delta t_{\alpha}\left(E_0, \rho_0, w_{24}, L_{24}, \beta_1, f_{24}, \delta E, \delta\rho, \delta w, \delta L, \delta\beta, \delta f\right) = 3.678 \times 10^{-8} \, \text{m}$$

Beam 4E 30 nm x 2 Al coating

$$\delta t_{\alpha 25} := \delta t_{\alpha}\left(E_0, \rho_0, w_{25}, L_{25}, \beta_1, f_{25}, \delta E, \delta\rho, \delta w, \delta L, \delta\beta, \delta f\right) = 6.323 \times 10^{-8} \, \text{m}$$

Beam 3C FORT

$$\delta t_{\alpha 26} := \delta t_{\alpha}\left(E_0, \rho_0, w_{26}, L_{26}, \beta_1, f_{26}, \delta E, \delta\rho, \delta w, \delta L, \delta\beta, \delta f\right) = 4.614 \times 10^{-8} \, \text{m}$$

5 nm   Al coating 26

$$\delta t_{\alpha 27} := \delta t_{\alpha}\left(E_0, \rho_0, w_{27}, L_{27}, \beta_1, f_{27}, \delta E, \delta\rho, \delta w, \delta L, \delta\beta, \delta f\right) = 4.574 \times 10^{-8} \, \text{m}$$

5 nm x 2   Al coating 27

$$\delta t_{\alpha 28} := \delta t_{\alpha}\left(E_0, \rho_0, w_{28}, L_{28}, \beta_1, f_{28}, \delta E, \delta\rho, \delta w, \delta L, \delta\beta, \delta f\right) = 4.781 \times 10^{-8} \, \text{m}$$

10 nm   Al coating 28

$$\delta t_{\alpha 29} := \delta t_{\alpha}\left(E_0, \rho_0, w_{29}, L_{29}, \beta_1, f_{29}, \delta E, \delta\rho, \delta w, \delta L, \delta\beta, \delta f\right) = 4.862 \times 10^{-8} \, \text{m}$$

10 nm   Al coating 29

$$\delta t_{\alpha 30} := \delta t_{\alpha}\left(E_0, \rho_0, w_{30}, L_{30}, \beta_1, f_{30}, \delta E, \delta\rho, \delta w, \delta L, \delta\beta, \delta f\right) = 4.78 \times 10^{-8} \, \text{m}$$

20 nm   Al coating 30

$$\delta t_{\alpha 31} := \delta t_{\alpha}\left(E_0, \rho_0, w_{31}, L_{31}, \beta_1, f_{31}, \delta E, \delta\rho, \delta w, \delta L, \delta\beta, \delta f\right) = 4.478 \times 10^{-8} \, \text{m}$$

20 nm   Al coating 31

$$\delta t_{\alpha 32} := \delta t_{\alpha}\left(E_0, \rho_0, w_{32}, L_{32}, \beta_1, f_{32}, \delta E, \delta\rho, \delta w, \delta L, \delta\beta, \delta f\right) = 3.883 \times 10^{-8} \, \text{m}$$

30 nm x 2   Al coating 32

$$\delta t_{\alpha 33} := \delta t_{\alpha}\left(E_0, \rho_0, w_{33}, L_{33}, \beta_1, f_{33}, \delta E, \delta\rho, \delta w, \delta L, \delta\beta, \delta f\right) = 3.88 \times 10^{-8} \, \text{m}$$

30 nm x 2   Al coating 33

Calculated Resonant Frequencies

$$f_{n1}(E,\rho,w,t,L) := \frac{\beta_1^2}{2\cdot\pi\, L^2}\cdot\sqrt{\frac{E\cdot I(w,t)}{\rho\cdot A(w,t)}} \qquad f_{n1}(E_0,\rho_0,w_0,t_0,L_0) = 13.44898\cdot KH_z$$

$$f_{n2}(E,\rho,w,t,L) := \frac{\beta_2^2}{2\cdot\pi\, L^2}\cdot\sqrt{\frac{E\cdot I(w,t)}{\rho\cdot A(w,t)}} \qquad f_{n2}(E_0,\rho_0,w_0,t_0,L_0) = 84.28938\cdot KH_z$$

$$f_{n3}(E,\rho,w,t,L) := \frac{\beta_3^2}{2\cdot\pi\, L^2}\cdot\sqrt{\frac{E\cdot I(w,t)}{\rho\cdot A(w,t)}} \qquad f_{n3}(E_0,\rho_0,w_0,t_0,L_0) = 236.03644\cdot KH_z$$

$$f_{n4}(E,\rho,w,t,L) := \frac{\beta_4^2}{2\cdot\pi\, L^2}\cdot\sqrt{\frac{E\cdot I(w,t)}{\rho\cdot A(w,t)}} \qquad f_{n4}(E_0,\rho_0,w_0,t_0,L_0) = 462.54729\cdot KH_z$$

$$f_{n5}(E,\rho,w,t,L) := \frac{\beta_5^2}{2\cdot\pi\, L^2}\cdot\sqrt{\frac{E\cdot I(w,t)}{\rho\cdot A(w,t)}} \qquad f_{n5}(E_0,\rho_0,w_0,t_0,L_0) = 764.54174\cdot KH_z$$

$$f_{n6}(E,\rho,w,t,L) := \frac{\beta_6^2}{2\cdot\pi\, L^2}\cdot\sqrt{\frac{E\cdot I(w,t)}{\rho\cdot A(w,t)}} \qquad f_{n6}(E_0,\rho_0,w_0,t_0,L_0) = 1142.15197\cdot KH_z$$

Air Damping

$$K_m := \sqrt{\frac{32\cdot M}{R\cdot T_0}} = 6.117\times 10^{-4}\frac{s}{m} \qquad Q_{air}(f_n,t,\rho,K_m,P) := \frac{2\cdot\pi\cdot f_n\cdot t\cdot\rho}{K_m\cdot P} \qquad \text{note, only valid in molecular region}$$

$$Q_{air}(f_9,t_9,\rho_0,K_m,P_1) = 7.235$$

$$Q_{air}(f_9,t_9,\rho_0,K_m,P_2) = 84.124$$

$$Q_{air}(f_9,t_9,\rho_0,K_m,P_3) = 723.468$$

$$Q_{air}(f_9,t_9,\rho_0,K_m,P_4) = 6.029\times 10^3$$

$$Q_{air}(f_9,t_9,\rho_0,K_m,P_5) = 7.235\times 10^4$$

$$Q_{air}(f_9,t_9,\rho_0,K_m,P_6) = 1.809\times 10^5$$

$$Q_{air}(f_9,t_9,\rho_0,K_m,P_7) = 5.168\times 10^5$$

$$Q_{air}(f_9,t_9,\rho_0,K_m,P_8) = 4.522\times 10^7$$

$$Q_{airtheory} := \begin{pmatrix} 7.234 \\ 84.113 \\ 723.371 \\ 6.028\times 10^3 \\ 7.234\times 10^4 \\ 1.808\times 10^5 \\ 5.167\times 10^5 \\ 4.521\times 10^7 \\ 1.34\times 10^8 \\ 2.893\times 10^8 \\ 1.148\times 10^9 \end{pmatrix} \qquad P := \begin{pmatrix} 1\cdot 10^5 \\ 8.6\cdot 10^3 \\ 1\cdot 10^3 \\ 1.2\cdot 10^2 \\ 1\cdot 10^1 \\ 4 \\ 1.4 \\ 1.6\cdot 10^{-2} \\ 5.4\cdot 10^{-3} \\ 2.5\cdot 10^{-3} \\ 6.3\cdot 10^{-4} \end{pmatrix} \qquad Q_{exp} := \begin{pmatrix} 47 \\ 148 \\ 198 \\ 593 \\ 5187 \\ 11334 \\ 21782 \\ 32787 \\ 34803 \\ 37154 \\ 39704 \end{pmatrix}$$

$$Q_{air}\left(f_9, t_9, \rho_0, K_m, P_9\right) = 1.34 \times 10^8$$

$$Q_{air}\left(f_9, t_9, \rho_0, K_m, P_{10}\right) = 2.894 \times 10^8$$

$$Q_{air}\left(f_9, t_9, \rho_0, K_m, P_{11}\right) = 1.148 \times 10^9$$

$$Q_{airexp1} := \left[\left(Q_{exp_0}\right)^{-1} - \left(Q_{exp_{10}}\right)^{-1}\right]^{-1} = 47.056$$

$$Q_{airexp2} := \left[\left(Q_{exp_1}\right)^{-1} - \left(Q_{exp_{10}}\right)^{-1}\right]^{-1} = 148.554$$

$$Q_{airexp3} := \left[\left(Q_{exp_2}\right)^{-1} - \left(Q_{exp_{10}}\right)^{-1}\right]^{-1} = 198.992$$

$$Q_{airexp4} := \left[\left(Q_{exp_3}\right)^{-1} - \left(Q_{exp_{10}}\right)^{-1}\right]^{-1} = 601.991$$

$$Q_{airexp5} := \left[\left(Q_{exp_4}\right)^{-1} - \left(Q_{exp_{10}}\right)^{-1}\right]^{-1} = 5.966 \times 10^3$$

$$Q_{airexp6} := \left[\left(Q_{exp_5}\right)^{-1} - \left(Q_{exp_{10}}\right)^{-1}\right]^{-1} = 1.586 \times 10^4$$

$$Q_{airexp7} := \left[\left(Q_{exp_6}\right)^{-1} - \left(Q_{exp_{10}}\right)^{-1}\right]^{-1} = 4.826 \times 10^4$$

$$Q_{airexp8} := \left[\left(Q_{exp_7}\right)^{-1} - \left(Q_{exp_{10}}\right)^{-1}\right]^{-1} = 1.882 \times 10^5$$

$$Q_{airexp9} := \left[\left(Q_{exp_8}\right)^{-1} - \left(Q_{exp_{10}}\right)^{-1}\right]^{-1} = 2.819 \times 10^5$$

$$Q_{airexp10} := \left[\left(Q_{exp_9}\right)^{-1} - \left(Q_{exp_{10}}\right)^{-1}\right]^{-1} = 5.785 \times 10^5$$

$$Q_{airexp} := \begin{pmatrix} 47.056 \\ 148.554 \\ 198.992 \\ 601.991 \\ 5.966 \times 10^3 \\ 1.586 \times 10^4 \\ 4.826 \times 10^4 \\ 1.882 \times 10^5 \\ 2.819 \times 10^5 \\ 5.785 \times 10^5 \\ 0 \end{pmatrix}$$
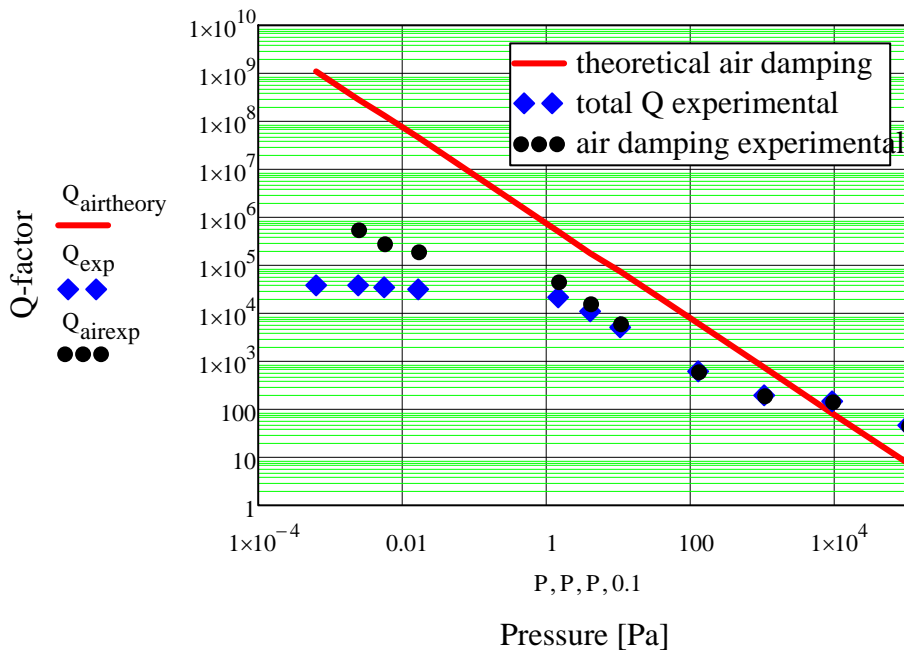
TED

$$F_0(k, \rho, c_p, t) := \frac{\pi \cdot k}{2 \cdot \rho \cdot c_p \cdot t^2}$$ characteristic damping frequency

$$\chi(k, c_p, \rho) := \frac{k}{c_p \cdot \rho}$$

$$\omega(E, \rho, w, t, L) := f_{n1}(E, \rho, w, t, L) \cdot 2 \cdot \pi$$

$$\tau_z(t, k, c_p, \rho) := \frac{t^2}{\pi^2 \cdot \chi(k, c_p, \rho)}$$

$$\xi(E, \rho, k, c_p, w, t, L) := t \cdot \sqrt{\frac{\omega(E, \rho, w, t, L)}{2\chi(k, c_p, \rho)}}$$

$$Q_Z(E, \rho, k, c_p, \alpha, T, w, t, L) := \left[\frac{E \cdot \alpha^2 \cdot T}{c_p \cdot \rho} \cdot \frac{\omega(E, \rho, w, t, L) \cdot \tau_z(t, k, c_p, \rho)}{1 + \left(\omega(E, \rho, w, t, L) \cdot \tau_z(t, k, c_p, \rho) \right)^2} \right]^{-1}$$ Zener Equation

114

$$Q_L\left(E, \rho, k, c_p, \alpha, T, w, t, L\right) := \cfrac{1}{\left[\cfrac{E \cdot \alpha^2 \cdot T}{c_p \cdot \rho}\left(\cfrac{6}{\xi\left(E, \rho, k, c_p, w, t, L\right)^2} - \cfrac{6}{\xi\left(E, \rho, k, c_p, w, t, L\right)^3} \cdot \cfrac{\sinh\left(\xi\left(E, \rho, k, c_p, w, t, L\right)\right) \dots + \sin\left(\xi\left(E, \rho, k, c_p, w, t, L\right)\right)}{\cosh\left(\xi\left(E, \rho, k, c_p, w, t, L\right)\right) \dots + \cos\left(\xi\left(E, \rho, k, c_p, w, t, L\right)\right)}\right)\right]}$$

Lifshitz Equation

prospective samples

$Q_Z\left(E_0, \rho_0, k_0, c_{p.0}, \alpha_0, T_0, w_0, t_0, L_0\right) = 1.4 \times 10^7$

$Q_Z\left(E_0, \rho_0, k_0, c_{p.0}, \alpha_0, T_0, w_1, t_1, L_1\right) = 2.801 \times 10^7$ $Q_Z\left(E_0, \rho_0, k_0, c_{p.0}, \alpha_0, T_0, w_5, t_5, L_5\right) = 4.612 \times 10^4$

$Q_Z\left(E_0, \rho_0, k_0, c_{p.0}, \alpha_0, T_0, w_2, t_2, L_2\right) = 7.17 \times 10^6$ $Q_Z\left(E_0, \rho_0, k_0, c_{p.0}, \alpha_0, T_0, w_6, t_6, L_6\right) = 7.967 \times 10^5$

$Q_Z\left(E_0, \rho_0, k_0, c_{p.0}, \alpha_0, T_0, w_3, t_3, L_3\right) = 1.037 \times 10^6$ $Q_Z\left(E_N, \rho_N, k_N, c_{p.N}, \alpha_N, T_0, w_7, t_7, L_7\right) = 1.225 \times 10^7$

$Q_Z\left(E_0, \rho_0, k_0, c_{p.0}, \alpha_0, T_0, w_4, t_4, L_4\right) = 9.511 \times 10^4$ $Q_Z\left(E_N, \rho_N, k_N, c_{p.N}, \alpha_N, T_0, w_8, t_8, L_8\right) = 7.26 \times 10^6$

Actual Beams

$Q_{Z9} := Q_Z\left(E_0, \rho_0, k_0, c_{p.0}, \alpha_0, T_0, w_9, t_9, L_9\right) = 1.172 \times 10^7$ Beam 2E 10 nm Al coating

$Q_{Z10} := Q_Z\left(E_0, \rho_0, k_0, c_{p.0}, \alpha_0, T_0, w_{10}, t_{10}, L_{10}\right) = 2.617 \times 10^7$ Beam 1A SICON

$Q_{Z11} := Q_Z\left(E_0, \rho_0, k_0, c_{p.0}, \alpha_0, T_0, w_{11}, t_{11}, L_{11}\right) = 2.88 \times 10^7$ Beam 1B SHOCON

$Q_{Z12} := Q_Z\left(E_0, \rho_0, k_0, c_{p.0}, \alpha_0, T_0, w_{12}, t_{12}, L_{12}\right) = 1.419 \times 10^6$ Beam 1C FORT

$Q_{Z13} := Q_Z\left(E_0, \rho_0, k_0, c_{p.0}, \alpha_0, T_0, w_{13}, t_{13}, L_{13}\right) = 1.432 \times 10^7$ Beam 1E 5 nm Al coating

$Q_{Z14} := Q_Z\left(E_0, \rho_0, k_0, c_{p.0}, \alpha_0, T_0, w_{14}, t_{14}, L_{14}\right) = 2.795 \times 10^7$ Beam 2A SICON

$Q_{Z15} := Q_Z\left(E_0, \rho_0, k_0, c_{p.0}, \alpha_0, T_0, w_{15}, t_{15}, L_{15}\right) = 3.681 \times 10^7$ Beam 2B SHOCON

$Q_{Z16} := Q_Z\left(E_0, \rho_0, k_0, c_{p.0}, \alpha_0, T_0, w_{16}, t_{16}, L_{16}\right) = 2.248 \times 10^6$ Beam 2C FORT

$Q_{Z17} := Q_Z\left(E_0, \rho_0, k_0, c_{p.0}, \alpha_0, T_0, w_{17}, t_{17}, L_{17}\right) = 2.956 \times 10^7$ Beam 3A SICON

$Q_{Z18} := Q_Z\left(E_0, \rho_0, k_0, c_{p.0}, \alpha_0, T_0, w_{18}, t_{18}, L_{18}\right) = 2.71 \times 10^7$ Beam 3B SHOCON

$Q_{Z19} := Q_Z\left(E_0, \rho_0, k_0, c_{p.0}, \alpha_0, T_0, w_{19}, t_{19}, L_{19}\right) = 9.977 \times 10^4$ Beam 3D ACL

$Q_{Z20} := Q_Z\left(E_0, \rho_0, k_0, c_{p.0}, \alpha_0, T_0, w_{20}, t_{20}, L_{20}\right) = 1.089 \times 10^7$ Beam 3E 20 nm Al coating

$Q_{Z21} := 9.317 \cdot 10^6$ Beam 4A 5 nm x 2 Al coating

$Q_{Z22} := Q_Z\left(E_0, \rho_0, k_0, c_{p.0}, \alpha_0, T_0, w_{22}, t_{22}, L_{22}\right) = 3.514 \times 10^7$ Beam 4B SHOCON

$$Q_{Z23} := Q_Z(E_0, \rho_0, k_0, c_{p.0}, \alpha_0, T_0, w_{23}, t_{23}, L_{23}) = 1.438 \times 10^6$$ Beam 4C FORT

$$Q_{Z24} := Q_Z(E_0, \rho_0, k_0, c_{p.0}, \alpha_0, T_0, w_{24}, t_{24}, L_{24}) = 2.503 \times 10^7$$ Beam 4E 30 nm x 2 Al coating

$$Q_{Z25} := Q_Z(E_0, \rho_0, k_0, c_{p.0}, \alpha_0, T_0, w_{25}, t_{25}, L_{25}) = 1.349 \times 10^6$$ Beam 3C FORT

$$Q_{Z26} := 1.262 \cdot 10^6$$ 5 nm   Al coating 26

$$Q_{Z27} := Q_Z(E_0, \rho_0, k_0, c_{p.0}, \alpha_0, T_0, w_{27}, t_{27}, L_{27}) = 1.303 \times 10^7$$ 5 nm x 2   Al coating 27

$$Q_{Z28} := Q_Z(E_0, \rho_0, k_0, c_{p.0}, \alpha_0, T_0, w_{28}, t_{28}, L_{28}) = 1.134 \times 10^7$$ 10 nm   Al coating 28

$$Q_{Z29} := Q_Z(E_0, \rho_0, k_0, c_{p.0}, \alpha_0, T_0, w_{29}, t_{29}, L_{29}) = 1.075 \times 10^7$$ 10 nm   Al coating 29

$$Q_{Z30} := Q_Z(E_0, \rho_0, k_0, c_{p.0}, \alpha_0, T_0, w_{30}, t_{30}, L_{30}) = 1.134 \times 10^7$$ 20 nm   Al coating 30

$$Q_{Z31} := 1.374 \cdot 10^6$$ 20 nm   Al coating 31

$$Q_{Z32} := Q_Z(E_0, \rho_0, k_0, c_{p.0}, \alpha_0, T_0, w_{32}, t_{32}, L_{32}) = 2.127 \times 10^7$$ 30 nm x 2   Al coating 32

$$Q_{Z33} := Q_Z(E_0, \rho_0, k_0, c_{p.0}, \alpha_0, T_0, w_{33}, t_{33}, L_{33}) = 2.138 \times 10^7$$ 30 nm x 2   Al coating 33

TED Lifshitz

$$Q_{L9} := Q_L(E_0, \rho_0, k_0, c_{p.0}, \alpha_0, T_0, w_9, t_9, L_9) = 1.187 \times 10^7$$ Beam 2E 10 nm Al coating

$$Q_{L10} := Q_L(E_0, \rho_0, k_0, c_{p.0}, \alpha_0, T_0, w_{10}, t_{10}, L_{10}) = 2.651 \times 10^7$$ Beam 1A SICON

$$Q_{L11} := Q_L(E_0, \rho_0, k_0, c_{p.0}, \alpha_0, T_0, w_{11}, t_{11}, L_{11}) = 2.918 \times 10^7$$ Beam 1B SHOCON

$$Q_{L12} := Q_L(E_0, \rho_0, k_0, c_{p.0}, \alpha_0, T_0, w_{12}, t_{12}, L_{12}) = 1.437 \times 10^6$$ Beam 1C FORT

$$Q_{L13} := Q_L(E_0, \rho_0, k_0, c_{p.0}, \alpha_0, T_0, w_{13}, t_{13}, L_{13}) = 1.451 \times 10^7$$ Beam 1E 5 nm Al coating

$$Q_{L14} := Q_L(E_0, \rho_0, k_0, c_{p.0}, \alpha_0, T_0, w_{14}, t_{14}, L_{14}) = 2.831 \times 10^7$$ Beam 2A SICON

$$Q_{L15} := Q_L(E_0, \rho_0, k_0, c_{p.0}, \alpha_0, T_0, w_{15}, t_{15}, L_{15}) = 3.729 \times 10^7$$ Beam 2B SHOCON

$$Q_{L16} := Q_L(E_0, \rho_0, k_0, c_{p.0}, \alpha_0, T_0, w_{16}, t_{16}, L_{16}) = 2.278 \times 10^6$$ Beam 2C FORT

$$Q_{L17} := Q_L(E_0, \rho_0, k_0, c_{p.0}, \alpha_0, T_0, w_{17}, t_{17}, L_{17}) = 2.995 \times 10^7$$ Beam 3A SICON

$$Q_{L18} := Q_L(E_0, \rho_0, k_0, c_{p.0}, \alpha_0, T_0, w_{18}, t_{18}, L_{18}) = 2.746 \times 10^7$$ Beam 3B SHOCON

$$Q_{L19} := Q_L(E_0, \rho_0, k_0, c_{p.0}, \alpha_0, T_0, w_{19}, t_{19}, L_{19}) = 1.011 \times 10^5$$ Beam 3D ACL

$$Q_{L20} := Q_L(E_0, \rho_0, k_0, c_{p.0}, \alpha_0, T_0, w_{20}, t_{20}, L_{20}) = 1.103 \times 10^7$$ Beam 3E 20 nm Al coating

$$Q_{L21} := Q_L(E_0, \rho_0, k_0, c_{p.0}, \alpha_0, T_0, w_{21}, t_{21}, L_{21}) = 9.44 \times 10^6$$ Beam 4A 5 nm x 2 Al coating

$$Q_{L22} := Q_L(E_0, \rho_0, k_0, c_{p.0}, \alpha_0, T_0, w_{22}, t_{22}, L_{22}) = 3.56 \times 10^7$$ Beam 4B SHOCON

$Q_{L23} := Q_L\left(E_0, \rho_0, k_0, c_{p.0}, \alpha_0, T_0, w_{23}, t_{23}, L_{23}\right) = 1.457 \times 10^6$ Beam 4C FORT

$Q_{L24} := Q_L\left(E_0, \rho_0, k_0, c_{p.0}, \alpha_0, T_0, w_{24}, t_{24}, L_{24}\right) = 2.536 \times 10^7$ Beam 4E 30 nm x 2 Al coating

$Q_{L25} := Q_L\left(E_0, \rho_0, k_0, c_{p.0}, \alpha_0, T_0, w_{25}, t_{25}, L_{25}\right) = 1.367 \times 10^6$ Beam 3C FORT

$Q_{L26} := Q_L\left(E_0, \rho_0, k_0, c_{p.0}, \alpha_0, T_0, w_{26}, t_{26}, L_{26}\right) = 1.279 \times 10^7$ 5 nm   Al coating 26

$Q_{L27} := Q_L\left(E_0, \rho_0, k_0, c_{p.0}, \alpha_0, T_0, w_{27}, t_{27}, L_{27}\right) = 1.32 \times 10^7$ 5 nm x 2   Al coating 27

$Q_{L28} := Q_L\left(E_0, \rho_0, k_0, c_{p.0}, \alpha_0, T_0, w_{28}, t_{28}, L_{28}\right) = 1.149 \times 10^7$ 10 nm   Al coating 28

$Q_{L29} := Q_L\left(E_0, \rho_0, k_0, c_{p.0}, \alpha_0, T_0, w_{29}, t_{29}, L_{29}\right) = 1.09 \times 10^7$ 10 nm   Al coating 29

$Q_{L30} := Q_L\left(E_0, \rho_0, k_0, c_{p.0}, \alpha_0, T_0, w_{30}, t_{30}, L_{30}\right) = 1.149 \times 10^7$ 20 nm   Al coating 30

$Q_{L31} := Q_L\left(E_0, \rho_0, k_0, c_{p.0}, \alpha_0, T_0, w_{31}, t_{31}, L_{31}\right) = 1.392 \times 10^7$ 20 nm   Al coating 31

$Q_{L32} := Q_L\left(E_0, \rho_0, k_0, c_{p.0}, \alpha_0, T_0, w_{32}, t_{32}, L_{32}\right) = 2.155 \times 10^7$ 30 nm x 2   Al coating 32

30 nm x 2   Al coating 33

$Q_{L33} := 2.166 \cdot 10^7$

uncertainty TED Zener

$$\delta Q_Z\left(E, \rho, k, c_p, \alpha, T, w, t, L, \delta E, \delta\rho, \delta k, \delta c_p, \delta\alpha, \delta T, \delta w, \delta t, \delta L\right) := \left[\begin{array}{l} \left[\left(\dfrac{d}{dE} Q_Z\left(E, \rho, k, c_p, \alpha, T, w, t, L\right)\right) \cdot \delta E\right]^2 \ldots \\[6pt] + \left[\left(\dfrac{d}{d\rho} Q_Z\left(E, \rho, k, c_p, \alpha, T, w, t, L\right)\right) \cdot \delta\rho\right]^2 \ldots \\[6pt] + \left[\left(\dfrac{d}{dk} Q_Z\left(E, \rho, k, c_p, \alpha, T, w, t, L\right)\right) \cdot \delta k\right]^2 \ldots \\[6pt] + \left[\left(\dfrac{d}{dc_p} Q_Z\left(E, \rho, k, c_p, \alpha, T, w, t, L\right)\right) \cdot \delta c_p\right]^2 \ldots \\[6pt] + \left[\left(\dfrac{d}{d\alpha} Q_Z\left(E, \rho, k, c_p, \alpha, T, w, t, L\right)\right) \cdot \delta\alpha\right]^2 \ldots \\[6pt] + \left[\left(\dfrac{d}{dT} Q_Z\left(E, \rho, k, c_p, \alpha, T, w, t, L\right)\right) \cdot \delta T\right]^2 \ldots \\[6pt] + \left[\left(\dfrac{d}{dw} Q_Z\left(E, \rho, k, c_p, \alpha, T, w, t, L\right)\right) \cdot \delta w\right]^2 \ldots \\[6pt] + \left[\left(\dfrac{d}{dt} Q_Z\left(E, \rho, k, c_p, \alpha, T, w, t, L\right)\right) \cdot \delta t\right]^2 \ldots \\[6pt] + \left[\left(\dfrac{d}{dL} Q_Z\left(E, \rho, k, c_p, \alpha, T, w, t, L\right)\right) \cdot \delta L\right]^2 \end{array} \right]^{\frac{1}{2}}$$

$$\delta Q_{Z9} := \delta Q_Z\left(E_0, \rho_0, k_0, c_{p.0}, \alpha_0, T_0, w_9, t_9, L_9, \delta E, \delta\rho, \delta k, \delta c_p, \delta\alpha, \delta T, \delta w, \delta t_{\alpha 9}, \delta L\right) = 1.559 \times 10^6$$ 2E 10 nm Al

$$\delta Q_{Z10} := \delta Q_Z\left(E_0, \rho_0, k_0, c_{p.0}, \alpha_0, T_0, w_{10}, t_{10}, L_{10}, \delta E, \delta\rho, \delta k, \delta c_p, \delta\alpha, \delta T, \delta w, \delta t_{\alpha 10}, \delta L\right) = 3.482 \times 10^6$$ 1A SICON

$$\delta Q_{Z11} := \delta Q_Z\left(E_0, \rho_0, k_0, c_{p.0}, \alpha_0, T_0, w_{11}, t_{11}, L_{11}, \delta E, \delta\rho, \delta k, \delta c_p, \delta\alpha, \delta T, \delta w, \delta t_{\alpha 11}, \delta L\right) = 3.891 \times 10^6$$ 1B SHOCON

$$\delta Q_{Z12} := \delta Q_Z\left(E_0, \rho_0, k_0, c_{p.0}, \alpha_0, T_0, w_{12}, t_{12}, L_{12}, \delta E, \delta\rho, \delta k, \delta c_p, \delta\alpha, \delta T, \delta w, \delta t_{\alpha 12}, \delta L\right) = 1.923 \times 10^5$$ 1C FORT

$$\delta Q_{Z13} := \delta Q_Z\left(E_0, \rho_0, k_0, c_{p.0}, \alpha_0, T_0, w_{13}, t_{13}, L_{13}, \delta E, \delta\rho, \delta k, \delta c_p, \delta\alpha, \delta T, \delta w, \delta t_{\alpha 13}, \delta L\right) = 1.905 \times 10^6$$ 1E 5 nm Al

$$\delta Q_{Z14} := \delta Q_Z\left(E_0, \rho_0, k_0, c_{p.0}, \alpha_0, T_0, w_{14}, t_{14}, L_{14}, \delta E, \delta\rho, \delta k, \delta c_p, \delta\alpha, \delta T, \delta w, \delta t_{\alpha 14}, \delta L\right) = 3.718 \times 10^6$$ 2A SICON

$$\delta Q_{Z15} := \delta Q_Z\left(E_0, \rho_0, k_0, c_{p.0}, \alpha_0, T_0, w_{15}, t_{15}, L_{15}, \delta E, \delta\rho, \delta k, \delta c_p, \delta\alpha, \delta T, \delta w, \delta t_{\alpha 15}, \delta L\right) = 4.974 \times 10^6$$ 2B SHOCON

$$\delta Q_{Z16} := \delta Q_Z\left(E_0, \rho_0, k_0, c_{p.0}, \alpha_0, T_0, w_{16}, t_{16}, L_{16}, \delta E, \delta\rho, \delta k, \delta c_p, \delta\alpha, \delta T, \delta w, \delta t_{\alpha 16}, \delta L\right) = 3.048 \times 10^5$$ 2C FORT

$$\delta Q_{Z17} := \delta Q_Z\left(E_0, \rho_0, k_0, c_{p.0}, \alpha_0, T_0, w_{17}, t_{17}, L_{17}, \delta E, \delta\rho, \delta k, \delta c_p, \delta\alpha, \delta T, \delta w, \delta t_{\alpha 17}, \delta L\right) = 3.933 \times 10^6$$ 3A SICON

$$\delta Q_{Z18} := \delta Q_Z\left(E_0, \rho_0, k_0, c_{p.0}, \alpha_0, T_0, w_{18}, t_{18}, L_{18}, \delta E, \delta\rho, \delta k, \delta c_p, \delta\alpha, \delta T, \delta w, \delta t_{\alpha 18}, \delta L\right) = 3.66 \times 10^6$$ 3B SHOCON

$$\delta Q_{Z19} := \delta Q_Z\left(E_0, \rho_0, k_0, c_{p.0}, \alpha_0, T_0, w_{19}, t_{19}, L_{19}, \delta E, \delta\rho, \delta k, \delta c_p, \delta\alpha, \delta T, \delta w, \delta t_{\alpha 19}, \delta L\right) = 1.344 \times 10^4$$ 3D ACL

$$\delta Q_{Z20} := \delta Q_Z\left(E_0, \rho_0, k_0, c_{p.0}, \alpha_0, T_0, w_{20}, t_{20}, L_{20}, \delta E, \delta\rho, \delta k, \delta c_p, \delta\alpha, \delta T, \delta w, \delta t_{\alpha 20}, \delta L\right) = 1.449 \times 10^6$$ 3E 20 nm Al

$$\delta Q_{Z21} := \delta Q_Z\left(E_0, \rho_0, k_0, c_{p.0}, \alpha_0, T_0, w_{21}, t_{21}, L_{21}, \delta E, \delta\rho, \delta k, \delta c_p, \delta\alpha, \delta T, \delta w, \delta t_{\alpha 21}, \delta L\right) = 1.24 \times 10^6$$ 4A 5 nm x 2 Al

$$\delta Q_{Z22} := \delta Q_Z\left(E_0, \rho_0, k_0, c_{p.0}, \alpha_0, T_0, w_{22}, t_{22}, L_{22}, \delta E, \delta\rho, \delta k, \delta c_p, \delta\alpha, \delta T, \delta w, \delta t_{\alpha 22}, \delta L\right) = 4.747 \times 10^6$$ 4B SHOCON

$$\delta Q_{Z23} := \delta Q_Z\left(E_0, \rho_0, k_0, c_{p.0}, \alpha_0, T_0, w_{23}, t_{23}, L_{23}, \delta E, \delta\rho, \delta k, \delta c_p, \delta\alpha, \delta T, \delta w, \delta t_{\alpha 23}, \delta L\right) = 1.949 \times 10^5$$ 4C FORT

$$\delta Q_{Z24} := \delta Q_Z\left(E_0, \rho_0, k_0, c_{p.0}, \alpha_0, T_0, w_{24}, t_{24}, L_{24}, \delta E, \delta\rho, \delta k, \delta c_p, \delta\alpha, \delta T, \delta w, \delta t_{\alpha 24}, \delta L\right) = 3.329 \times 10^6$$ 4E 30 nm x 2 Al

$$\delta Q_{Z25} := \delta Q_Z\left(E_0, \rho_0, k_0, c_{p.0}, \alpha_0, T_0, w_{25}, t_{25}, L_{25}, \delta E, \delta\rho, \delta k, \delta c_p, \delta\alpha, \delta T, \delta w, \delta t_{\alpha 25}, \delta L\right) = 1.829 \times 10^5$$ 3C FORT

$$\delta Q_{Z26} := \delta Q_Z\left(E_0, \rho_0, k_0, c_{p.0}, \alpha_0, T_0, w_{26}, t_{26}, L_{26}, \delta E, \delta\rho, \delta k, \delta c_p, \delta\alpha, \delta T, \delta w, \delta t_{\alpha 26}, \delta L\right) = 1.679 \times 10^6$$ 5 nm   Al

$$\delta Q_{Z27} := \delta Q_Z\left(E_0, \rho_0, k_0, c_{p.0}, \alpha_0, T_0, w_{27}, t_{27}, L_{27}, \delta E, \delta\rho, \delta k, \delta c_p, \delta\alpha, \delta T, \delta w, \delta t_{\alpha 27}, \delta L\right) = 1.733 \times 10^6$$ 5 nm x 2   Al

$$\delta Q_{Z28} := \delta Q_Z\left(E_0, \rho_0, k_0, c_{p.0}, \alpha_0, T_0, w_{28}, t_{28}, L_{28}, \delta E, \delta\rho, \delta k, \delta c_p, \delta\alpha, \delta T, \delta w, \delta t_{\alpha 28}, \delta L\right) = 1.508 \times 10^6$$ 10 nm   Al

$$\delta Q_{Z29} := \delta Q_Z\left(E_0, \rho_0, k_0, c_{p.0}, \alpha_0, T_0, w_{29}, t_{29}, L_{29}, \delta E, \delta\rho, \delta k, \delta c_p, \delta\alpha, \delta T, \delta w, \delta t_{\alpha 29}, \delta L\right) = 1.431 \times 10^6$$ 10 nm   Al

$$\delta Q_{Z30} := \delta Q_Z\left(E_0, \rho_0, k_0, c_{p.0}, \alpha_0, T_0, w_{30}, t_{30}, L_{30}, \delta E, \delta\rho, \delta k, \delta c_p, \delta\alpha, \delta T, \delta w, \delta t_{\alpha 30}, \delta L\right) = 1.509 \times 10^6$$ 20 nm   Al

$$\delta Q_{Z31} := \delta Q_Z\left(E_0, \rho_0, k_0, c_{p.0}, \alpha_0, T_0, w_{31}, t_{31}, L_{31}, \delta E, \delta\rho, \delta k, \delta c_p, \delta\alpha, \delta T, \delta w, \delta t_{\alpha 31}, \delta L\right) = 1.828 \times 10^6$$ 20 nm   Al

$$\delta Q_{Z32} := \delta Q_Z\left(E_0, \rho_0, k_0, c_{p.0}, \alpha_0, T_0, w_{32}, t_{32}, L_{32}, \delta E, \delta\rho, \delta k, \delta c_p, \delta\alpha, \delta T, \delta w, \delta t_{\alpha 32}, \delta L\right) = 2.829 \times 10^6$$ 30 nm x 2   Al

$$\delta Q_{Z33} := \delta Q_Z\left(E_0, \rho_0, k_0, c_{p.0}, \alpha_0, T_0, w_{33}, t_{33}, L_{33}, \delta E, \delta\rho, \delta k, \delta c_p, \delta\alpha, \delta T, \delta w, \delta t_{\alpha 33}, \delta L\right) = 2.844 \times 10^6$$ 30 nm x 2   Al

Individual Contributions to uncertainty in TED

$$\%\delta Qz\delta E\left(E,\rho,k,c_p,\alpha,T,w,t,L,\delta E,\delta\rho,\delta k,\delta c_p,\delta\alpha,\delta T,\delta w,\delta t,\delta L\right) := \frac{\left[\left(\dfrac{d}{dE}Q_Z\left(E,\rho,k,c_p,\alpha,T,w,t,L\right)\right)\cdot\delta E\right]^2}{\delta Q_Z\left(E,\rho,k,c_p,\alpha,T,w,t,L,\delta E,\delta\rho,\delta k,\delta c_p,\delta\alpha,\delta T,\delta w,\delta t,\delta L\right)^2}$$

$$\%\delta Qz\delta E_9 := 0.184$$

$$\%\delta Qz\delta\rho\left(E,\rho,k,c_p,\alpha,T,w,t,L,\delta E,\delta\rho,\delta k,\delta c_p,\delta\alpha,\delta T,\delta w,\delta t,\delta L\right) := \frac{\left[\left(\dfrac{d}{d\rho}Q_Z\left(E,\rho,k,c_p,\alpha,T,w,t,L\right)\right)\cdot\delta\rho\right]^2}{\delta Q_Z\left(E,\rho,k,c_p,\alpha,T,w,t,L,\delta E,\delta\rho,\delta k,\delta c_p,\delta\alpha,\delta T,\delta w,\delta t,\delta L\right)^2}$$

$$\%\delta Qz\delta\rho_9 := \%\delta Qz\delta\rho\left(E_0,\rho_0,k_0,c_{p.0},\alpha_0,T_0,w_9,t_9,L_9,\delta E,\delta\rho,\delta k,\delta c_p,\delta\alpha,\delta T,\delta w,\delta t_{\alpha 9},\delta L\right) = 0.007$$

$$\%\delta Qz\delta k\left(E,\rho,k,c_p,\alpha,T,w,t,L,\delta E,\delta\rho,\delta k,\delta c_p,\delta\alpha,\delta T,\delta w,\delta t,\delta L\right) := \frac{\left[\left(\dfrac{d}{dk}Q_Z\left(E,\rho,k,c_p,\alpha,T,w,t,L\right)\right)\cdot\delta k\right]^2}{\delta Q_Z\left(E,\rho,k,c_p,\alpha,T,w,t,L,\delta E,\delta\rho,\delta k,\delta c_p,\delta\alpha,\delta T,\delta w,\delta t,\delta L\right)^2}$$

$$\%\delta Qz\delta k_9 := \%\delta Qz\delta k\left(E_0,\rho_0,k_0,c_{p.0},\alpha_0,T_0,w_9,t_9,L_9,\delta E,\delta\rho,\delta k,\delta c_p,\delta\alpha,\delta T,\delta w,\delta t_{\alpha 9},\delta L\right) = 0.221$$

$$\%\delta Qz\delta c_p\left(E,\rho,k,c_p,\alpha,T,w,t,L,\delta E,\delta\rho,\delta k,\delta c_p,\delta\alpha,\delta T,\delta w,\delta t,\delta L\right) := \frac{\left[\left(\dfrac{d}{dc_p}Q_Z\left(E,\rho,k,c_p,\alpha,T,w,t,L\right)\right)\cdot\delta c_p\right]^2}{\delta Q_Z\left(E,\rho,k,c_p,\alpha,T,w,t,L,\delta E,\delta\rho,\delta k,\delta c_p,\delta\alpha,\delta T,\delta w,\delta t,\delta L\right)^2}$$

$$\%\delta Qz\delta c_{p.9} := \%\delta Qz\delta c_p\left(E_0,\rho_0,k_0,c_{p.0},\alpha_0,T_0,w_9,t_9,L_9,\delta E,\delta\rho,\delta k,\delta c_p,\delta\alpha,\delta T,\delta w,\delta t_{\alpha 9},\delta L\right) = 0$$

$$\%\delta Qz\delta\alpha\left(E,\rho,k,c_p,\alpha,T,w,t,L,\delta E,\delta\rho,\delta k,\delta c_p,\delta\alpha,\delta T,\delta w,\delta t,\delta L\right) := \frac{\left[\left(\dfrac{d}{d\alpha}Q_Z\left(E,\rho,k,c_p,\alpha,T,w,t,L\right)\right)\cdot\delta\alpha\right]^2}{\delta Q_Z\left(E,\rho,k,c_p,\alpha,T,w,t,L,\delta E,\delta\rho,\delta k,\delta c_p,\delta\alpha,\delta T,\delta w,\delta t,\delta L\right)^2}$$

$$\%\delta Qz\delta\alpha_9 := \%\delta Qz\delta\alpha\left(E_0,\rho_0,k_0,c_{p.0},\alpha_0,T_0,w_9,t_9,L_9,\delta E,\delta\rho,\delta k,\delta c_p,\delta\alpha,\delta T,\delta w,\delta t_{\alpha 9},\delta L\right) = 0.334$$

$$\%\delta Qz\delta T\left(E,\rho,k,c_p,\alpha,T,w,t,L,\delta E,\delta\rho,\delta k,\delta c_p,\delta\alpha,\delta T,\delta w,\delta t,\delta L\right) := \dfrac{\left[\left(\dfrac{d}{dT}Q_Z\left(E,\rho,k,c_p,\alpha,T,w,t,L\right)\right)\cdot\delta T\right]^2}{\delta Q_Z\left(E,\rho,k,c_p,\alpha,T,w,t,L,\delta E,\delta\rho,\delta k,\delta c_p,\delta\alpha,\delta T,\delta w,\delta t,\delta L\right)^2}$$

$$\%\delta Qz\delta T_9 := \%\delta Qz\delta T\left(E_0,\rho_0,k_0,c_{p.0},\alpha_0,T_0,w_9,t_9,L_9,\delta E,\delta\rho,\delta k,\delta c_p,\delta\alpha,\delta T,\delta w,\delta t_{\alpha 9},\delta L\right) = 0.001$$

$$\%\delta Qz\delta w\left(E,\rho,k,c_p,\alpha,T,w,t,L,\delta E,\delta\rho,\delta k,\delta c_p,\delta\alpha,\delta T,\delta w,\delta t,\delta L\right) := \dfrac{\left[\left(\dfrac{d}{dw}Q_Z\left(E,\rho,k,c_p,\alpha,T,w,t,L\right)\right)\cdot\delta w\right]^2}{\delta Q_Z\left(E,\rho,k,c_p,\alpha,T,w,t,L,\delta E,\delta\rho,\delta k,\delta c_p,\delta\alpha,\delta T,\delta w,\delta t,\delta L\right)^2}$$

$$\%\delta Qz\delta w_9 := \%\delta Qz\delta w\left(E_0,\rho_0,k_0,c_{p.0},\alpha_0,T_0,w_9,t_9,L_9,\delta E,\delta\rho,\delta k,\delta c_p,\delta\alpha,\delta T,\delta w,\delta t_{\alpha 9},\delta L\right) = 0$$

$$\%\delta Qz\delta L\left(E,\rho,k,c_p,\alpha,T,w,t,L,\delta E,\delta\rho,\delta k,\delta c_p,\delta\alpha,\delta T,\delta w,\delta t,\delta L\right) := \dfrac{\left[\left(\dfrac{d}{dL}Q_Z\left(E,\rho,k,c_p,\alpha,T,w,t,L\right)\right)\cdot\delta L\right]^2}{\delta Q_Z\left(E,\rho,k,c_p,\alpha,T,w,t,L,\delta E,\delta\rho,\delta k,\delta c_p,\delta\alpha,\delta T,\delta w,\delta t,\delta L\right)^2}$$

$$\%\delta Qz\delta L_9 := \%\delta Qz\delta L\left(E_0,\rho_0,k_0,c_{p.0},\alpha_0,T_0,w_9,t_9,L_9,\delta E,\delta\rho,\delta k,\delta c_p,\delta\alpha,\delta T,\delta w,\delta t_{\alpha 9},\delta L\right) = 0.001$$

$$\%\delta Qz\delta t\left(E,\rho,k,c_p,\alpha,T,w,t,L,\delta E,\delta\rho,\delta k,\delta c_p,\delta\alpha,\delta T,\delta w,\delta t,\delta L\right) := \dfrac{\left[\left(\dfrac{d}{dt}Q_Z\left(E,\rho,k,c_p,\alpha,T,w,t,L\right)\right)\cdot\delta t\right]^2}{\delta Q_Z\left(E,\rho,k,c_p,\alpha,T,w,t,L,\delta E,\delta\rho,\delta k,\delta c_p,\delta\alpha,\delta T,\delta w,\delta t,\delta L\right)^2}$$

$$\%\delta Qz\delta t_9 := \%\delta Qz\delta t\left(E_0,\rho_0,k_0,c_{p.0},\alpha_0,T_0,w_9,t_9,L_9,\delta E,\delta\rho,\delta k,\delta c_p,\delta\alpha,\delta T,\delta w,\delta t_{\alpha 9},\delta L\right) = 0.253$$

Uncertainty TED Lifshitz

$$\delta Q_L\left(E,\rho,k,c_p,\alpha,T,w,t,L,\delta E,\delta\rho,\delta k,\delta c_p,\delta\alpha,\delta T,\delta w,\delta t,\delta L\right) := \left[\left[\left(\frac{d}{dE}Q_L\left(E,\rho,k,c_p,\alpha,T,w,t,L\right)\right)\cdot\delta E\right]^2 \ldots\right.$$
$$+\left[\left(\frac{d}{d\rho}Q_L\left(E,\rho,k,c_p,\alpha,T,w,t,L\right)\right)\cdot\delta\rho\right]^2 \ldots$$
$$+\left[\left(\frac{d}{dk}Q_L\left(E,\rho,k,c_p,\alpha,T,w,t,L\right)\right)\cdot\delta k\right]^2 \ldots$$
$$+\left[\left(\frac{d}{dc_p}Q_L\left(E,\rho,k,c_p,\alpha,T,w,t,L\right)\right)\cdot\delta c_p\right]^2 \ldots$$
$$+\left[\left(\frac{d}{d\alpha}Q_L\left(E,\rho,k,c_p,\alpha,T,w,t,L\right)\right)\cdot\delta\alpha\right]^2 \ldots$$
$$+\left[\left(\frac{d}{dT}Q_L\left(E,\rho,k,c_p,\alpha,T,w,t,L\right)\right)\cdot\delta T\right]^2 \ldots$$
$$+\left[\left(\frac{d}{dw}Q_L\left(E,\rho,k,c_p,\alpha,T,w,t,L\right)\right)\cdot\delta w\right]^2 \ldots$$
$$+\left[\left(\frac{d}{dt}Q_L\left(E,\rho,k,c_p,\alpha,T,w,t,L\right)\right)\cdot\delta t\right]^2 \ldots$$
$$\left.+\left[\left(\frac{d}{dL}Q_L\left(E,\rho,k,c_p,\alpha,T,w,t,L\right)\right)\cdot\delta L\right]^2\right]^{\frac{1}{2}}$$

$\delta Q_{L9} := \delta Q_L\left(E_0,\rho_0,k_0,c_{p.0},\alpha_0,T_0,w_9,t_9,L_9,\delta E,\delta\rho,\delta k,\delta c_p,\delta\alpha,\delta T,\delta w,\delta t_{\alpha 9},\delta L\right) = 1.579\times 10^6$ — Beam 2E 10 nm Al coating

$\delta Q_{L10} := \delta Q_L\left(E_0,\rho_0,k_0,c_{p.0},\alpha_0,T_0,w_{10},t_{10},L_{10},\delta E,\delta\rho,\delta k,\delta c_p,\delta\alpha,\delta T,\delta w,\delta t_{\alpha 10},\delta L\right) = 3.343\times 10^6$ — Beam 1A SICON

$\delta Q_{L11} := \delta Q_L\left(E_0,\rho_0,k_0,c_{p.0},\alpha_0,T_0,w_{11},t_{11},L_{11},\delta E,\delta\rho,\delta k,\delta c_p,\delta\alpha,\delta T,\delta w,\delta t_{\alpha 11},\delta L\right) = 3.573\times 10^6$ — Beam 1B SHOCON

$\delta Q_{L12} := \delta Q_L\left(E_0,\rho_0,k_0,c_{p.0},\alpha_0,T_0,w_{12},t_{12},L_{12},\delta E,\delta\rho,\delta k,\delta c_p,\delta\alpha,\delta T,\delta w,\delta t_{\alpha 12},\delta L\right) = 1.949\times 10^5$ — Beam 1C FORT

$\delta Q_{L13} := 1.742\times 10^6$ — Beam 1E 5 nm Al coating

$\delta Q_{L14} := \delta Q_L\left(E_0,\rho_0,k_0,c_{p.0},\alpha_0,T_0,w_{14},t_{14},L_{14},\delta E,\delta\rho,\delta k,\delta c_p,\delta\alpha,\delta T,\delta w,\delta t_{\alpha 14},\delta L\right) = 3.403\times 10^6$ — Beam 2A SICON

$\delta Q_{L15} := 4.984\times 10^6$ — Beam 2B SHOCON

$\delta Q_{L16} := \delta Q_L\left(E_0,\rho_0,k_0,c_{p.0},\alpha_0,T_0,w_{16},t_{16},L_{16},\delta E,\delta\rho,\delta k,\delta c_p,\delta\alpha,\delta T,\delta w,\delta t_{\alpha 16},\delta L\right) = 3.088\times 10^5$ — Beam 2C FORT

$\delta Q_{L17} := \delta Q_L\left(E_0,\rho_0,k_0,c_{p.0},\alpha_0,T_0,w_{17},t_{17},L_{17},\delta E,\delta\rho,\delta k,\delta c_p,\delta\alpha,\delta T,\delta w,\delta t_{\alpha 17},\delta L\right) = 3.776\times 10^6$ — Beam 3A SICON

$\delta Q_{L18} := \delta Q_L\left(E_0,\rho_0,k_0,c_{p.0},\alpha_0,T_0,w_{18},t_{18},L_{18},\delta E,\delta\rho,\delta k,\delta c_p,\delta\alpha,\delta T,\delta w,\delta t_{\alpha 18},\delta L\right) = 3.483\times 10^6$ — Beam 3B SHOCON

$$\delta Q_{L19} := \delta Q_L\left(E_0, \rho_0, k_0, c_{p.0}, \alpha_0, T_0, w_{19}, t_{19}, L_{19}, \delta E, \delta \rho, \delta k, \delta c_p, \delta \alpha, \delta T, \delta w, \delta t_{\alpha 19}, \delta L\right) = 1.362 \times 10^4$$

Beam 3D ACL

$$\delta Q_{L20} := \delta Q_L\left(E_0, \rho_0, k_0, c_{p.0}, \alpha_0, T_0, w_{20}, t_{20}, L_{20}, \delta E, \delta \rho, \delta k, \delta c_p, \delta \alpha, \delta T, \delta w, \delta t_{\alpha 20}, \delta L\right) = 1.326 \times 10^6$$

Beam 3E 20 nm Al coating

$$\delta Q_{L21} := \delta Q_L\left(E_0, \rho_0, k_0, c_{p.0}, \alpha_0, T_0, w_{21}, t_{21}, L_{21}, \delta E, \delta \rho, \delta k, \delta c_p, \delta \alpha, \delta T, \delta w, \delta t_{\alpha 21}, \delta L\right) = 1.19 \times 10^6$$

Beam 4A 5 nm x 2 Al coating

$$\delta Q_{L22} := \delta Q_L\left(E_0, \rho_0, k_0, c_{p.0}, \alpha_0, T_0, w_{22}, t_{22}, L_{22}, \delta E, \delta \rho, \delta k, \delta c_p, \delta \alpha, \delta T, \delta w, \delta t_{\alpha 22}, \delta L\right) = 4.409 \times 10^6$$

Beam 4B SHOCON

$$\delta Q_{L23} := \delta Q_L\left(E_0, \rho_0, k_0, c_{p.0}, \alpha_0, T_0, w_{23}, t_{23}, L_{23}, \delta E, \delta \rho, \delta k, \delta c_p, \delta \alpha, \delta T, \delta w, \delta t_{\alpha 23}, \delta L\right) = 1.974 \times 10^5$$

Beam 4C FORT

$$\delta Q_{L24} := \delta Q_L\left(E_0, \rho_0, k_0, c_{p.0}, \alpha_0, T_0, w_{24}, t_{24}, L_{24}, \delta E, \delta \rho, \delta k, \delta c_p, \delta \alpha, \delta T, \delta w, \delta t_{\alpha 24}, \delta L\right) = 3.196 \times 10^6$$

Beam 4E 30 nm x 2 Al coating

$$\delta Q_{L25} := \delta Q_L\left(E_0, \rho_0, k_0, c_{p.0}, \alpha_0, T_0, w_{25}, t_{25}, L_{25}, \delta E, \delta \rho, \delta k, \delta c_p, \delta \alpha, \delta T, \delta w, \delta t_{\alpha 25}, \delta L\right) = 1.853 \times 10^5$$

Beam 3C FORT

$$\delta Q_{L26} := \delta Q_L\left(E_0, \rho_0, k_0, c_{p.0}, \alpha_0, T_0, w_{26}, t_{26}, L_{26}, \delta E, \delta \rho, \delta k, \delta c_p, \delta \alpha, \delta T, \delta w, \delta t_{\alpha 26}, \delta L\right) = 1.702 \times 10^6$$

5 nm Al coating

$$\delta Q_{L27} := 1.591 \times 10^6$$

5 nm x 2 Al coating

$$\delta Q_{L28} := 1.74 \times 10^6$$

10 nm Al coating

$$\delta Q_{L29} := \delta Q_L\left(E_0, \rho_0, k_0, c_{p.0}, \alpha_0, T_0, w_{29}, t_{29}, L_{29}, \delta E, \delta \rho, \delta k, \delta c_p, \delta \alpha, \delta T, \delta w, \delta t_{\alpha 29}, \delta L\right) = 1.31 \times 10^6$$

10 nm Al coating

$$\delta Q_{L30} := \delta Q_L\left(E_0, \rho_0, k_0, c_{p.0}, \alpha_0, T_0, w_{30}, t_{30}, L_{30}, \delta E, \delta \rho, \delta k, \delta c_p, \delta \alpha, \delta T, \delta w, \delta t_{\alpha 30}, \delta L\right) = 1.544 \times 10^6$$

20 nm Al coating

$$\delta Q_{L31} := 1.853 \times 10^6$$

20 nm Al coating

$$\delta Q_{L32} := \delta Q_L\left(E_0, \rho_0, k_0, c_{p.0}, \alpha_0, T_0, w_{32}, t_{32}, L_{32}, \delta E, \delta \rho, \delta k, \delta c_p, \delta \alpha, \delta T, \delta w, \delta t_{\alpha 32}, \delta L\right) = 2.589 \times 10^6$$

30 nm x 2 Al coating

$$\delta Q_{L33} := \delta Q_L\left(E_0, \rho_0, k_0, c_{p.0}, \alpha_0, T_0, w_{33}, t_{33}, L_{33}, \delta E, \delta \rho, \delta k, \delta c_p, \delta \alpha, \delta T, \delta w, \delta t_{\alpha 33}, \delta L\right) = 2.701 \times 10^6$$

30 nm x 2 Al coating

Characteristic damping frequency

$$F_9 := F_0\left(k_0, \rho_0, c_{p.0}, t_9\right) = 3.449 \times 10^7 \frac{1}{s}$$

Beam 2E 10 nm Al coating

$$F_{10} := F_0\left(k_0, \rho_0, c_{p.0}, t_{10}\right) = 59.914 \cdot MHz$$

Beam 1A SICON

$$F_{11} := F_0\left(k_0, \rho_0, c_{p.0}, t_{11}\right) = 1.535 \times 10^8 \frac{1}{s}$$

Beam 1B SHOCON

$$F_{12} := F_0\left(k_0, \rho_0, c_{p.0}, t_{12}\right) = 2.292 \times 10^7 \frac{1}{s}$$

Beam 1C FORT

$$F_{19} := F_0\left(k_0, \rho_0, c_{p.0}, t_{19}\right) = 3.49 \times 10^6 \frac{1}{s}$$

Beam 3D ACL

Anchor Losses

$$Q_{A2}(L, t) := \frac{1}{2 \cdot .23 \cdot \left(\dfrac{t^3}{L^3} \right)}$$

$Q_{A2}(L_0, t_0) = 2.476 \times 10^7$ Prospective samples

$Q_{A2}(L_1, t_1) = 2.476 \times 10^7$

$Q_{A2}(L_2, t_2) = 1.268 \times 10^7$

$Q_{A2}(L_3, t_3) = 9.171 \times 10^5$

$Q_{A2}(L_4, t_4) = 4.659 \times 10^4$

$Q_{A2}(L_5, t_5) = 4.032 \times 10^4$

$Q_{A2}(L_6, t_6) = 4.696 \times 10^5$

$Q_{A2}(L_7, t_7) = 3.397 \times 10^7$

$Q_{A2}(L_8, t_8) = 8.052 \times 10^7$

$Q_{A9} := Q_{A2}(L_9, t_9) = 2.078 \times 10^7$ Beam 2E 10 nm Al coating

$Q_{A10} := Q_{A2}(L_{10}, t_{10}) = 4.586 \times 10^7$ Beam 1A SICON

$Q_{A11} := Q_{A2}(L_{11}, t_{11}) = 2.614 \times 10^7$ Beam 1B SHOCON

$Q_{A12} := Q_{A2}(L_{12}, t_{12}) = 1.19 \times 10^6$ Beam 1C FORT

$Q_{A13} := Q_{A2}(L_{13}, t_{13}) = 2.515 \times 10^7$ Beam 1E 5 nm Al coating

$Q_{A14} := Q_{A2}(L_{14}, t_{14}) = 4.908 \times 10^7$ Beam 2A SICON

$Q_{A15} := Q_{A2}(L_{15}, t_{15}) = 3.312 \times 10^7$ Beam 2B SHOCON

$Q_{A16} := Q_{A2}(L_{16}, t_{16}) = 1.881 \times 10^6$ Beam 2C FORT

$Q_{A17} := Q_{A2}(L_{17}, t_{17}) = 5.181 \times 10^7$ Beam 3A SICON

$Q_{A18} := Q_{A2}(L_{18}, t_{18}) = 2.485 \times 10^7$ Beam 3B SHOCON

$Q_{A19} := Q_{A2}(L_{19}, t_{19}) = 9.073 \times 10^4$ Beam 3D ACL

$Q_{A20} := Q_{A2}(L_{20}, t_{20}) = 1.917 \times 10^7$ Beam 3E 20 nm Al coating

$Q_{A21} := Q_{A2}(L_{21}, t_{21}) = 1.646 \times 10^7$ Beam 4A 5 nm x 2 Al coating

$Q_{A22} := Q_{A2}(L_{22}, t_{22}) = 3.196 \times 10^7$ Beam 4B SHOCON

$Q_{A23} := Q_{A2}(L_{23}, t_{23}) = 1.211 \times 10^6$ Beam 4C FORT

$Q_{A24} := Q_{A2}(L_{24}, t_{24}) = 4.433 \times 10^7$ Beam 4E 30 nm x 2 Al coating

$Q_{A25} := Q_{A2}(L_{25}, t_{25}) = 1.137 \times 10^6$ Beam 3C FORT

$Q_{A26} := Q_{A2}(L_{26}, t_{26}) = 2.231 \times 10^7$ 5 nm   Al coating 26

$Q_{A27} := Q_{A2}(L_{27}, t_{27}) = 2.309 \times 10^7$ 5 nm x 2   Al coating 27

$Q_{A28} := Q_{A2}(L_{28}, t_{28}) = 2.002 \times 10^7$ 10 nm   Al coating 28

$Q_{A29} := Q_{A2}(L_{29}, t_{29}) = 1.897 \times 10^7$ 10 nm   Al coating 29

$Q_{A30} := Q_{A2}(L_{30}, t_{30}) = 2.003 \times 10^7$ 20 nm   Al coating 30

$Q_{A31} := Q_{A2}(L_{31}, t_{31}) = 2.421 \times 10^7$ 20 nm   Al coating 31

$Q_{A32} := Q_{A2}(L_{32}, t_{32}) = 3.766 \times 10^7$ 30 nm x 2   Al coating 32

$Q_{A33} := Q_{A2}(L_{33}, t_{33}) = 3.793 \times 10^7$ 30 nm x 2   Al coating 33

Uncertainty in Anchor loss

$$\delta Q_{A2}(L, t, \delta L, \delta t) := \left[\left[\left(\frac{d}{dL} Q_{A2}(L, t) \right) \cdot \delta L \right]^2 + \left[\left(\frac{d}{dt} Q_{A2}(L, t) \right) \cdot \delta t \right]^2 \right]^{\frac{1}{2}}$$

$\delta Q_{A9} := \delta Q_{A2}(L_9, t_9, \delta L, \delta t_{\alpha 9}) = 1.397 \times 10^6$ Beam 2E 10 nm Al coating

$\delta Q_{A10} := \delta Q_{A2}(L_{10}, t_{10}, \delta L, \delta t_{\alpha 10}) = 3.084 \times 10^6$ Beam 1A SICON

$\delta Q_{A11} := \delta Q_{A2}(L_{11}, t_{11}, \delta L, \delta t_{\alpha 11}) = 1.874 \times 10^6$ Beam 1B SHOCON

$\delta Q_{A12} := \delta Q_{A2}(L_{12}, t_{12}, \delta L, \delta t_{\alpha 12}) = 8.649 \times 10^4$ Beam 1C FORT

$\delta Q_{A13} := \delta Q_{A2}(L_{13}, t_{13}, \delta L, \delta t_{\alpha 13}) = 1.691 \times 10^6$ Beam 1E 5 nm Al coating

$\delta Q_{A14} := \delta Q_{A2}(L_{14}, t_{14}, \delta L, \delta t_{\alpha 14}) = 3.3 \times 10^6$ Beam 2A SICON

$\delta Q_{A15} := \delta Q_{A2}(L_{15}, t_{15}, \delta L, \delta t_{\alpha 15}) = 2.377 \times 10^6$ Beam 2B SHOCON

$\delta Q_{A16} := \delta Q_{A2}(L_{16}, t_{16}, \delta L, \delta t_{\alpha 16}) = 1.368 \times 10^5$ Beam 2C FORT

$\delta Q_{A17} := \delta Q_{A2}(L_{17}, t_{17}, \delta L, \delta t_{\alpha 17}) = 3.484 \times 10^6$ Beam 3A SICON

$$\delta Q_{A18} := \delta Q_{A2}(L_{18}, t_{18}, \delta L, \delta t_{\alpha18}) = 1.778 \times 10^6 \qquad \text{Beam 3B SHOCON}$$

$$\delta Q_{A19} := \delta Q_{A2}(L_{19}, t_{19}, \delta L, \delta t_{\alpha19}) = 6.499 \times 10^3 \qquad \text{Beam 3D ACL}$$

$$\delta Q_{A20} := \delta Q_{A2}(L_{20}, t_{20}, \delta L, \delta t_{\alpha20}) = 1.288 \times 10^6 \qquad \text{Beam 3E 20 nm Al coating}$$

$$\delta Q_{A21} := \delta Q_{A2}(L_{21}, t_{21}, \delta L, \delta t_{\alpha21}) = 1.106 \times 10^6 \qquad \text{Beam 4A 5 nm x 2 Al coating}$$

$$\delta Q_{A22} := \delta Q_{A2}(L_{22}, t_{22}, \delta L, \delta t_{\alpha22}) = 2.29 \times 10^6 \qquad \text{Beam 4B SHOCON}$$

$$\delta Q_{A23} := \delta Q_{A2}(L_{23}, t_{23}, \delta L, \delta t_{\alpha23}) = 8.792 \times 10^4 \qquad \text{Beam 4C FORT}$$

$$\delta Q_{A24} := \delta Q_{A2}(L_{24}, t_{24}, \delta L, \delta t_{\alpha24}) = 2.979 \times 10^6 \qquad \text{Beam 4E 30 nm x 2 Al coating}$$

$$\delta Q_{A25} := \delta Q_{A2}(L_{25}, t_{25}, \delta L, \delta t_{\alpha25}) = 8.259 \times 10^4 \qquad \text{Beam 3C FORT}$$

$$\delta Q_{A26} := \delta Q_{A2}(L_{26}, t_{26}, \delta L, \delta t_{\alpha26}) = 1.499 \times 10^6 \qquad \text{5 nm   Al coating 26}$$

$$\delta Q_{A27} := \delta Q_{A2}(L_{27}, t_{27}, \delta L, \delta t_{\alpha27}) = 1.552 \times 10^6 \qquad \text{5 nm x 2   Al coating 27}$$

$$\delta Q_{A28} := \delta Q_{A2}(L_{28}, t_{28}, \delta L, \delta t_{\alpha28}) = 1.346 \times 10^6 \qquad \text{10 nm   Al coating 28}$$

$$\delta Q_{A29} := \delta Q_{A2}(L_{29}, t_{29}, \delta L, \delta t_{\alpha29}) = 1.275 \times 10^6 \qquad \text{10 nm   Al coating 29}$$

$$\delta Q_{A30} := \delta Q_{A2}(L_{30}, t_{30}, \delta L, \delta t_{\alpha30}) = 1.346 \times 10^6 \qquad \text{20 nm   Al coating 30}$$

$$\delta Q_{A31} := \delta Q_{A2}(L_{31}, t_{31}, \delta L, \delta t_{\alpha31}) = 1.627 \times 10^6 \qquad \text{20 nm   Al coating 31}$$

$$\delta Q_{A32} := \delta Q_{A2}(L_{32}, t_{32}, \delta L, \delta t_{\alpha32}) = 2.531 \times 10^6 \qquad \text{30 nm x 2   Al coating 32}$$

$$\delta Q_{A33} := \delta Q_{A2}(L_{33}, t_{33}, \delta L, \delta t_{\alpha33}) = 2.549 \times 10^6 \qquad \text{30 nm x 2   Al coating 33}$$

Surface Losses

$$E_{D\_Hao} := 0.81 \frac{\text{kg}}{\text{s}^2} \qquad \text{from Hao} \qquad \text{where } E_D = \delta \, E_{ds}$$

$$Q_S(w, t, E) := \frac{w \cdot t}{2 \cdot (3 \cdot w + t)} \cdot \frac{E}{E_{D\_Hao}}$$

$$Q_S(w_0, t_0, E_0) = 6.703 \times 10^4 \qquad \text{Prospective samples}$$

$$Q_S(w_1, t_1, E_0) = 3.381 \times 10^4$$

$$Q_S(w_2, t_2, E_0) = 8.345 \times 10^4$$

$$Q_S(w_3, t_3, E_0) = 9.892 \times 10^4$$

$$Q_S(w_4, t_4, E_0) = 1.47 \times 10^5$$

$$Q_S(w_5, t_5, E_0) = 2.705 \times 10^5$$

$$Q_S(w_6, t_6, E_0) = 8.244 \times 10^4$$

$$Q_S(w_7, t_7, E_N) = 1.191 \times 10^4$$

$$Q_S(w_8, t_8, E_N) = 3.562 \times 10^4$$

$$Q_{SD}(Q, Q_A, Q_{TED}) := \left(\frac{1}{Q} - \frac{1}{Q_A} - \frac{1}{Q_{TED}} \right)^{-1}$$

$$\delta E_D(w, t, E, Q_{SD}) := \frac{w \cdot t \cdot E}{2 \cdot (3 \cdot w + t) \cdot Q_{SD}}$$

$$E_D(\delta E_D, \delta) := \frac{\delta E_D}{\delta}$$

$$Q_{SD9} := Q_{SD}(Q_9, Q_{A9}, Q_{L9}) = 3.991 \times 10^4 \qquad\qquad \text{Beam 2E 10 nm Al coating}$$

$$\delta E_{D9} := \delta E_D(w_9, t_9, E_0, Q_{SD9}) = 1.449 \frac{kg}{s^2}$$

$$\delta_9 := 10 \cdot nm \qquad E_{D9} := \frac{\delta E_{D9}}{\delta_9} = 1.449 \times 10^8 \, Pa$$

$$Q_{SD10} := \left(\frac{1}{Q_{10}} - \frac{1}{Q_{A10}} - \frac{1}{Q_{L10}} \right)^{-1} = 1.043 \times 10^5 \qquad \text{Beam 1A SICON}$$

$$\delta E_{D10} := \delta E_D(w_{10}, t_{10}, E_0, Q_{SD10}) = 0.422 \frac{kg}{s^2}$$

$$Q_{SD11} := \left(\frac{1}{Q_{11}} - \frac{1}{Q_{A11}} - \frac{1}{Q_{L11}} \right)^{-1} = 5.522 \times 10^4 \qquad \text{Beam 1B SHOCON}$$

$$\delta E_{D11} := \delta E_D(w_{11}, t_{11}, E_0, Q_{SD11}) = 0.5 \frac{kg}{s^2}$$

$$Q_{SD12} := \left(\frac{1}{Q_{12}} - \frac{1}{Q_{A12}} - \frac{1}{Q_{L12}} \right)^{-1} = 1.254 \times 10^5 \qquad \text{Beam 1C FORT}$$

$$\delta E_{D12} := \delta E_D(w_{12}, t_{12}, E_0, Q_{SD12}) = 0.558 \frac{kg}{s^2}$$

$$Q_{SD13} := \left(\frac{1}{Q_{13}} - \frac{1}{Q_{A13}} - \frac{1}{Q_{L13}} \right)^{-1} = 6.43 \times 10^4 \qquad \text{Beam 1E 5 nm Al coating}$$

$$\delta E_{D13} := \delta E_D \left(w_{13}, t_{13}, E_0, Q_{SD13} \right) = 0.836 \frac{kg}{s^2}$$

$$\delta_{13} := 5 \cdot nm \qquad E_{D13} := \frac{\delta E_{D13}}{\delta_{13}} = 1.672 \times 10^8 \, Pa$$

$$Q_{SD14} := \left(\frac{1}{Q_{14}} - \frac{1}{Q_{A14}} - \frac{1}{Q_{L14}} \right)^{-1} = 1.126 \times 10^5 \qquad \text{Beam 2A SICON}$$

$$\delta E_{D14} := \delta E_D \left(w_{14}, t_{14}, E_0, Q_{SD14} \right) = 0.383 \frac{kg}{s^2}$$

$$Q_{SD15} := \left(\frac{1}{Q_{15}} - \frac{1}{Q_{A15}} - \frac{1}{Q_{L15}} \right)^{-1} = 5.782 \times 10^4 \qquad \text{Beam 2B SHOCON}$$

$$\delta E_{D15} := \delta E_D \left(w_{15}, t_{15}, E_0, Q_{SD15} \right) = 0.438 \frac{kg}{s^2}$$

$$Q_{SD16} := \left(\frac{1}{Q_{16}} - \frac{1}{Q_{A16}} - \frac{1}{Q_{L16}} \right)^{-1} = 3.268 \times 10^4 \qquad \text{Beam 2C FORT}$$

$$\delta E_{D16} := \delta E_D \left(w_{16}, t_{16}, E_0, Q_{SD16} \right) = 1.839 \frac{kg}{s^2}$$

$$Q_{SD17} := \left(\frac{1}{Q_{17}} - \frac{1}{Q_{A17}} - \frac{1}{Q_{L17}} \right)^{-1} = 1.001 \times 10^5 \qquad \text{Beam 3A SICON}$$

$$\delta E_{D17} := \delta E_D \left(w_{17}, t_{17}, E_0, Q_{SD17} \right) = 0.423 \frac{kg}{s^2}$$

$$Q_{SD18} := \left(\frac{1}{Q_{18}} - \frac{1}{Q_{A18}} - \frac{1}{Q_{L18}} \right)^{-1} = 5.09 \times 10^4 \qquad \text{Beam 3B SHOCON}$$

$$\delta E_{D18} := \delta E_D \left(w_{18}, t_{18}, E_0, Q_{SD18} \right) = 0.557 \frac{kg}{s^2}$$

$$Q_{SD19} := \left(\frac{1}{Q_{19}} - \frac{1}{Q_{A19}} - \frac{1}{Q_{L19}} \right)^{-1} = 1.019 \times 10^5 \qquad \text{Beam 3D ACL}$$

$$\delta E_{D19} := \delta E_D \left(w_{19}, t_{19}, E_0, Q_{SD19} \right) = 1.718 \frac{kg}{s^2}$$

$$Q_{SD20} := \left(\frac{1}{Q_{20}} - \frac{1}{Q_{A20}} - \frac{1}{Q_{L20}} \right)^{-1} = 2.18 \times 10^4 \qquad \text{Beam 3E 20 nm Al coating}$$

$$\delta E_{D20} := \delta E_D(w_{20}, t_{20}, E_0, Q_{SD20}) = 2.703 \frac{kg}{s^2}$$

$$\delta_{20} := 20 \cdot nm \qquad E_{D20} := \frac{\delta E_{D20}}{\delta_{20}} = 1.351 \times 10^8 \, Pa$$

$$Q_{SD21} := \left(\frac{1}{Q_{21}} - \frac{1}{Q_{A21}} - \frac{1}{Q_{L21}} \right)^{-1} = 4.355 \times 10^4 \qquad \text{Beam 4A 5 nm x 2 Al coating}$$

$$\delta E_{D21} := \delta E_D(w_{21}, t_{21}, E_0, Q_{SD21}) = 1.428 \frac{kg}{s^2}$$

$$\delta_{21} := 10 \cdot nm \qquad E_{D21} := \frac{\delta E_{D21}}{\delta_{21}} = 1.428 \times 10^8 \, Pa$$

$$Q_{SD22} := \left(\frac{1}{Q_{22}} - \frac{1}{Q_{A22}} - \frac{1}{Q_{L22}} \right)^{-1} = 4.427 \times 10^4 \qquad \text{Beam 4B SHOCON}$$

$$\delta E_{D22} := \delta E_D(w_{22}, t_{22}, E_0, Q_{SD22}) = 0.585 \frac{kg}{s^2}$$

$$Q_{SD23} := \left(\frac{1}{Q_{23}} - \frac{1}{Q_{A23}} - \frac{1}{Q_{L23}} \right)^{-1} = 1.296 \times 10^5 \qquad \text{Beam 4C FORT}$$

$$\delta E_{D23} := \delta E_D(w_{23}, t_{23}, E_0, Q_{SD23}) = 0.539 \frac{kg}{s^2}$$

$$Q_{SD24} := \left(\frac{1}{Q_{24}} - \frac{1}{Q_{A24}} - \frac{1}{Q_{L24}} \right)^{-1} = 3.687 \times 10^3 \qquad \text{Beam 4E 30 nm x 2 Al coating}$$

$$\delta E_{D24} := \delta E_D(w_{24}, t_{24}, E_0, Q_{SD24}) = 12.206 \frac{kg}{s^2}$$

$$\delta_{24} := 60 \cdot nm \qquad E_{D24} := \frac{\delta E_{D24}}{\delta_{24}} = 2.034 \times 10^8 \, Pa$$

$$Q_{SD25} := \left(\frac{1}{Q_{25}} - \frac{1}{Q_{A25}} - \frac{1}{Q_{L25}} \right)^{-1} = 1.492 \times 10^5 \qquad \text{Beam 3C FORT}$$

$$\delta E_{D25} := \delta E_D(w_{25}, t_{25}, E_0, Q_{SD25}) = 0.479 \frac{kg}{s^2}$$

$$Q_{SD26} := \left(\frac{1}{Q_{26}} - \frac{1}{Q_{A26}} - \frac{1}{Q_{L26}} \right)^{-1} = 7.876 \times 10^4$$
5 nm   Al coating 26

$$\delta E_{D26} := \delta E_D\left(w_{26}, t_{26}, E_0, Q_{SD26} \right) = 0.715 \frac{kg}{s^2}$$

$$\delta_{26} := 5 \cdot nm \qquad E_{D26} := \frac{\delta E_{D26}}{\delta_{26}} = 1.43 \times 10^8 \, Pa$$

$$Q_{SD27} := \left(\frac{1}{Q_{27}} - \frac{1}{Q_{A27}} - \frac{1}{Q_{L27}} \right)^{-1} = 4.019 \times 10^4$$

5 nm x 2   Al coating 27

$$\delta E_{D27} := \delta E_D\left(w_{27}, t_{27}, E_0, Q_{SD27} \right) = 1.389 \frac{kg}{s^2}$$

$$\delta_{27} := 10 \cdot nm \qquad E_{D27} := \frac{\delta E_{D27}}{\delta_{27}} = 1.389 \times 10^8 \, Pa$$

$$Q_{SD28} := \left(\frac{1}{Q_{28}} - \frac{1}{Q_{A28}} - \frac{1}{Q_{L28}} \right)^{-1} = 3.921 \times 10^4$$

10 nm   Al coating 28

$$\delta E_{D28} := \delta E_D\left(w_{28}, t_{28}, E_0, Q_{SD28} \right) = 1.487 \frac{kg}{s^2}$$

$$\delta_{28} := 10 \cdot nm \qquad E_{D28} := \frac{\delta E_{D28}}{\delta_{28}} = 1.487 \times 10^8 \, Pa$$

$$Q_{SD29} := \left(\frac{1}{Q_{29}} - \frac{1}{Q_{A29}} - \frac{1}{Q_{L29}} \right)^{-1} = 3.882 \times 10^4$$

10 nm   Al coating 29

$$\delta E_{D29} := \delta E_D\left(w_{29}, t_{29}, E_0, Q_{SD29} \right) = 1.527 \frac{kg}{s^2}$$

$$\delta_{29} := 10 \cdot nm \qquad E_{D29} := \frac{\delta E_{D29}}{\delta_{29}} = 1.527 \times 10^8 \, Pa$$

$$Q_{SD30} := \left(\frac{1}{Q_{30}} - \frac{1}{Q_{A30}} - \frac{1}{Q_{L30}} \right)^{-1} = 2.458 \times 10^4$$

20 nm   Al coating 30

$$\delta E_{D30} := \delta E_D\left(w_{30}, t_{30}, E_0, Q_{SD30} \right) = 2.371 \frac{kg}{s^2}$$

$$\delta_{30} := 20 \cdot nm \qquad E_{D30} := \frac{\delta E_{D30}}{\delta_{30}} = 1.185 \times 10^8 \, Pa$$

129

$$Q_{SD31} := \left(\frac{1}{Q_{31}} - \frac{1}{Q_{A31}} - \frac{1}{Q_{L31}} \right)^{-1} = 2.205 \times 10^4 \qquad \text{20 nm Al coating 31}$$

$$\delta E_{D31} := \delta E_D\left(w_{31}, t_{31}, E_0, Q_{SD31}\right) = 2.478 \frac{kg}{s^2}$$

$$\delta_{31} := 20 \cdot nm \qquad E_{D31} := \frac{\delta E_{D31}}{\delta_{31}} = 1.239 \times 10^8 \, Pa$$

$$Q_{SD32} := \left(\frac{1}{Q_{32}} - \frac{1}{Q_{A32}} - \frac{1}{Q_{L32}} \right)^{-1} = 4.802 \times 10^3 \qquad \text{30 nm x 2 Al coating 32}$$

$$\delta E_{D32} := \delta E_D\left(w_{32}, t_{32}, E_0, Q_{SD32}\right) = 9.89 \frac{kg}{s^2}$$

$$\delta_{32} := 60 \cdot nm \qquad E_{D32} := \frac{\delta E_{D32}}{\delta_{32}} = 1.648 \times 10^8 \, Pa$$

$$Q_{SD33} := \left(\frac{1}{Q_{33}} - \frac{1}{Q_{A33}} - \frac{1}{Q_{L33}} \right)^{-1} = 4.682 \times 10^3 \qquad \text{30 nm x 2 Al coating 33}$$

$$\delta E_{D33} := \delta E_D\left(w_{33}, t_{33}, E_0, Q_{SD33}\right) = 10.135 \frac{kg}{s^2}$$

$$\delta_{33} := 60 \cdot nm \qquad E_{D33} := \frac{\delta E_{D33}}{\delta_{33}} = 1.689 \times 10^8 \, Pa$$

uncertainty in surface losses

$$\% \delta Q := 0.043$$

$$\delta Q_{SD}\left(Q, Q_A, Q_L, \delta Q_A, \delta Q_L\right) := \left[\left[\left(\frac{d}{dQ} Q_{SD}\left(Q, Q_A, Q_L\right) \right) \cdot \% \delta Q \cdot Q \right]^2 \dots \right.$$
$$\left. + \left[\left(\frac{d}{dQ_A} Q_{SD}\left(Q, Q_A, Q_L\right) \right) \cdot \delta Q_A \right]^2 \dots \right.$$
$$\left. + \left[\left(\frac{d}{dQ_L} Q_{SD}\left(Q, Q_A, Q_L\right) \right) \cdot \delta Q_L \right]^2 \right]^{\frac{1}{2}}$$

$$\delta Q_{SD9} := \delta Q_{SD}\left(Q_9, Q_{A9}, Q_{L9}, \delta Q_{A9}, \delta Q_{L9}\right) = 1.725 \times 10^3 \qquad \text{Beam 2E 10 nm Al coating}$$

$$\delta Q_{SD10} := \delta Q_{SD}\left(Q_{10}, Q_{A10}, Q_{L10}, \delta Q_{A10}, \delta Q_{L10}\right) = 4.515 \times 10^3 \qquad \text{Beam 1A SICON}$$

$$\delta Q_{SD11} := \delta Q_{SD}(Q_{11}, Q_{A11}, Q_{L11}, \delta Q_{A11}, \delta Q_{L11}) = 2.384 \times 10^3$$

Beam 1B SHOCON

$$\delta Q_{SD12} := \delta Q_{SD}(Q_{12}, Q_{A12}, Q_{L12}, \delta Q_{A12}, \delta Q_{L12}) = 6.671 \times 10^3$$

Beam 1C FORT

$$\delta Q_{SD13} := \delta Q_{SD}(Q_{13}, Q_{A13}, Q_{L13}, \delta Q_{A13}, \delta Q_{L13}) = 2.785 \times 10^3$$

Beam 1E 5 nm Al coating

$$\delta Q_{SD14} := \delta Q_{SD}(Q_{14}, Q_{A14}, Q_{L14}, \delta Q_{A14}, \delta Q_{L14}) = 4.87 \times 10^3$$

Beam 2A SICON

$$\delta Q_{SD15} := \delta Q_{SD}(Q_{15}, Q_{A15}, Q_{L15}, \delta Q_{A15}, \delta Q_{L15}) = 2.494 \times 10^3$$

Beam 2B SHOCON

$$\delta Q_{SD16} := \delta Q_{SD}(Q_{16}, Q_{A16}, Q_{L16}, \delta Q_{A16}, \delta Q_{L16}) = 1.452 \times 10^3$$

Beam 2C FORT

$$\delta Q_{SD17} := \delta Q_{SD}(Q_{17}, Q_{A17}, Q_{L17}, \delta Q_{A17}, \delta Q_{L17}) = 4.326 \times 10^3$$

Beam 3A SICON

$$\delta Q_{SD18} := \delta Q_{SD}(Q_{18}, Q_{A18}, Q_{L18}, \delta Q_{A18}, \delta Q_{L18}) = 2.197 \times 10^3$$

Beam 3B SHOCON

$$\delta Q_{SD19} := \delta Q_{SD}(Q_{19}, Q_{A19}, Q_{L19}, \delta Q_{A19}, \delta Q_{L19}) = 2.113 \times 10^4$$

Beam 3D ACL

$$\delta Q_{SD20} := \delta Q_{SD}(Q_{20}, Q_{A20}, Q_{L20}, \delta Q_{A20}, \delta Q_{L20}) = 940.451$$

Beam 3E 20 nm Al coating

$$\delta Q_{SD21} := \delta Q_{SD}(Q_{21}, Q_{A21}, Q_{L21}, \delta Q_{A21}, \delta Q_{L21}) = 1.886 \times 10^3$$

Beam 4A 5 nm x 2 Al coating

$$\delta Q_{SD22} := \delta Q_{SD}(Q_{22}, Q_{A22}, Q_{L22}, \delta Q_{A22}, \delta Q_{L22}) = 1.909 \times 10^3$$

Beam 4B SHOCON

$$\delta Q_{SD23} := \delta Q_{SD}(Q_{23}, Q_{A23}, Q_{L23}, \delta Q_{A23}, \delta Q_{L23}) = 6.918 \times 10^3$$

Beam 4C FORT

$$\delta Q_{SD24} := \delta Q_{SD}(Q_{24}, Q_{A24}, Q_{L24}, \delta Q_{A24}, \delta Q_{L24}) = 158.57$$

Beam 4E 30 nm x 2 Al coating

$$\delta Q_{SD25} := \delta Q_{SD}(Q_{25}, Q_{A25}, Q_{L25}, \delta Q_{A25}, \delta Q_{L25}) = 8.377 \times 10^3$$

Beam 3C FORT

$$\delta Q_{SD26} := \delta Q_{SD}(Q_{26}, Q_{A26}, Q_{L26}, \delta Q_{A26}, \delta Q_{L26}) = 3.42 \times 10^3$$

5 nm   Al coating

$$\delta Q_{SD27} := \delta Q_{SD}(Q_{27}, Q_{A27}, Q_{L27}, \delta Q_{A27}, \delta Q_{L27}) = 1.737 \times 10^3$$

5 nm x 2   Al coating

$$\delta Q_{SD28} := \delta Q_{SD}(Q_{28}, Q_{A28}, Q_{L28}, \delta Q_{A28}, \delta Q_{L28}) = 1.695 \times 10^3$$

10 nm   Al coating

$$\delta Q_{SD29} := \delta Q_{SD}(Q_{29}, Q_{A29}, Q_{L29}, \delta Q_{A29}, \delta Q_{L29}) = 1.679 \times 10^3$$

10 nm   Al coating

$$\delta Q_{SD30} := \delta Q_{SD}(Q_{30}, Q_{A30}, Q_{L30}, \delta Q_{A30}, \delta Q_{L30}) = 1.061 \times 10^3$$

20 nm   Al coating

$$\delta Q_{SD31} := \delta Q_{SD}(Q_{31}, Q_{A31}, Q_{L31}, \delta Q_{A31}, \delta Q_{L31}) = 950.74$$

20 nm   Al coating

$$\delta Q_{SD32} := \delta Q_{SD}(Q_{32}, Q_{A32}, Q_{L32}, \delta Q_{A32}, \delta Q_{L32}) = 206.545$$

30 nm x 2   Al coating

$$\delta Q_{SD33} := \delta Q_{SD}(Q_{33}, Q_{A33}, Q_{L33}, \delta Q_{A33}, \delta Q_{L33}) = 201.377$$

30 nm x 2   Al coating

Uncertainty in δ E$_D$

$$\delta \mathcal{E}_D(w,t,E,Q_{SD},\delta w,\delta t,\delta E,\delta Q_{SD}) := \left[\left[\left(\frac{d}{dw}\delta E_D(w,t,E,Q_{SD})\right)\cdot \delta w\right]^2 + \left[\left(\frac{d}{dt}\delta E_D(w,t,E,Q_{SD})\right)\cdot \delta t\right]^2 \ldots \right.$$
$$\left. + \left[\left(\frac{d}{dE}\delta E_D(w,t,E,Q_{SD})\right)\cdot \delta E\right]^2 \ldots \right.$$
$$\left. + \left[\left(\frac{d}{dQ_{SD}}\delta E_D(w,t,E,Q_{SD})\right)\cdot \delta Q_{SD}\right]^2 \right]^{\frac{1}{2}}$$

$\delta \mathcal{E}_{D9} := \delta \mathcal{E}_D(w_9,t_9,E_0,Q_{SD9},\delta w,\delta t_{\alpha 9},\delta E,\delta Q_{SD9}) = 0.089\frac{kg}{s^2}$ Beam 2E 10 nm Al coating

$\delta \mathcal{E}_{D10} := \delta \mathcal{E}_D(w_{10},t_{10},E_0,Q_{SD10},\delta w,\delta t_{\alpha 10},\delta E,\delta Q_{SD10}) = 0.026\frac{kg}{s^2}$ Beam 1A SICON

$\delta \mathcal{E}_{D11} := \delta \mathcal{E}_D(w_{11},t_{11},E_0,Q_{SD11},\delta w,\delta t_{\alpha 11},\delta E,\delta Q_{SD11}) = 0.031\frac{kg}{s^2}$ Beam 1B SHOCON

$\delta \mathcal{E}_{D12} := \delta \mathcal{E}_D(w_{12},t_{12},E_0,Q_{SD12},\delta w,\delta t_{\alpha 12},\delta E,\delta Q_{SD12}) = 0.039\frac{kg}{s^2}$ Beam 1C FORT

$\delta \mathcal{E}_{D13} := \delta \mathcal{E}_D(w_{13},t_{13},E_0,Q_{SD13},\delta w,\delta t_{\alpha 13},\delta E,\delta Q_{SD13}) = 0.052\frac{kg}{s^2}$ Beam 1E 5 nm Al coating

$\delta \mathcal{E}_{D14} := \delta \mathcal{E}_D(w_{14},t_{14},E_0,Q_{SD14},\delta w,\delta t_{\alpha 14},\delta E,\delta Q_{SD14}) = 0.024\frac{kg}{s^2}$ Beam 2A SICON

$\delta \mathcal{E}_{D15} := \delta \mathcal{E}_D(w_{15},t_{15},E_0,Q_{SD15},\delta w,\delta t_{\alpha 15},\delta E,\delta Q_{SD15}) = 0.027\frac{kg}{s^2}$ Beam 2B SHOCON

$\delta \mathcal{E}_{D16} := \delta \mathcal{E}_D(w_{16},t_{16},E_0,Q_{SD16},\delta w,\delta t_{\alpha 16},\delta E,\delta Q_{SD16}) = 0.116\frac{kg}{s^2}$ Beam 2C FORT

$\delta \mathcal{E}_{D17} := \delta \mathcal{E}_D(w_{17},t_{17},E_0,Q_{SD17},\delta w,\delta t_{\alpha 17},\delta E,\delta Q_{SD17}) = 0.026\frac{kg}{s^2}$ Beam 3A SICON

$\delta \mathcal{E}_{D18} := \delta \mathcal{E}_D(w_{18},t_{18},E_0,Q_{SD18},\delta w,\delta t_{\alpha 18},\delta E,\delta Q_{SD18}) = 0.035\frac{kg}{s^2}$ Beam 3B SHOCON

$\delta \mathcal{E}_{D19} := \delta \mathcal{E}_D(w_{19},t_{19},E_0,Q_{SD19},\delta w,\delta t_{\alpha 19},\delta E,\delta Q_{SD19}) = 0.364\frac{kg}{s^2}$ Beam 3D ACL

$\delta \mathcal{E}_{D20} := \delta \mathcal{E}_D(w_{20},t_{20},E_0,Q_{SD20},\delta w,\delta t_{\alpha 20},\delta E,\delta Q_{SD20}) = 0.166\frac{kg}{s^2}$ Beam 3E 20 nm Al coating

$\delta E_{D21} := \delta E_D(w_{21}, t_{21}, E_0, Q_{SD21}, \delta w, \delta t_{\alpha 21}, \delta E, \delta Q_{SD21}) = 0.088 \frac{kg}{s^2}$ Beam 4A 5 nm x 2 Al coating

$\delta E_{D22} := \delta E_D(w_{22}, t_{22}, E_0, Q_{SD22}, \delta w, \delta t_{\alpha 22}, \delta E, \delta Q_{SD22}) = 0.036 \frac{kg}{s^2}$ Beam 4B SHOCON

$\delta E_{D23} := \delta E_D(w_{23}, t_{23}, E_0, Q_{SD23}, \delta w, \delta t_{\alpha 23}, \delta E, \delta Q_{SD23}) = 0.037 \frac{kg}{s^2}$ Beam 4C FORT

$\delta E_{D24} := \delta E_D(w_{24}, t_{24}, E_0, Q_{SD24}, \delta w, \delta t_{\alpha 24}, \delta E, \delta Q_{SD24}) = 0.751 \frac{kg}{s^2}$ Beam 4E 30 nm x 2 Al coating

$\delta E_{D25} := \delta E_D(w_{25}, t_{25}, E_0, Q_{SD25}, \delta w, \delta t_{\alpha 25}, \delta E, \delta Q_{SD25}) = 0.034 \frac{kg}{s^2}$ Beam 3C FORT

$\delta E_{D26} := \delta E_D(w_{26}, t_{26}, E_0, Q_{SD26}, \delta w, \delta t_{\alpha 26}, \delta E, \delta Q_{SD26}) = 0.044 \frac{kg}{s^2}$ 5 nm   Al coating 26

$\delta E_{D27} := \delta E_D(w_{27}, t_{27}, E_0, Q_{SD27}, \delta w, \delta t_{\alpha 27}, \delta E, \delta Q_{SD27}) = 0.086 \frac{kg}{s^2}$ 5 nm x 2   Al coating 27

$\delta E_{D28} := \delta E_D(w_{28}, t_{28}, E_0, Q_{SD28}, \delta w, \delta t_{\alpha 28}, \delta E, \delta Q_{SD28}) = 0.092 \frac{kg}{s^2}$ 10 nm   Al coating 28

$\delta E_{D29} := \delta E_D(w_{29}, t_{29}, E_0, Q_{SD29}, \delta w, \delta t_{\alpha 29}, \delta E, \delta Q_{SD29}) = 0.094 \frac{kg}{s^2}$ 10 nm   Al coating 29

$\delta E_{D30} := \delta E_D(w_{30}, t_{30}, E_0, Q_{SD30}, \delta w, \delta t_{\alpha 30}, \delta E, \delta Q_{SD30}) = 0.146 \frac{kg}{s^2}$ 20 nm   Al coating 30

$\delta E_{D31} := \delta E_D(w_{31}, t_{31}, E_0, Q_{SD31}, \delta w, \delta t_{\alpha 31}, \delta E, \delta Q_{SD31}) = 0.152 \frac{kg}{s^2}$ 20 nm   Al coating 31

$\delta E_{D32} := \delta E_D(w_{32}, t_{32}, E_0, Q_{SD32}, \delta w, \delta t_{\alpha 32}, \delta E, \delta Q_{SD32}) = 0.608 \frac{kg}{s^2}$ 30 nm x 2   Al coating 32

$\delta E_{D33} := \delta E_D(w_{33}, t_{33}, E_0, Q_{SD33}, \delta w, \delta t_{\alpha 33}, \delta E, \delta Q_{SD33}) = 0.623 \frac{kg}{s^2}$ 30 nm x 2   Al coating 33

Uncertainty in E_D

$$\Delta E_D(\delta E_D, \delta, \delta E_D, \delta\delta) := \left[\left[\left(\frac{d}{d\delta E_D} E_D(\delta E_D, \delta) \right) \cdot \delta E_D \right]^2 + \left[\left(\frac{d}{d\delta} E_D(\delta E_D, \delta) \right) \cdot \delta\delta \right]^2 \right]^{\frac{1}{2}}$$

$\delta\delta_1 := 1 \cdot nm$

$\delta\delta_2 := 2 \cdot nm$ uncertainty in coating thickness

$\delta\delta_3 := 4 \cdot nm$

$\delta\delta_4 := 12 \cdot nm$

$\Delta E_{D9} := \Delta E_D(\delta E_{D9}, \delta_9, \delta\delta E_{D9}, \delta\delta_2) = 3.032 \times 10^7 \, Pa$ Beam 2E 10 nm Al coating

$\Delta E_{D13} := \Delta E_D(\delta E_{D13}, \delta_{13}, \delta\delta E_{D13}, \delta\delta_1) = 3.5 \times 10^7 \, Pa$ Beam 1E 5 nm Al coating

$\Delta E_{D20} := \Delta E_D(\delta E_{D20}, \delta_{20}, \delta\delta E_{D20}, \delta\delta_3) = 2.828 \times 10^7 \, Pa$ Beam 3E 20 nm Al coating

$\Delta E_{D21} := \Delta E_D(\delta E_{D21}, \delta_{21}, \delta\delta E_{D21}, \delta\delta_2) = 2.989 \times 10^7 \, Pa$ Beam 4A 5 nm x 2 Al coating

$\Delta E_{D24} := \Delta E_D(\delta E_{D24}, \delta_{24}, \delta\delta E_{D24}, \delta\delta_4) = 4.257 \times 10^7 \, Pa$ Beam 4E 30 nm x 2 Al coating

$\Delta E_{D26} := \Delta E_D(\delta E_{D26}, \delta_{26}, \delta\delta E_{D26}, \delta\delta_1) = 2.993 \times 10^7 \, Pa$ 5 nm   Al coating

$\Delta E_{D27} := \Delta E_D(\delta E_{D27}, \delta_{27}, \delta\delta E_{D27}, \delta\delta_2) = 2.907 \times 10^7 \, Pa$ 5 nm x 2   Al coating

$\Delta E_{D28} := \Delta E_D(\delta E_{D28}, \delta_{28}, \delta\delta E_{D28}, \delta\delta_2) = 3.112 \times 10^7 \, Pa$ 10 nm   Al coating

$\Delta E_{D29} := \Delta E_D(\delta E_{D29}, \delta_{29}, \delta\delta E_{D29}, \delta\delta_2) = 3.197 \times 10^7 \, Pa$ 10 nm   Al coating

$\Delta E_{D30} := \Delta E_D(\delta E_{D30}, \delta_{30}, \delta\delta E_{D30}, \delta\delta_3) = 2.48 \times 10^7 \, Pa$ 20 nm   Al coating

$\Delta E_{D31} := \Delta E_D(\delta E_{D31}, \delta_{31}, \delta\delta E_{D31}, \delta\delta_3) = 2.592 \times 10^7 \, Pa$ 20 nm   Al coating

$\Delta E_{D32} := \Delta E_D(\delta E_{D32}, \delta_{32}, \delta\delta E_{D32}, \delta\delta_4) = 3.449 \times 10^7 \, Pa$ 30 nm x 2   Al coating 32

$\Delta E_{D33} := \Delta E_D(\delta E_{D33}, \delta_{33}, \delta\delta E_{D33}, \delta\delta_4) = 3.534 \times 10^7 \, Pa$ 30 nm x 2   Al coating 33

$$J(\delta E_D, \delta, \delta\delta E_D, \delta\delta) := \frac{\left[\left(\frac{d}{d\delta}E_D(\delta E_D, \delta)\right) \cdot \delta\delta\right]^2}{\Delta E_D(\delta E_D, \delta, \delta\delta E_D, \delta\delta)^2}$$ % contributions for coating thickness

$J9 := J(\delta E_{D9}, \delta_9, \delta\delta E_{D9}, \delta\delta_2) = 0.913$

Damping due to AuPd coating

$$Q_{coating}(Q_{Au}, Q) := \left(\frac{1}{Q_{Au}} - \frac{1}{Q}\right)^{-1}$$

$Q_{coating10} := Q_{coating}(Q_{Au10}, Q_{10}) = 7.915 \times 10^3$ Beam 1A SICON with 28 nm AuPd

$$\delta E_{DAu10} := \delta E_D\left(w_{10}, t_{10}, E_0, Q_{coating10}\right) = 5.563 \frac{kg}{s^2}$$

$$\delta_{Au10} := 28 \cdot nm \qquad E_{DAu10} := \frac{\delta E_{DAu10}}{\delta_{Au10}} = 1.987 \times 10^8 \, Pa$$

$$Q_{coating11} := Q_{coating}\left(Q_{Au11}, Q_{11}\right) = 2.876 \times 10^3 \qquad \text{\color{blue}Beam 1B SHOCON with 28 nm AuPd}$$

$$\delta E_{DAu11} := \delta E_D\left(w_{11}, t_{11}, E_0, Q_{coating11}\right) = 9.602 \frac{kg}{s^2}$$

$$\delta_{Au11} := 28 \cdot nm \qquad E_{DAu11} := \frac{\delta E_{DAu11}}{\delta_{Au11}} = 3.429 \times 10^8 \, Pa$$

$$Q_{coating12} := Q_{coating}\left(Q_{Au12}, Q_{12}\right) = 8.024 \times 10^3 \qquad \text{\color{blue}Beam 1C FORT with 28 nm AuPd}$$

$$\delta E_{DAu12} := \delta E_D\left(w_{12}, t_{12}, E_0, Q_{coating12}\right) = 8.72 \frac{kg}{s^2}$$

$$\delta_{Au12} := 28 \cdot nm \qquad E_{DAu12} := \frac{\delta E_{DAu12}}{\delta_{Au12}} = 3.114 \times 10^8 \, Pa$$

$$Q_{coating13} := Q_{coating}\left(Q_{Au13}, Q_{13}\right) = 8.831 \times 10^3 \qquad \text{\color{blue}Beam 1E 5 nm Al coating with 28 nm AuPd}$$

$$\delta E_{DAu13} := \delta E_D\left(w_{13}, t_{13}, E_0, Q_{coating13}\right) = 6.088 \frac{kg}{s^2}$$

$$\delta_{Au13} := 28 \cdot nm \qquad E_{DAu13} := \frac{\delta E_{DAu13}}{\delta_{Au13}} = 2.174 \times 10^8 \, Pa$$

$$\text{\color{blue}Beam 4A 5 nm x 2 Al coating with 28 nm AuPd}$$

$$Q_{coating21} := Q_{coating}\left(Q_{Au21}, Q_{21}\right) = 8.662 \times 10^3$$

$$\delta E_{DAu21} := \delta E_D\left(w_{21}, t_{21}, E_0, Q_{coating21}\right) = 7.181 \frac{kg}{s^2}$$

$$\delta_{Au21} := 28 \cdot nm \qquad E_{DAu21} := \frac{\delta E_{DAu21}}{\delta_{Au21}} = 2.565 \times 10^8 \, Pa$$

$$Q_{coating22} := Q_{coating}\left(Q_{Au22}, Q_{22}\right) = 2.299 \times 10^3 \qquad \text{\color{blue}Beam 4B SHOCON with 28 nm AuPd}$$

$$\delta E_{DAu22} := \delta E_D\left(w_{22}, t_{22}, E_0, Q_{coating22}\right) = 11.264 \frac{kg}{s^2}$$

$$\delta_{Au22} := 28 \cdot nm \qquad E_{DAu22} := \frac{\delta E_{DAu22}}{\delta_{Au22}} = 4.023 \times 10^8 \, Pa$$

$Q_{coating23} := Q_{coating}(Q_{Au23}, Q_{23}) = 5.458 \times 10^3$

$\delta E_{DAu23} := \delta E_D(w_{23}, t_{23}, E_0, Q_{coating23}) = 12.802 \dfrac{kg}{s^2}$

$\delta_{Au23} := 28 \cdot nm \qquad E_{DAu23} := \dfrac{\delta E_{DAu23}}{\delta_{Au23}} = 4.572 \times 10^8 \, Pa$

$Q_{coating24} := Q_{coating}(Q_{Au24}, Q_{24}) = 1.091 \times 10^4$

$\delta E_{DAu24} := \delta E_D(w_{24}, t_{24}, E_0, Q_{coating24}) = 4.126 \dfrac{kg}{s^2}$

$\delta_{Au24} := 28 \cdot nm \qquad E_{DAu24} := \dfrac{\delta E_{DAu24}}{\delta_{Au24}} = 1.473 \times 10^8 \, Pa$

Uncertainty in coated samples

$\% \delta Q_{Au} := 0.04$

$\delta \delta_{Au} := 10 \cdot nm$

$$\delta Q_{coating}(Q_{Au}, Q) := \left[\left[\left(\frac{d}{dQ} Q_{coating}(Q_{Au}, Q) \right) \cdot \% \delta Q \cdot Q \right]^2 \ldots \\ + \left[\left(\frac{d}{dQ_{Au}} Q_{coating}(Q_{Au}, Q) \right) \cdot \% \delta Q_{Au} \cdot Q_{Au} \right]^2 \right]^{\frac{1}{2}}$$

$\delta Q_{coating10} := \delta Q_{coating}(Q_{Au10}, Q_{10}) = 341.774$

$\delta \delta E_{DAu10} := \delta \delta E_D(w_{10}, t_{10}, E_0, Q_{coating10}, \delta w, \delta t_{\alpha10}, \delta E, \delta Q_{coating10}) = 0.343 \dfrac{kg}{s^2}$

$\Delta E_{DAu10} := \Delta E_D(\delta E_{DAu10}, \delta_{Au10}, \delta \delta E_{DAu10}, \delta \delta_{Au}) = 7.2 \times 10^7 \, Pa$

$\delta Q_{coating11} := \delta Q_{coating}(Q_{Au11}, Q_{11}) = 121.224$

$\delta \delta E_{DAu11} := \delta \delta E_D(w_{11}, t_{11}, E_0, Q_{coating11}, \delta w, \delta t_{\alpha11}, \delta E, \delta Q_{coating11}) = 0.589 \dfrac{kg}{s^2}$

$\Delta E_{DAu11} := \Delta E_D(\delta E_{DAu11}, \delta_{Au11}, \delta \delta E_{DAu11}, \delta \delta_{Au}) = 1.243 \times 10^8 \, Pa$

$\delta Q_{coating12} := \delta Q_{coating}(Q_{Au12}, Q_{12}) = 346.439$

$\Delta E_{DAu12} := \Delta E_D\left(\delta \!\!E_{DAu12}, \delta_{Au12}, \delta \!\!E_{DAu12}, \delta \delta_{Au}\right) = 1.129 \times 10^8 \, Pa$

$\delta Q_{coating13} := \delta Q_{coating}\left(Q_{Au13}, Q_{13}\right) = 405.498$ Beam 1E 5 nm Al coating with 28 nm AuPd

$\delta \!\!E_{DAu13} := \delta \!\!E_D\left(w_{13}, t_{13}, E_0, Q_{coating13}, \delta w, \delta t_{\alpha13}, \delta E, \delta Q_{coating13}\right) = 0.387 \dfrac{kg}{s^2}$

$\Delta E_{DAu13} := \Delta E_D\left(\delta \!\!E_{DAu13}, \delta_{Au13}, \delta \!\!E_{DAu13}, \delta \delta_{Au}\right) = 7.887 \times 10^7 \, Pa$

$\delta Q_{coating21} := \delta Q_{coating}\left(Q_{Au21}, Q_{21}\right) = 422.517$ Beam 4A 5 nm x 2 Al coating with 28 nm AuPd

$\delta \!\!E_{DAu21} := \delta \!\!E_D\left(w_{21}, t_{21}, E_0, Q_{coating21}, \delta w, \delta t_{\alpha21}, \delta E, \delta Q_{coating21}\right) = 0.471 \dfrac{kg}{s^2}$

$\Delta E_{DAu21} := \Delta E_D\left(\delta \!\!E_{DAu21}, \delta_{Au21}, \delta \!\!E_{DAu21}, \delta \delta_{Au}\right) = 9.313 \times 10^7 \, Pa$

$\delta Q_{coating22} := \delta Q_{coating}\left(Q_{Au22}, Q_{22}\right) = 96.874$ Beam 4B SHOCON with 28 nm AuPd

$\delta \!\!E_{DAu22} := \delta \!\!E_D\left(w_{22}, t_{22}, E_0, Q_{coating22}, \delta w, \delta t_{\alpha22}, \delta E, \delta Q_{coating22}\right) = 0.691 \dfrac{kg}{s^2}$

$\Delta E_{DAu22} := \Delta E_D\left(\delta \!\!E_{DAu22}, \delta_{Au22}, \delta \!\!E_{DAu22}, \delta \delta_{Au}\right) = 1.458 \times 10^8 \, Pa$

$\delta Q_{coating23} := \delta Q_{coating}\left(Q_{Au23}, Q_{23}\right) = 229.612$ Beam 4C FORT with 28 nm AuPd

$\delta \!\!E_{DAu23} := \delta \!\!E_D\left(w_{23}, t_{23}, E_0, Q_{coating23}, \delta w, \delta t_{\alpha23}, \delta E, \delta Q_{coating23}\right) = 0.784 \dfrac{kg}{s^2}$

$\Delta E_{DAu23} := \Delta E_D\left(\delta \!\!E_{DAu23}, \delta_{Au23}, \delta \!\!E_{DAu23}, \delta \delta_{Au}\right) = 1.657 \times 10^8 \, Pa$

$\delta Q_{coating24} := \delta Q_{coating}\left(Q_{Au24}, Q_{24}\right) = 2.216 \times 10^3$ Beam 4E 30 nm x 2 Al coating with 28 nm AuPd

$\delta \!\!E_{DAu24} := \delta \!\!E_D\left(w_{24}, t_{24}, E_0, Q_{coating24}, \delta w, \delta t_{\alpha24}, \delta E, \delta Q_{coating24}\right) = 0.858 \dfrac{kg}{s^2}$

$\Delta E_{DAu24} := \Delta E_D\left(\delta \!\!E_{DAu24}, \delta_{Au24}, \delta \!\!E_{DAu24}, \delta \delta_{Au}\right) = 6.089 \times 10^7 \, Pa$

$$J\left(\delta \!\!E_D, \delta, \delta \!\!E_D, \delta \delta\right) := \frac{\left[\left(\dfrac{d}{d\delta} E_D\left(\delta \!\!E_D, \delta\right)\right) \cdot \delta \delta\right]^2}{\Delta E_D\left(\delta \!\!E_D, \delta, \delta \!\!E_D, \delta \delta\right)^2}$$ % contributions for coating thickness

$J9 := J\left(\delta \!\!E_{DAu10}, \delta_{Au10}, \delta \!\!E_{DAu10}, \delta \delta_{Au}\right) = 0.971$

Total Q

$$Q_1 := \cfrac{1}{\dfrac{1}{Q_Z\left(E_0, \rho_0, k_0, c_{p.0}, \alpha_0, T_0, w_1, t_1, L_1\right)} + \dfrac{1}{Q_{A2}\left(L_1, t_1\right)} + \dfrac{1}{Q_S\left(w_1, t_1, E_0\right)}} = 3.373 \times 10^4$$

$$Q_2 := \cfrac{1}{\cfrac{1}{Q_Z\left(E_0,\rho_0,k_0,c_{p.0},\alpha_0,T_0,w_2,t_2,L_2\right)} + \cfrac{1}{Q_{A2}\left(L_2,t_2\right)} + \cfrac{1}{Q_S\left(w_2,t_2,E_0\right)}} = 8.195 \times 10^4$$

$$Q_3 := \cfrac{1}{\cfrac{1}{Q_Z\left(E_0,\rho_0,k_0,c_{p.0},\alpha_0,T_0,w_3,t_3,L_3\right)} + \cfrac{1}{Q_{A2}\left(L_3,t_3\right)} + \cfrac{1}{Q_S\left(w_3,t_3,E_0\right)}} = 8.222 \times 10^4$$

$$Q_4 := \cfrac{1}{\cfrac{1}{Q_Z\left(E_0,\rho_0,k_0,c_{p.0},\alpha_0,T_0,w_4,t_4,L_4\right)} + \cfrac{1}{Q_{A2}\left(L_4,t_4\right)} + \cfrac{1}{Q_S\left(w_4,t_4,E_0\right)}} = 2.579 \times 10^4$$

$$Q_5 := \cfrac{1}{\cfrac{1}{Q_Z\left(E_0,\rho_0,k_0,c_{p.0},\alpha_0,T_0,w_5,t_5,L_5\right)} + \cfrac{1}{Q_{A2}\left(L_5,t_5\right)} + \cfrac{1}{Q_S\left(w_5,t_5,E_0\right)}} = 1.993 \times 10^4$$

$$Q_6 := \cfrac{1}{\cfrac{1}{Q_Z\left(E_0,\rho_0,k_0,c_{p.0},\alpha_0,T_0,w_6,t_6,L_6\right)} + \cfrac{1}{Q_{A2}\left(L_6,t_6\right)} + \cfrac{1}{Q_S\left(w_6,t_6,E_0\right)}} = 6.445 \times 10^4$$

Aspect Ratio

$$A_1(L,t) := \frac{L}{t} \qquad A_2(w,t) := \frac{w}{t}$$

$A_1\left(L_0,t_0\right) = 225 \qquad A_2\left(w_0,t_0\right) = 20$

$A_1\left(L_1,t_1\right) = 225 \qquad A_2\left(w_1,t_1\right) = 43 \qquad t_1 = 1 \times 10^{-6}\,m \qquad$ SHOCUN

$A_1\left(L_2,t_2\right) = 180 \qquad A_2\left(w_2,t_2\right) = 16 \qquad t_2 = 2.5 \times 10^{-6}\,m \qquad$ SICON

$A_1\left(L_3,t_3\right) = 75 \qquad A_2\left(w_3,t_3\right) = 10 \qquad t_3 = 3 \times 10^{-6}\,m \qquad$ FORT

$A_1\left(L_4,t_4\right) = 27.778 \qquad A_2\left(w_4,t_4\right) = 7.778 \qquad t_4 = 4.5 \times 10^{-6}\,m \qquad$ ACT

$A_1\left(L_5,t_5\right) = 26.471 \qquad A_2\left(w_5,t_5\right) = 4.706 \qquad t_5 = 8.5 \times 10^{-6}\,m \qquad$ ACL

$A_1\left(L_6,t_6\right) = 60 \qquad A_2\left(w_6,t_6\right) = 10 \qquad t_6 = 2.5 \times 10^{-6}\,m \qquad$ ACST

$$\text{th} := \begin{pmatrix} t_1 \\ t_2 \\ t_3 \\ t_4 \\ t_5 \\ t_6 \end{pmatrix} = \begin{pmatrix} 1 \times 10^{-6} \\ 2.5 \times 10^{-6} \\ 3 \times 10^{-6} \\ 4.5 \times 10^{-6} \\ 8.5 \times 10^{-6} \\ 2.5 \times 10^{-6} \end{pmatrix} m \qquad AR_L := \begin{pmatrix} A_1(L_1, t_1) \\ A_1(L_2, t_2) \\ A_1(L_3, t_3) \\ A_1(L_4, t_4) \\ A_1(L_5, t_5) \\ A_1(L_6, t_6) \end{pmatrix} = \begin{pmatrix} 225 \\ 180 \\ 75 \\ 27.778 \\ 26.471 \\ 60 \end{pmatrix}$$

SHOCUN
SICON
FORT
ACT
ACL
ACST

$$AR_w := \begin{pmatrix} A_2(w_1, t_1) \\ A_2(w_2, t_2) \\ A_2(w_3, t_3) \\ A_2(w_4, t_4) \\ A_2(w_5, t_5) \\ A_2(w_6, t_6) \end{pmatrix} = \begin{pmatrix} 43 \\ 16 \\ 10 \\ 7.778 \\ 4.706 \\ 10 \end{pmatrix} \qquad Q_{total} := \begin{pmatrix} Q_1 \\ Q_2 \\ Q_3 \\ Q_4 \\ Q_5 \\ Q_6 \end{pmatrix} = \begin{pmatrix} 3.373 \times 10^4 \\ 8.195 \times 10^4 \\ 8.222 \times 10^4 \\ 2.579 \times 10^4 \\ 1.993 \times 10^4 \\ 6.445 \times 10^4 \end{pmatrix}$$

SHOCUN
SICON
FORT
ACT
ACL
ACST

$$Q_{TED} := \begin{pmatrix} Q_Z(E_0, \rho_0, k_0, c_{p.0}, \alpha_0, T_0, w_1, t_1, L_1) \\ Q_Z(E_0, \rho_0, k_0, c_{p.0}, \alpha_0, T_0, w_2, t_2, L_2) \\ Q_Z(E_0, \rho_0, k_0, c_{p.0}, \alpha_0, T_0, w_3, t_3, L_3) \\ Q_Z(E_0, \rho_0, k_0, c_{p.0}, \alpha_0, T_0, w_4, t_4, L_4) \\ Q_Z(E_0, \rho_0, k_0, c_{p.0}, \alpha_0, T_0, w_5, t_5, L_5) \\ Q_Z(E_0, \rho_0, k_0, c_{p.0}, \alpha_0, T_0, w_6, t_6, L_6) \end{pmatrix} = \begin{pmatrix} 2.801 \times 10^7 \\ 7.17 \times 10^6 \\ 1.037 \times 10^6 \\ 9.511 \times 10^4 \\ 4.612 \times 10^4 \\ 7.967 \times 10^5 \end{pmatrix}$$

SHOCUN
SICON
FORT
ACT
ACL
ACST

$$Q_{Surface} := \begin{pmatrix} Q_S(w_1, t_1, E_0) \\ Q_S(w_2, t_2, E_0) \\ Q_S(w_3, t_3, E_0) \\ Q_S(w_4, t_4, E_0) \\ Q_S(w_5, t_5, E_0) \\ Q_S(w_6, t_6, E_0) \end{pmatrix} = \begin{pmatrix} 3.381 \times 10^4 \\ 8.345 \times 10^4 \\ 9.892 \times 10^4 \\ 1.47 \times 10^5 \\ 2.705 \times 10^5 \\ 8.244 \times 10^4 \end{pmatrix}$$

SHOCUN
SICON
FORT
ACT
ACL
ACST

$$Q_{anchor} := \begin{pmatrix} Q_{A2}(L_1, t_1) \\ Q_{A2}(L_2, t_2) \\ Q_{A2}(L_3, t_3) \\ Q_{A2}(L_4, t_4) \\ Q_{A2}(L_5, t_5) \\ Q_{A2}(L_6, t_6) \end{pmatrix} = \begin{pmatrix} 2.476 \times 10^7 \\ 1.268 \times 10^7 \\ 9.171 \times 10^5 \\ 4.659 \times 10^4 \\ 4.032 \times 10^4 \\ 4.696 \times 10^5 \end{pmatrix}$$

SHOCUN
SICON
FORT
ACT
ACL
ACST

$$Q_{exp} := \begin{pmatrix} 103690 \\ 111850 \\ 99550 \\ 55000 \\ 57627 \\ 50706 \\ 44154 \\ 105170 \\ 31680 \\ 120270 \\ 108340 \\ 32540 \end{pmatrix} \qquad th_{exp} := \begin{pmatrix} 1.614 \times 10^{-6} \\ 1.582 \times 10^{-6} \\ 1.550 \times 10^{-6} \\ 1.008 \times 10^{-6} \\ 0.924 \times 10^{-6} \\ 1.036 \times 10^{-6} \\ 0.945 \times 10^{-6} \\ 2.610 \times 10^{-6} \\ 2.235 \times 10^{-6} \\ 2.662 \times 10^{-6} \\ 2.605 \times 10^{-6} \\ 6.869 \times 10^{-6} \end{pmatrix}$$

thickness [m]

Q-TED

Q_{TED} ●●●

th

thickness [m]

Q-Surface

$Q_{Surface}$ ●●●

th

thickness [m]
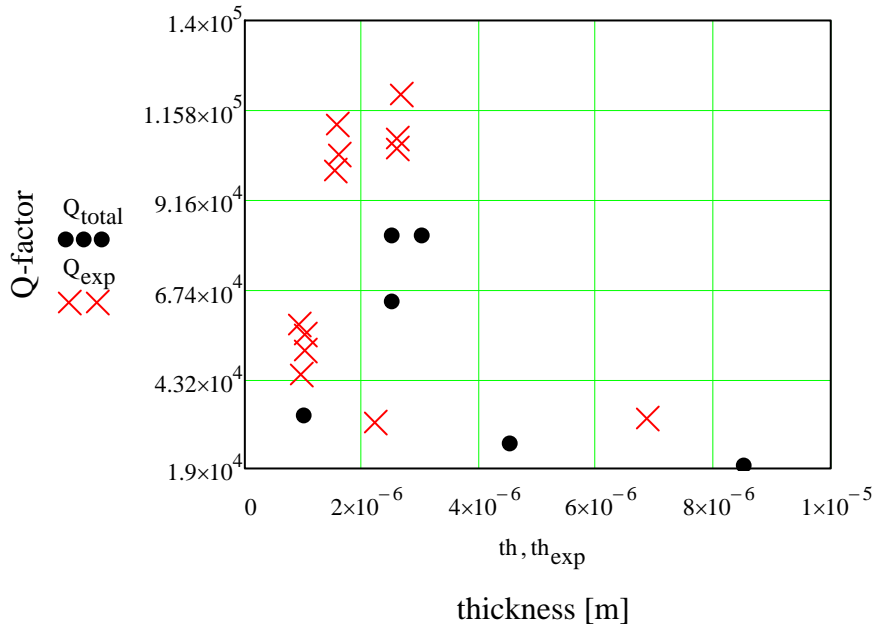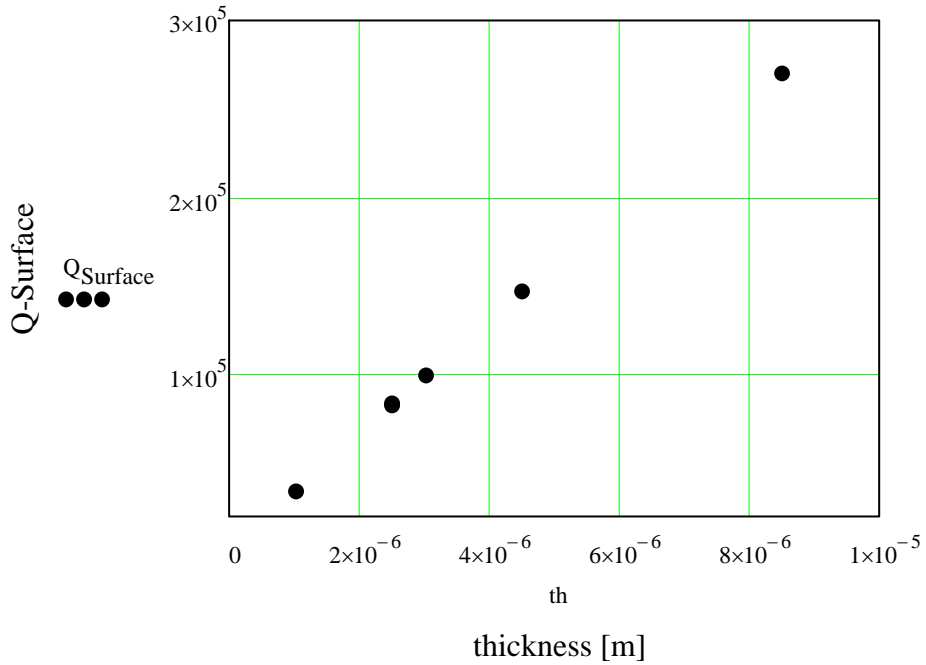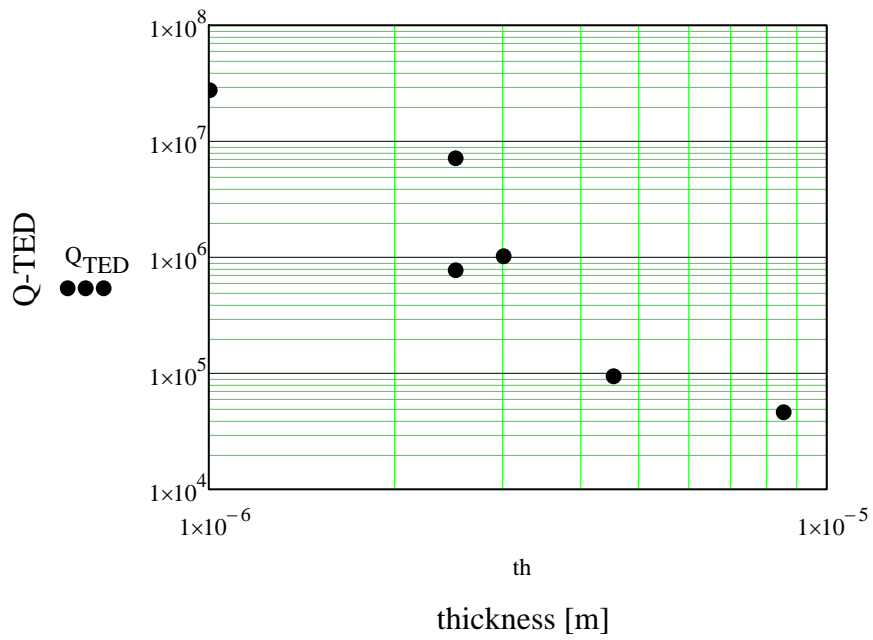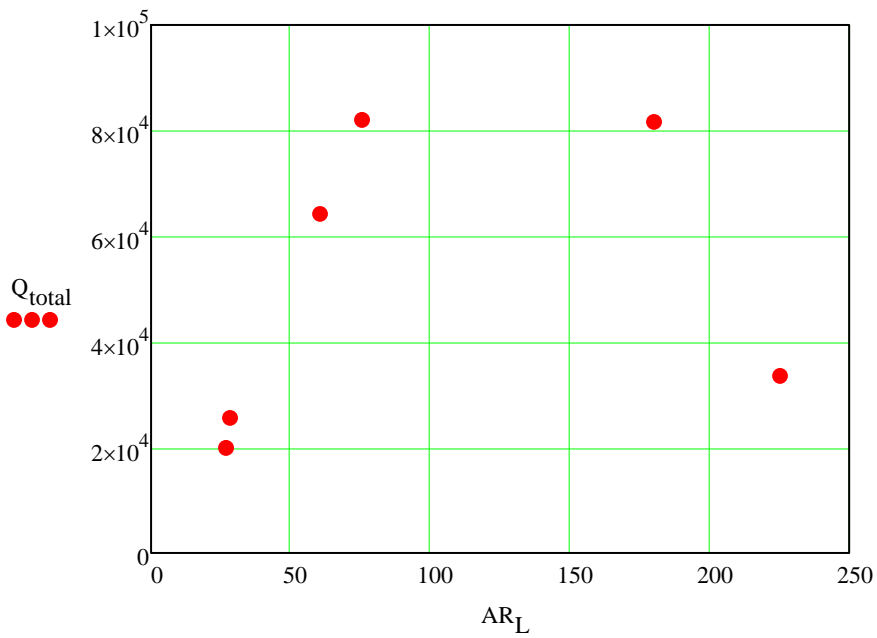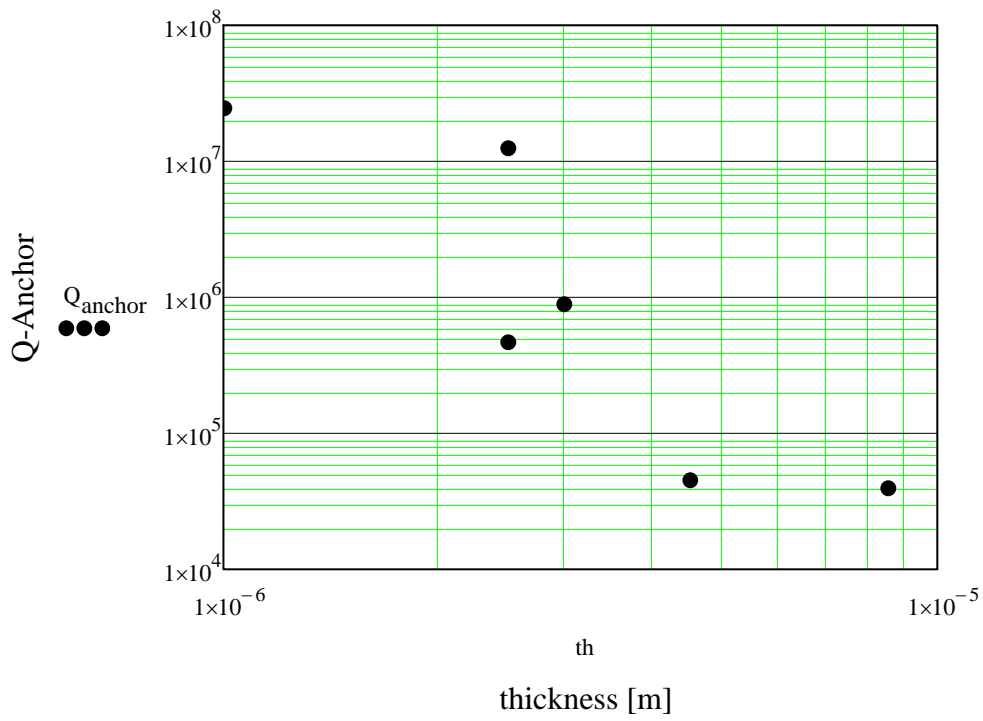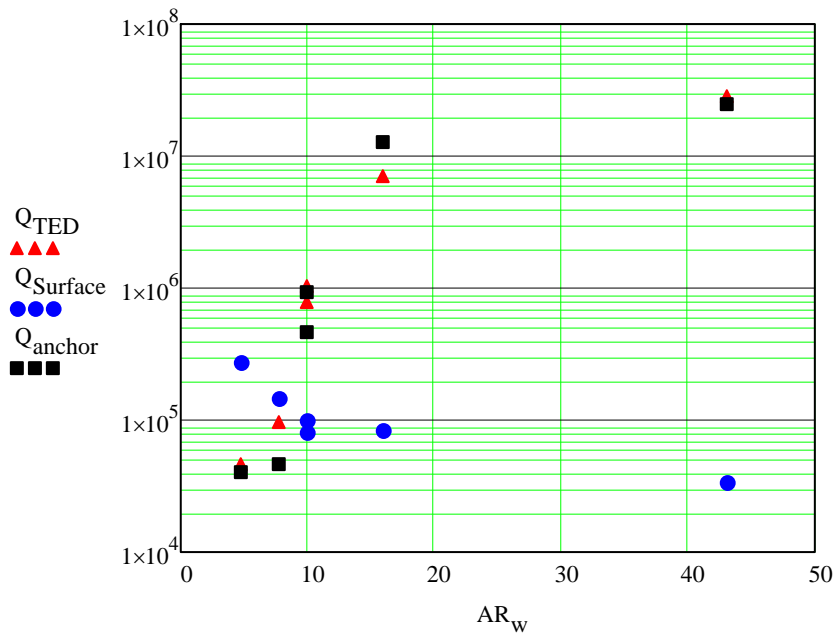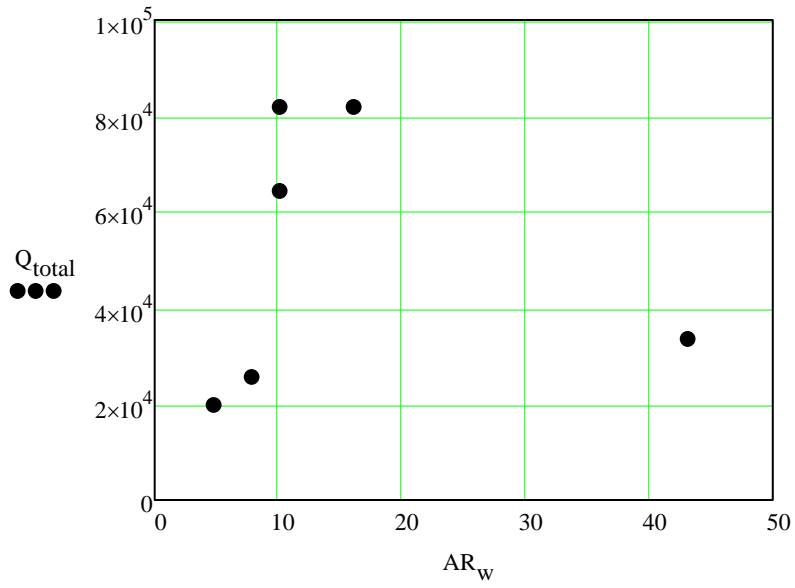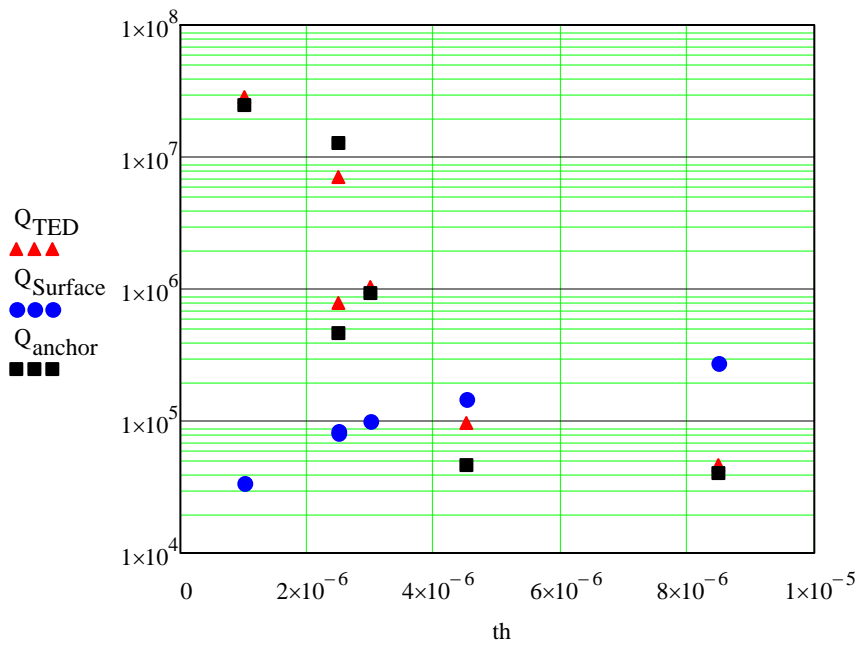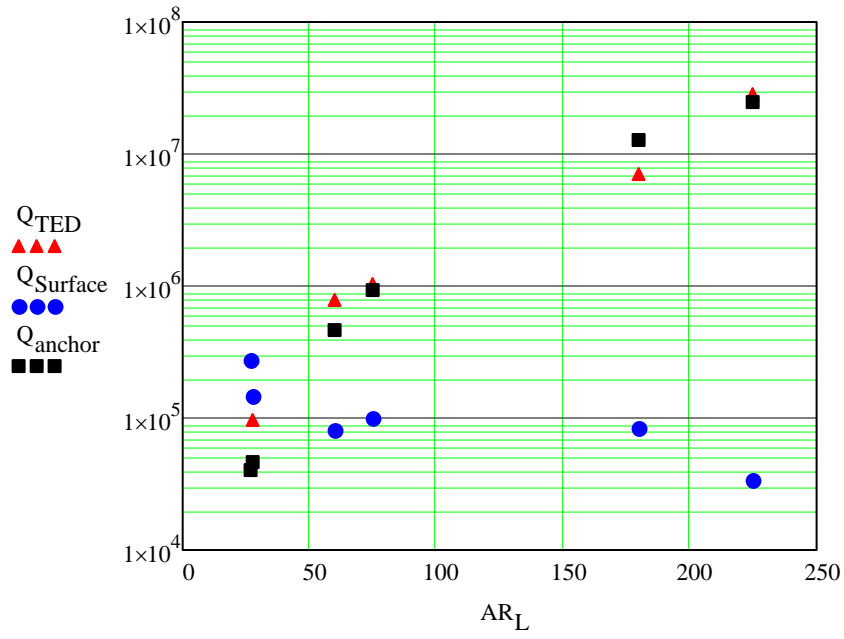
$AR_w := 0.1, 0.2.. 500$ $t := 1 \cdot \mu m$ $AR_L := 225$

$$L := AR_L \cdot t \qquad\qquad w\left(AR_w\right) := AR_w \cdot t$$

$$Q_Z\left(E, \rho, k, c_p, \alpha, T, AR_w\right) := \left[\frac{E \cdot \alpha^2 \cdot T}{c_p \cdot \rho} \cdot \frac{\omega\left(E, \rho, w\left(AR_w\right), t, L\right) \cdot \tau_z\left(t, k, c_p, \rho\right)}{1 + \left(\omega\left(E, \rho, w\left(AR_w\right), t, L\right) \cdot \tau_z\left(t, k, c_p, \rho\right)\right)^2}\right]^{-1}$$

$$Q_S\left(AR_w, E\right) := \frac{w\left(AR_w\right) \cdot t}{2 \cdot \left(3 \cdot w\left(AR_w\right) + t\right)} \cdot \frac{E}{E_{D\_Hao}} \qquad Q_{A2} := \frac{1}{2 \cdot .23 \cdot \left(\dfrac{t^3}{L^3}\right)}$$

$Q_Z\left(E_0, \rho_0, k_0, c_{p.0}, \alpha_0, T_0, AR_w\right)$ —— (red line)

$Q_S\left(AR_w, E_0\right)$ —— (blue line)

Q_{A2} —— (black line)
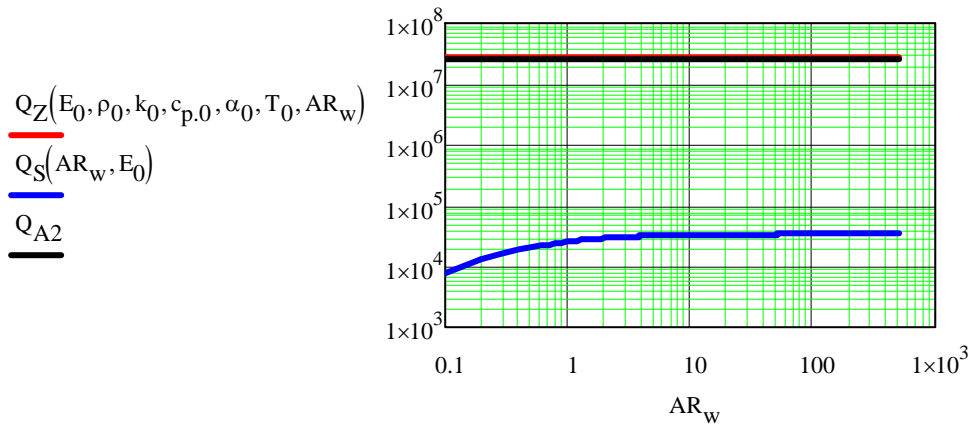
$$w := 0.1 \cdot \mu m, 0.2 \mu m .. 100 \mu m \qquad AR_W := 4.706 \qquad t(w) := \frac{w}{AR_w}$$

$$AR_L := 26.471 \qquad L(w) := AR_L \cdot t(w)$$

$$Q_Z\left(E, \rho, k, c_p, \alpha, T, w\right) := \left[\frac{E \cdot \alpha^2 \cdot T}{c_p \cdot \rho} \cdot \frac{\omega(E, \rho, w, t(w), L(w)) \cdot \tau_z\left(t(w), k, c_p, \rho\right)}{1 + \left(\omega(E, \rho, w, t(w), L(w)) \cdot \tau_z\left(t(w), k, c_p, \rho\right)\right)^2}\right]^{-1}$$

$$Q_S(w, E) := \frac{w \cdot t(w)}{2 \cdot (3 \cdot w + t(w))} \cdot \frac{E}{E_{D\_Hao}}$$

$$Q_{A2}(w) := \frac{1}{2 \cdot .23 \cdot \left(\dfrac{t(w)^3}{L(w)^3}\right)}$$

145

$$Q_Z\left(E_0, \rho_0, k_0, c_{p.0}, \alpha_0, T_0, w\right)$$

<hr/>

$$Q_S\left(w, E_0\right)$$

<hr/>

$$Q_{A2}(w)$$

<hr/>
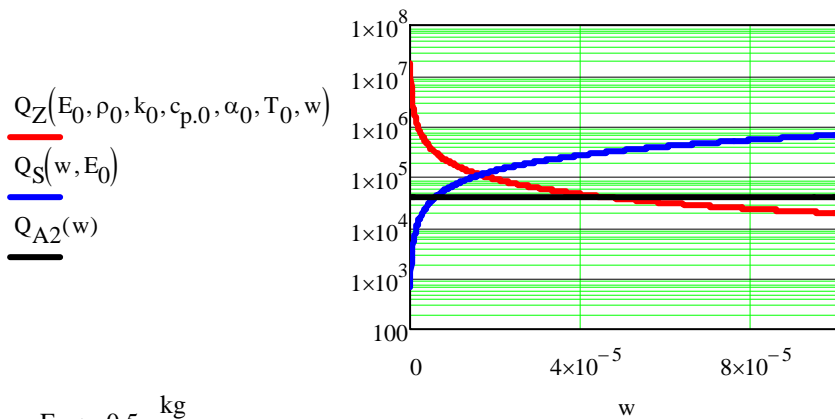
$$E_D := 0.5 \cdot \frac{kg}{s^2}$$

$$E := E_0$$

$$w := 1\mu m, 2\mu m .. 100\mu m$$

$$t := 0.1\mu m, 0.2\mu m .. 10\mu m$$

let L=Nw, N=5,10,15,20,25

$$Q_{Sur}(w, t) := \frac{w \cdot t}{2 \cdot (3 \cdot w + t)} \cdot \frac{E}{E_D}$$

Q Surface vs width and thickness
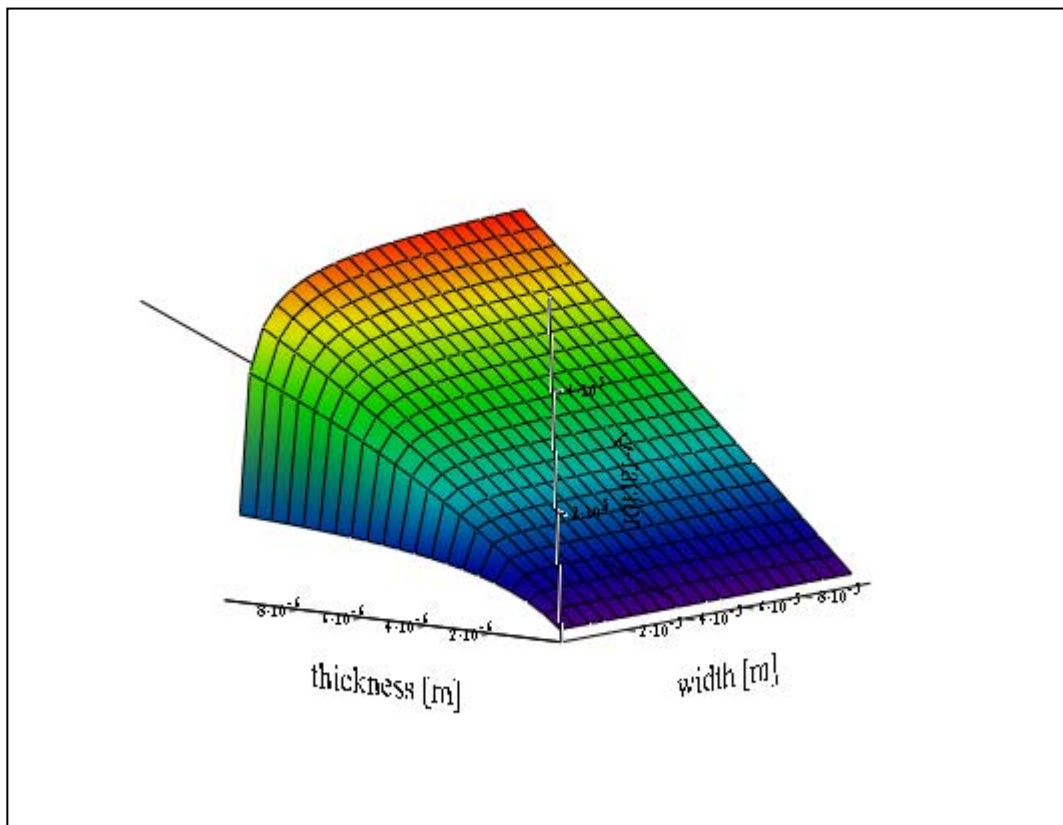
Q_{Sur}

$L(w) := 10 \cdot w$

$$Q_{TED}(w,t) := \left[\frac{E_0 \cdot \alpha_0^2 \cdot T_0}{c_{p.0} \cdot \rho_0} \cdot \frac{\dfrac{\beta_1^2}{2 \cdot \pi \, L(w)^2} \cdot \sqrt{\dfrac{E_0 \cdot I(w,t)}{\rho_0 \cdot A(w,t)}} \cdot 2 \cdot \pi \cdot \dfrac{t^2}{\pi^2 \cdot \dfrac{k_0}{c_{p.0} \cdot \rho_0}}}{1 + \left(\dfrac{\beta_1^2}{2 \cdot \pi \, L(w)^2} \cdot \sqrt{\dfrac{E_0 \cdot I(w,t)}{\rho_0 \cdot A(w,t)}} \cdot 2 \cdot \pi \cdot \dfrac{t^2}{\pi^2 \cdot \dfrac{k_0}{c_{p.0} \cdot \rho_0}} \right)^2} \right]^{-1}$$
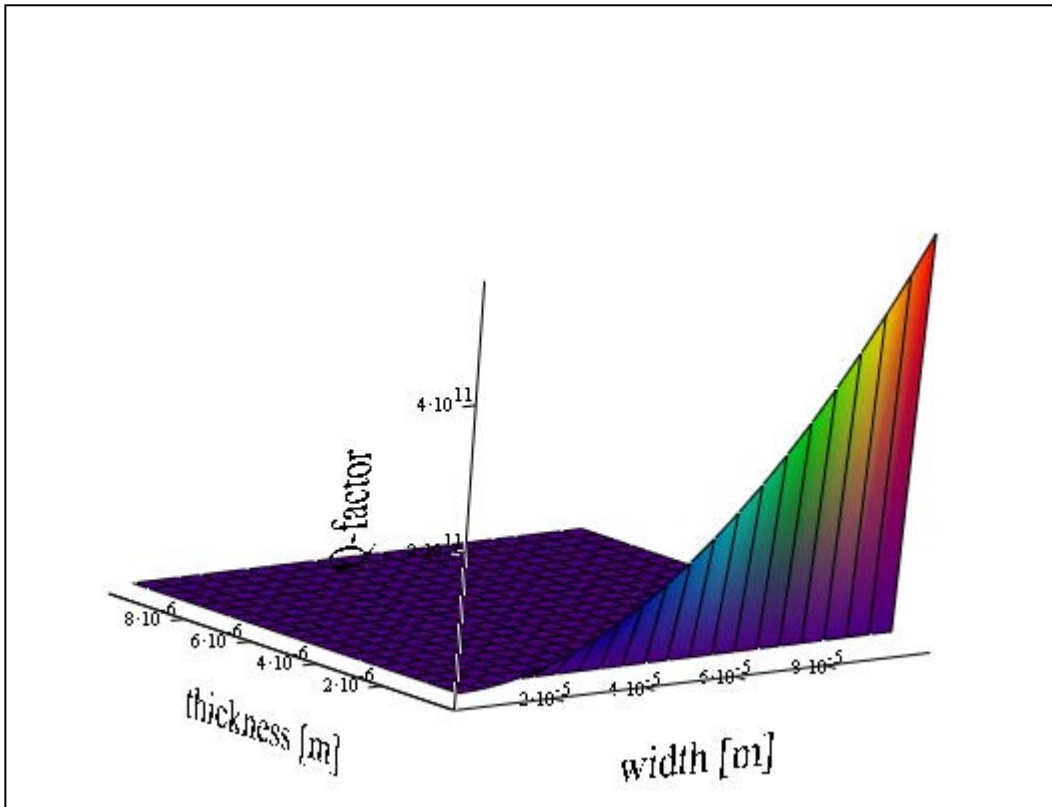
Q_{TED}

$$Q_{Anchor}(w,t) := \frac{1}{2 \cdot .23 \cdot \left(\dfrac{t^3}{L(w)^3} \right)}$$

147
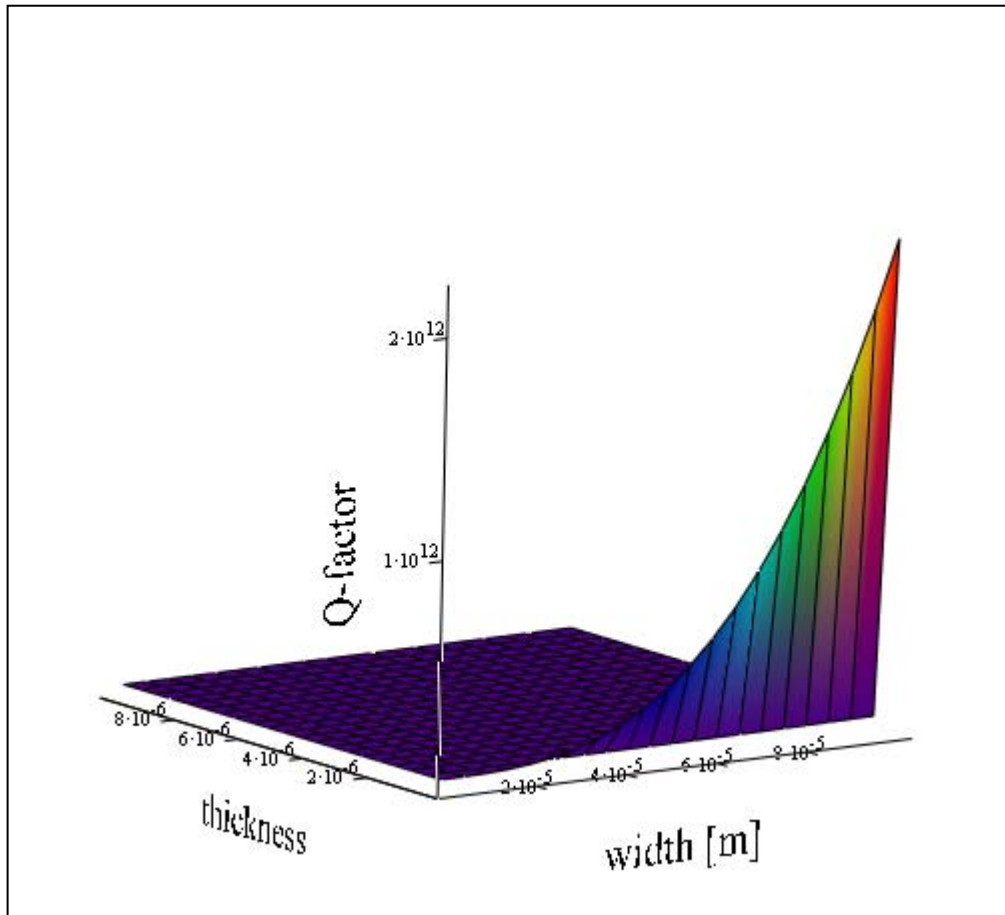
Q_{Anchor}

$$Q_{total}(w, t) := \left(\frac{1}{Q_{Anchor}(w, t)} + \frac{1}{Q_{TED}(w, t)} + \frac{1}{Q_{Sur}(w, t)} \right)^{-1}$$

Q_{total}